Exciton, Excimer, Exciplex: Study of Triplet State Harvesting in Organic Molecules for Organic Light-Emitting Diode Applications

PANDER, PIOTR,HENRYK

Exciton, Excimer, Exciplex:
Study of Triplet State Harvesting in Organic Molecules for Organic Light-Emitting Diode Applications

Piotr Pander

A Thesis Presented for the Degree of Doctor of Philosophy

Department of Physics
University of Durham
Durham, 2019

Abstract

Triplet state harvesting is an important issue in the area of organic electronics, including organic light emitting diode (OLED) technology that has already entered the global market. In the aim to achieve efficient light-emitting diodes the photophysical properties of OLED emitters need to be understood in great detail. This work is devoted to triplet state harvesting in OLEDs. In this work a set of triplet-harvesting systems comprising exciton, excimer or exciplex emitters are characterized and used to fabricate prototype devices. The first system is based on metal-free emitters, using acridone or phenothiazine, which show thermally activated delayed fluorescence (TADF) or room-temperature phosphorescence (RTP). The competition between the rate of deactivation pathways affecting the triplet state and the reverse intersystem crossing (RISC) rate determine whether these molecules emit through TADF or RTP. The second system explores the effects of different substitution patterns on the properties of excitonic tetradentate ONNO Pt(II) complexes, and their performance in OLEDs, revealing a complicated host-to-guest energy transfer mechanism in doped films. The third work in this thesis explores the properties of newly synthesized Pt(II) metal complexes that have been found to efficiently form photoluminescent excimers and have strong potential to be used in solution-processed OLED devices. The photophysical characterisation of these complexes doped in film has revealed co-existence of excimer and aggregate emissions. Finally, the last two works in this thesis are focused on small molecule and polymer-based exciplex blends that exhibit efficient TADF emissions and can be used to fabricate solution-processed or vacuum-deposited OLEDs. The photophysics of these exciplex systems is characterised in-depth and undoubtedly demonstrates that local triplet states are not involved in the RISC process in this blends, which is in clear contrast with most exciton small molecule TADF systems. Furthermore, in this work a clear rationale for the observation of emission decaying in power law regimes is obtained for the first time.

Table of contents

List of abbreviations

Al – aluminium

CT – charge-transfer

CzSi – 9-(4-tert -butylphenyl)-3,6-bis(triphenylsilyl)-9*H*-carbazole

DNTPD – *N*1,*N*1'-(Biphenyl-4,4'-diyl)bis(*N*1-phenyl-*N*4,*N*4-di-m-tolylbenzene-1,4-diamine)

FRET – Förster energy transfer

HFC – hyperfine coupling

HIL 1.3N – Heraeus Clevios HIL 1.3N

IC – internal conversion

ICT – intramolecular charge-transfer

ISC – intersystem crossing

LED – light-emitting diode

LiF – lithium fluoride

mCP – (1,3-Bis(carbazol-9-yl)benzene)

mCPPO1 – 9-(3-(9*H*-Carbazol-9-yl)phenyl)-3-(diphenylphosphoryl)-9*H*-carbazole

MLCT – metal-ligand charge transfer

MMLCT – metal-metal-ligand charge transfer

MW – molecular weight, g mol^{-1}

NIR – near infrared

NPB – *N*,*N*′-di(1-naphthyl)-*N*,*N*′-diphenyl-(1,1′-biphenyl)-4,4′-diamine

OLED – organic light-emitting diode

OXD-7 – 1,3-Bis[2-(4-tert -butylphenyl)-1,3,4-oxadiazo-5-yl]benzene

PEDOT:PSS – Poly(3,4-ethylenedioxythiophene)-poly(styrenesulfonate)

PO-T2T – 2,4,6-tris[3-(diphenylphosphinyl)phenyl]-1,3,5-triazine

PVK – poly(9-vinylcarbazole) (MW = 90 000)

PVKH – poly(9-vinylcarbazole) (MW = 1 100 000)

RIC – reverse internal conversion

RISC – reverse intersystem crossing

RTP – room temperature phosphorescence

SOC – spin-orbit coupling

TADF – thermally activated delayed fluorescence

TAPC – 4,4′-Cyclohexylidenebis[*N*,*N*-bis(4-methylphenyl)benzenamine]

TCBPA – 4,4'-(Diphenylmethylene)bis(*N*,*N*-diphenylaniline)), NPB, TPD (*N*,*N*′-Bis(3-methylphenyl)-*N*,*N*′-diphenylbenzidine

TCTA – Tris(4-carbazoyl-9-ylphenyl)amine

TPBi – 2,2',2''-(1,3,5-Benzinetriyl)-tris(1-phenyl-1-*H*-benzimidazole)

TPD – *N*,*N*′-Bis(3-methylphenyl)-*N*,*N*′-diphenylbenzidine

TSBPA – (4,4'-(Diphenylsilanediyl)bis(*N*,*N*-diphenylaniline))

VSEPR - valence shell electron pair repulsion

Declaration

All material contained in this thesis is original and is the result the author's work except where explicit reference is made to the work of others.

This thesis has not been submitted in whole or part for the award of a degree at this or any other university.

Statement of copyright

Acknowledgments

Thanks go to my parents: Ewa and Henryk, who always supported my decision to do doctoral studies in the UK.

Special acknowledgment to EXCILIGHT project members: Marharyta, Pavel, Anastasia, Oleh, Xiaofeng, Ramin, Yangyang, Antonio, Amruth, Marian, Manish, Gintas, Marco and Daniel (last two also members of the OEM group) and their supervisors for fantastic collaboration, friendly atmosphere and good vibes.

I would like to express my deep gratitude to Przemek Data, coordinator of the EXCILIGHT project and great friend.

Many thanks go to current and former members of the Organic Electroactive Materials research group: Daniel, Rongjuan, Marco, David, Gareth, Hameed, Chunyong, Paloma, Andrew, Chris, Murat, Yun, Larissa, Kleitos and Ines for maintaining a friendly atmosphere at the workplace, Patrycja, Roberto, and Marc for fruitful discussions, Heather for ensuring the wellbeing of the group members and always being friendly and helpful. Great thanks go to Andy Monkman for providing access to the research equipment, his helpful advices and suggestions.

And finally, I would like to express my very great appreciation to my supervisor Fernando Dias for his patience, support, and supervision.

This work was supported by the EXCILIGHT project funded by the European Union's Horizon 2020 Research and Innovation Programme under grant agreement No. 674990.

1 Introduction & motivations

The existence of developed societies is largely dependent upon artificial lighting. This is a crucial factor in transportation, housing, trade, industry and many more. However, the increasing needs for artificial lighting have led to rising consumption of electrical power, thus energy-efficient light sources became of major importance over the last years.[1–3] The development of the first incandescent lightbulbs triggered the search for artificial light sources with improved performance, in order to comply with the need for more energy-efficient solutions. This has led to the development of fluorescent tubes and light-emitting diodes (LED) that are far superior in efficiency. However, since Tang and VanSlyke[4] have shown a first organic light-emitting diode (OLED), scientists and industry partners have been interested in developing this technology. In fact, OLEDs have found more predominant role in luminescent displays, such as OLED TV's or smartphone screens. These solutions require emitters in the red, green and blue regions. However, an increasing interest is given to near infrared OLED emitters nowadays due to their potential in wearable optoelectronic devices with application in sensing, anti-counterfeit labelling, medical treatment of skin diseases and development of user-device interface systems.[5,6]

A growing need for energy-efficient OLEDs has led to new scientific discoveries related to the use of so-called triplet-harvesting molecules, [7,8] which are able to harvest all excited states generated in an OLED and therefore improve significantly the quantum efficiency of these devices. The growing need to analyse and understand the physical properties of organic π-conjugated molecules as OLED emitters – to make them more efficient and tailored for specific needs – has given a ground and became a motivation for this thesis. The author believes the results contained in this work will improve the understanding of mechanisms governing triplet-harvesting systems. The main focus of this work is to explore different photophysical mechanisms involving excitonic, excimer

and exciplex forming systems to tailor their luminescence properties and realise their application in OLED devices.

Currently, molecules with efficient triplet harvesting properties that can be used in devices are divided in two types: phosphorescent metal-containing complexes and TADF emitters.[3,5,9,10] Out of these two groups all three types of excited states discussed in this work are being used: exciton, excimer, and exciplex.[11–14] Specific properties of each group of emitters make them suitable for certain applications. For example, phosphorescent metal complexes have found an important role as standard OLED emitters due to their triplet-harvesting properties, short photoluminescence lifetime, high photoluminescence efficiency and high stability. They are currently being used in OLED screens, as red and green dopants also due to their narrow electroluminescence spectrum (important for colour purity). Unfortunately, blue phosphorescent complexes have been found to be insufficiently stable.[1] No stable blue metal complex that meets commercial requirements has been developed so far, despite decades of intense research.

TADF emitters, mostly excitonic, are believed to have potential to supersede phosphorescent metal complexes in their role as OLED emitters, mostly in display technology.[15] These emitters are mostly based on charge-transfer states that generate broad emission spectra.[5,16] Consequently, emitters with narrow spectra are increasingly requiered.[17]

Exciplex and excimer emitters typically exhibit broad emission spectra, thus their primary practical use is as component of white electroluminescence. Majority of exciplex emitters comprise of two non-metal organic molecules.[16,18] They exhibit fluorescent or TADF properties, although phosphorescent exciplexes have also been postulated to exist[19]. Excimer emitters are predominately Pt(II) metal complexes as non-metal molecules usually form excimers with low photoluminescence quantum yield.[14,20] Interestingly, due to the involvement of two metal centres in the excimers of metal

complexes, the phosphorescence radiative rate constant in these systems is very high, even for deep red and near infrared emissions. This opens an interesting pathway for excimer-forming Pt(II) complexes to be used as efficient near infrared emitters in OLEDs.

The main motivation of this work is thus to explore the photophysical properties in excitonic, excimer and exciplex systems in the context of their application in OLEDs. There are still many and very interesting questions to clarify in order to learn how these systems can be tailored to obtain the desirable properties for the fabrication of efficient OLEDs, with electroluminescence in the different regions of the visible and NIR electromagnetic spectrum. The author believes this work will significantly contribute to help on the understanding of the properties of these systems in general, especially their solid-state properties, and potential to be used in context of OLEDs in particular.

Publications contained within the thesis:

From the 26 published scientific papers (listed below) 24 were published during the course of the doctoral studies. From these the author has selected five to use in this thesis. These are shown below and are disclosed at the beginning of each experimental chapter.

Chapter 4

P. Pander, A. Swist, R. Motyka, J. Soloducho, F. B. Dias and P. Data, *J. Mater. Chem. C*, 2018, **6**, 5434–5443.

Author's contribution*: All photophysical measurements and half of OLED work. Writing the manuscript.*

Chapter 5

P. Pander, R. Bulmer, R. Martinscroft, S. Thompson, F. W. Lewis, T. J. Penfold, F. B. Dias and V. N. Kozhevnikov, *Inorg. Chem.*, 2018, **57**, 3825–3832.

Author's contribution*: All photophysical measurements and all OLED devices made and characterised. Electrochemical analysis. Writing parts of the manuscript related to the performed experimental work.*

Chapter 6

M. T. Walden, **P. Pander**, D. S. Yufit, F. B. Dias and J. A. G. Williams, *J. Mater. Chem. C*, 2019 DOI: 10.1039/C9TC00768G.

Author's contribution*: All solid-state photophysical measurements, electrochemical analysis and all OLED devices. Writing parts of the manuscript.*

Chapter 7

P. Pander, S. Gogoc, M. Colella, P. Data and F. B. Dias, *ACS Appl. Mater. Interfaces*, 2018, **10**, 28796–28802.

***Author's contribution**: All experiments and writing the manuscript.*

Chapter 8 (also **Chapter 2.4**)

M. Chapran, **P. Pander**, M. Vasylieva, G. Wiosna-Salyga, J. Ulanski, F. B. Dias and P. Data, *ACS Appl. Mater. Interfaces*, 2019, **11**, 13460–13471.

***Author's contribution**: Nearly all photophysical experiments (except for laser fluence) and formulation of the theory explaining photophysical exciplex behaviours.*

Publication included as a part of the Experimental (Chapter 3):

Chapter 3.4

P. Pander, P. Data and F.B. Dias, *J. Vis. Exp.*, 2018, e56614.

***Author's contribution**: All experiments and writing the manuscript.*

Other publications by the author:

1 M. Z. Shafikov, R. Daniels, **P. Pander**, F. B. Dias, J. A. G. Williams and V. N. Kozhevnikov, *ACS Appl. Mater. Interfaces*, 2019, **11**, 8182–8193.

2 **P. Pander**, A. Swist, R. Turczyn, S. Pouget, D. Djurado, A. Lazauskas, R. Pashazadeh, J. V. Grazulevicius, R. Motyka, A. Klimash, P. J. Skabara, P. Data, J. Soloducho and F. B. Dias, *J. Phys. Chem. C*, 2018, acs.jpcc.8b08329.

3 C. Chen, R. Huang, A. S. Batsanov, **P. Pander**, Y.-T. Hsu, Z. Chi, F. B. Dias and M. R. Bryce, *Angew. Chemie*, 2018, **130**, 16645–16649.

4 R. Pashazadeh, **P. Pander**, A. Lazauskas, F. B. Dias and J. V Grazulevicius, *J. Phys. Chem. Lett.*, 2018, **9**, 1172–1177.

5 **P. Pander**, R. Motyka, P. Zassowski, M. K. Etherington, D. Varsano, T. J. da Silva, M. J. Caldas, P. Data and A. P. Monkman, *J. Phys. Chem. C*, 2018, **122**, 23934–23942.

6 R. Pashazadeh, **P. Pander**, A. Bucinskas, P. J. Skabara, F. B. Dias and J. V Grazulevicius, *Chem. Commun.*, 2018, **54**, 13857–13860.

7 M. Colella, **P. Pander**, D. de S. Pereira and A. P. Monkman, *ACS Appl. Mater. Interfaces*, 2018, **10**, 40001–40007.

8 M. Colella, **P. Pander** and A. P. Monkman, *Org. Electron.*, 2018, **62**, 168–173.

9 A. Klimash, **P. Pander**, W. T. Klooster, S. J. Coles, P. Data, F. B. Dias and P. J. Skabara, *J. Mater. Chem. C*, 2018, **6**, 10557–10568.

10 Y. Qu, **P. Pander**, A. Bucinskas, M. Vasylieva, Y. Tian, F. Miomandre, F. B. Dias, G. Clavier, P. Data and P. Audebert, *Chem. - A Eur. J.*, 2019, **25**, 2457–2462.

11 **P. Pander**, A. Swist, J. Soloducho and F. B. Dias, *Dye. Pigment.*, 2017, **142**, 315–322.

12 M. Okazaki, Y. Takeda, P. Data, **P. Pander**, H. Higginbotham, A. P. Monkman and S. Minakata, *Chem. Sci.*, 2017, **8**, 2677–2686.

13 P. Data, **P. Pander**, M. Okazaki, Y. Takeda, S. Minakata and A. P. Monkman, *Angew. Chemie Int. Ed.*, 2016, **55**, 5739–5744.

14 P. Data, **P. Pander**, P. Zassowski, V. Mimaite, K. Karon, M. Lapkowski, J. V. Grazulevicius, P. Slepski and K. Darowicki, *Electrochim. Acta*, 2017, **230**, 10–21.

15 **P. Pander**, R. Motyka, P. Zassowski, M. Lapkowski, A. Swist and P. Data, *J. Phys. Chem. C*, 2017, **121**, 11027–11036.

16 P. Data, A. Kurowska, S. Pluczyk, P. Zassowski, **P. Pander**, R. Jedrysiak, M. Czwartosz, L. Otulakowski, J. Suwinski, M. Lapkowski and A. P. Monkman, *J. Phys. Chem. C*, 2016, **120**, 2070–2078.

17 **P. Pander**, A. Swist, P. Zassowski, J. Soloducho, M. Lapkowski and P. Data, *Electrochim. Acta*, 2017, **257**, 192–202.

18 **P. Pander**, P. Data, R. Turczyn, M. Lapkowski, A. Swist, J. Soloducho and A. P. Monkman, *Electrochim. Acta*, 2016, **210**, 773–782.

19 P. Data, **P. Pander**, M. Lapkowski, A. Swist, J. Soloducho, R. R. Reghu and J. V. Grazulevicius, *Electrochim. Acta*, 2014, **128**, 430–438.

20 K. Laba, P. Data, P. Zassowski, **P. Pander**, M. Lapkowski, K. Pluta and A. P. Monkman, *J. Phys. Chem. C*, 2015, **119**, 13129–13137.

2 Theoretical background

2.1 Electronic structure of π-conjugated molecules

π-conjugated molecules are at the foundation of OLED lighting. These molecules are composed of one or many conjugated systems that are formed by mixing the p-orbitals of neighbouring sp^2-hybrydized atoms, such as carbon, nitrogen or sometimes oxygen, boron and others. The most useful π-conjugated systems for OLEDs are aromatic due to their stability (lesser susceptibility towards chemical reactions) and ability to emit photoluminescence in the visible, as well as in UV and NIR regions. Aromatic systems are those fulfilling the Hückel's rule. That is the total number of electrons in the overlapping p-orbitals has to be 4n + 2, where n is a natural number. All discussions in this work relate to organic aromatic π-conjugated molecules. Interaction of orbitals is related to the geometrical orientation such that the orbital branches with the same sign (+/-) can align, forming a hybrid (bonding) orbital. This is why the aromatic molecules are planar, as in this case all p orbitals are parallel allowing the best possible overlap. If the orbitals are orthogonal, there is no interaction, thus no conjugation.[21]

2.2 Excited states of π-conjugated molecules

Electron transitions between the ground and excited states of molecules can be best described by the Jabłoński diagram (**Figure 2.1**). This diagram is called after the Polish Physicist Aleksander Jabłoński that first suggested the existence of a metastable state (currently known as triplet state) and depicted his hypothesis on a diagram,[22] that is used until today in its expanded and modernised forms. Jabłoński diagram is useful in the schematic representations of radiative and non-radiative processes in organic molecules. The diagram shows the electron energy levels associated with the ground state (S_0) and the excited states (S_1, S_2…, T_1, T_2, ….), of singlet and triplet characters, respectively. It also depicts the different electronic transitions occurring between these electronic states: internal conversion (IC), reverse internal conversion (RIC), absorption, and fluorescence are all allowed transitions; intersystem crossing (ISC), reverse

intersystem crossing (RISC), and phosphorescence are all spin forbidden transitions (i.e. transitions requiring an electron to change its spin). Typically, absorption is a transition from the ground state to the singlet excited state, $S_0 \rightarrow S_1$ (and also to upper singlet states S_2, S_3, etc.).

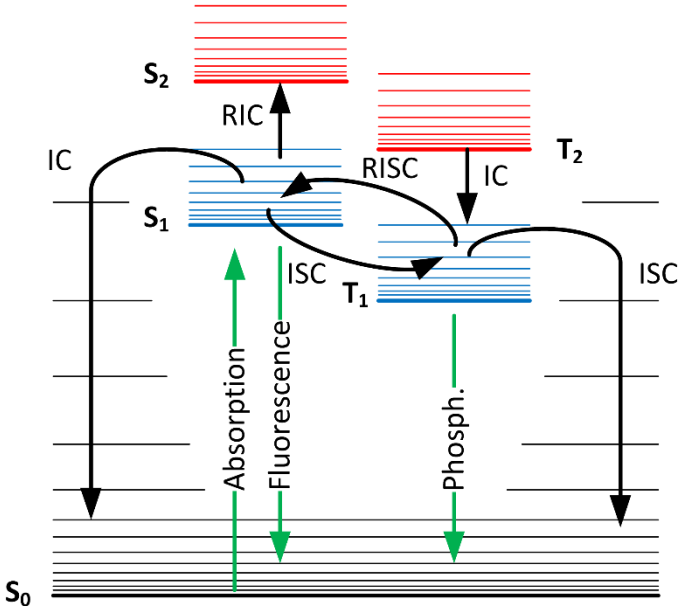

Figure 2.1. Jabłoński diagram depicting the radiative: absorption, fluorescence, and phosphorescence (green lines) and non-radiative: internal conversion (IC), intersystem crossing (ISC), reverse internal conversion (RIC), and reverse intersystem crossing (RISC) (black lines) electron transitions in organic molecules. S_1, S_2 – first and second singlet energy levels; T_1, T_2 – first and second triplet energy levels. Adapted from ref. [23]

Electronic transitions are governed by selection rules that state which ones are more probable to occur or faster. In general, optical transitions can be named as forbidden or allowed. Allowed transitions are relatively fast / probable whereas forbidden transitions are slow / improbable. Slow / fast is used to describe spontaneous transitions, such as radiative transition from the excited state to the ground state. On the other hand, probable / improbable refer to stimulated transitions, such as absorption. Therefore, allowed transitions, such as absorption ($S_0 \rightarrow S_1$), occurring with a 10^{15} s^{-1} rate, or fluorescence ($S_1 \rightarrow S_0$), occurring with a rate between 10^{10}-10^{8} s^{-1} are fast, whereas forbidden transitions, such as phosphorescence ($T_1 \rightarrow S_0$) require much more time, from

≈1 μs up to ≈1 s. Interestingly, intersystem crossing ($S_1 \rightarrow T_1$) can be much faster and may occur even within less than 1 ns in special cases.[5,23,24]

2.3 Hyperfine coupling

Hyperfine coupling is the effect caused by the interaction between two spins of electron or spins of electron and the nucleus. It is widely used in spectroscopy, such as nuclear magnetic resonance (NMR) or electron paramagnetic resonance (EPR). In organic molecules the hyperfine coupling (HFC) is considered a mechanism of interaction between electron energy levels, competitive to spin-orbit coupling.[25,26] In general, hyperfine coupling constants are miniscule, ≈0.2 cm^{-1} (≈2×10^{-5} eV)[27,28] and require the interacting singlet and the triplet states to differ in energy in the same order of magnitude. This means, only nearly isoenergetic states with $\Delta E_{ST} \approx 10^{-5}$ eV or less can interact this way. This situation may occur in charge-transfer states where the ^{1}CT – ^{3}CT gap is in order of 10^{-6}-10^{-5} eV. As shown by Ogiwara *et al.*[27] the intersystem crossing mediated through HFC in some TADF molecules is much more important than spin-orbit coupling.

2.4 Spin-orbit coupling

Spin-orbit coupling (SOC) describes the interaction between the electron magnetic moment due to the electron spin (determined by its spin quantum number) and orbital magnetic moment associated with an electron orbit (determined by angular/orbital quantum number). In simple words it is the interaction occurring from the motion of the electron within a specific geometry of the occupied subshell (orbital, “orbit”). Electron spin is constant, thus the spin-orbit interaction is orbital-dependent. It has been observed that spin-orbit coupling intensifies as the orbital quantum number rises, so it is larger for d- and f-orbitals than p-orbitals. SOC causes effectively splitting of triplet energy levels (zero-field splitting, ZFS), but also mixes the properties of singlet and triplet states. In example, due to SOC the triplet state in heavy metal complexes has a partial singlet

character (i.e. high radiative rate constant) allowing for short-lived and efficient phosphorescence and applicability in OLED devices.[13,29,30]

2.5 Use of triplet harvesting in OLED

Guidelines for improving the efficiency of OLEDs are obtained directly from the principal equation (2.1) describing the external quantum efficiency (EQE) of an OLED.[1,7,30,31]

$$\mathrm{EQE} = \eta_{\mathrm{out}}\eta_{\mathrm{fl}}\gamma\eta_{\mathrm{fr}} \qquad (2.1)$$

η_{out} – the outcoupling factor that is typically equal to 0.2-0.3 in a planar device built on glass. The outcoupling is related to the way light propagates in its path from the emissive material and glass with larger refractive index to air. Therefore, the light emitted by the device is affected by total internal reflection that causes light waveguiding, and also by scattering and even absorption. In order to overcome this issue, various different patterns can be built on a flat glass surface, such as semispheres, using transparent polymer media or even nanoparticles. On the other hand, ordering of molecules in the emissive layer may also be beneficial for the light outcoupling factor. By orienting the molecules in the emissive layer the actual effect is orientation of the transition dipole moment: horizontal orientation (perpendicular to the device plane) increases the light out coupling factor.[32]

η_{fl} – photoluminescence quantum yield (PLQY) of the emitter/emissive layer. This is a property of material/matrix and changes upon several factors. First of all the emitter has to be designed to reduce non-radiative decay. On the other hand the host/matrix is used (for the purpose of improving this parameter) to reduce aggregation quenching or self-quenching in the emitting material as well as to provide rigid environment to suppress non-radiative decay processes. PLQY in principle can vary from 0 to 1 and emitter/matrix systems with PLQY=1 are already well known.

γ – charge balance factor is related to the way the device is designed. Using adequate electron/hole transport/blocking and emissive layers of suitable thickness the value of 1 can be achieved. This means the fraction of injected holes and electrons that recombine to form excitons is close to 100%.

η_{fr} – fraction of emissive excited states. This describes the fraction of total excitons formed from charge recombination that are potentially emissive excited states.

The triplet state harvesting mechanisms discussed in this work are of great importance to improve the fraction of emissive excited states. In the way OLEDs work, singlets and triplet states are formed upon charge recombination on a ratio of 25% singlet states and 75% triplet states.[5,7,10,24] In many molecules, such as the purely organic fluorescent systems, the triplet states are often non-emissive at room temperature, which means that 75% of the states formed (triplets) are never transformed into light. In order to improve this factor, triplet harvesting systems have been used with relative success. This work focuses on the investigation of two mechanisms of triplet harvesting: 1) direct radiative decay from the triplet state, phosphorescence at room-temperature, and 2) thermally activated delayed fluorescence. In both cases triplet and singlet excited states can be harvested up to 100%.

2.5.1 Why is there 75 % of triplets?

Hole and electron bear a ½ spin. There is a random distribution of spins thus there is equal number of charge carriers with secondary spin quantum number $m_S = \pm ½$ (schematically represented as ↑ and ↓). This gives four possible ways the spins can be arranged: ↑↑, ↓↓, ↓↑, and ↑↓, resulting on one state with spin quantum number S = 0 (singlet) and three states with S = 1 (triplet). Each state can be described by its spin quantum number S and the secondary spin quantum number m_S which can have values from -S to +S with the interval of 1. In other words, the recombination of hole an electron bearing $m_S = \pm ½$ will give four states with equal probability: S = 0, m_S = 0

(singlet); S = 1, m_S = -1 (triplet); S = 1, m_S = 0 (triplet); S = 1, m_S = 1 (triplet). For this reason the spin statistics, under absence of other phenomena affecting it, inevitably leads to a conclusion that singlet states are formed with ¼ probability, while triplet states with the probability of ¾.[5,10,24]

2.6 Mechanisms for triplet harvesting in organic molecules

As it has been shown above triplet harvesting is of vital importance in OLEDs. Two main ways of triplet harvesting have been developed upon years of intense research in this topic: 1) delayed fluorescence, appearing as a result of triplet-triplet annihilation (TTA) or due to thermally activated reverse intersystem crossing (TADF). However, TTA is rarely used nowadays upon the emergence of TADF compounds; 2) room-temperature phosphorescence (RTP), appearing as a result of enhanced SOC due to the presence of heavy-metals, and more rarely RTP in metal-free molecules that have been specifically designed to show fast ISC rate and suppressed IC. Pure fluorescent emitters, i.e. those not harvesting triplets, are also discussed below as a matter of reference.[5]

2.6.1 Fluorescent emitters (not harvesting triplet states)

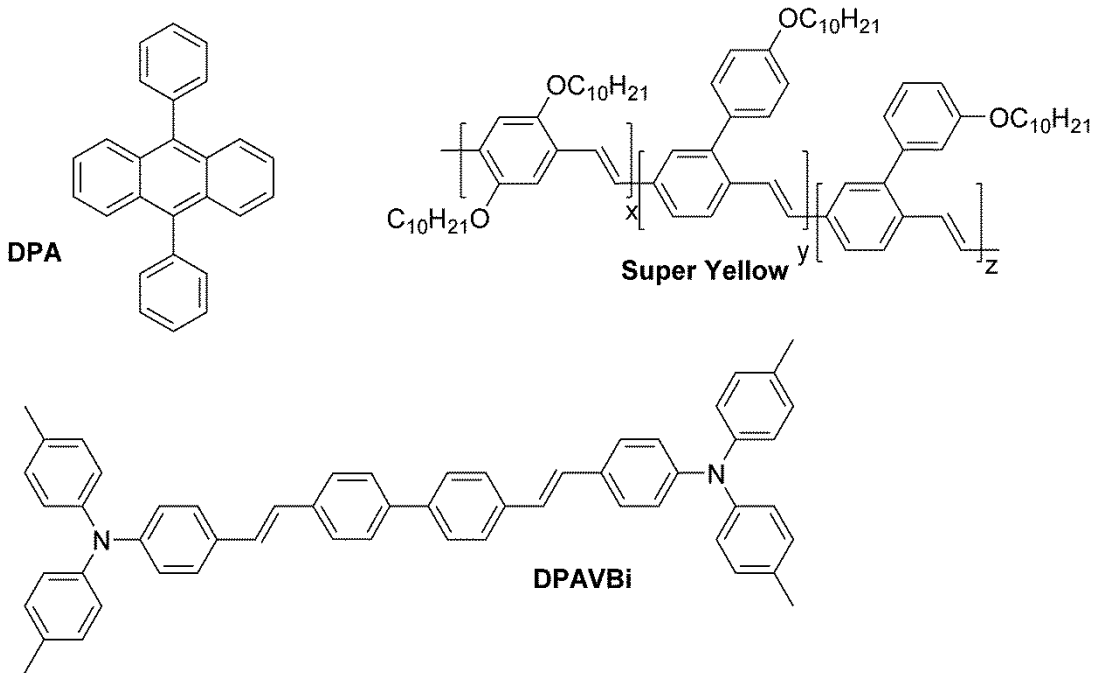

Figure 2.2. Examples of fluorescent small molecules DPA, DPAVBi, and polymer Super Yellow used in OLED.

Fluorescent emitters can be described as π-conjugated systems with large radiative rate constant of the singlet excited state and high photoluminescence quantum yield (**Figure 2.2**). These types of molecules usually possess energetically low excited triplet state that usually does not play any significant role in the emissive properties of these molecules (**Figure 2.3**). Therefore the maximum internal quantum efficiency of OLEDs based on pure fluorescent emitters is 25%. Fluorescent emitters can also perform as fluorescent dopants to TADF materials and phosphors using the so-called hyperfluorescence mechanism to achieve narrow emission with faster decaying rate.[33]

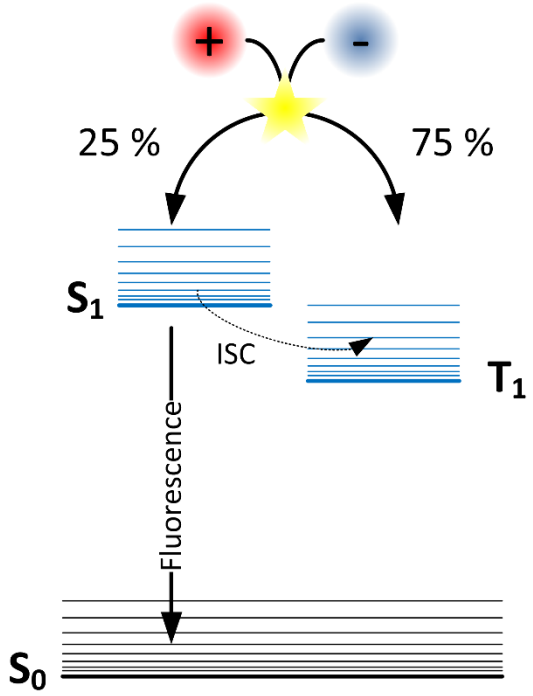

Figure 2.3.Fluorescent emitters in OLED. 75 % of excited states generated in OLED are not harvested. Furthermore, limited intersystem crossing might decrease singlet population below 25 % in favour of the triplet states. This gives a maximum of 25 % of excited states to be harvested by the fluorescent emitter.

2.6.2 Direct radiative decay of triplet state

Phosphorescent emitters are typically metal complexes that contain specific metal ions at selected oxidation states (**Figure 2.4**). In order to achieve brightly luminescent metal complexes several conditions must be met. Owing to the strong spin-orbit coupling resulting from the d-orbitals of open shell transition metal ions, such as Pt^{2+} (configuration d^8) or Ir^{3+} (configuration d^6) in their complexes, high triplet radiative rates have been achieved. The development of these emitters is also related to designing new ligands that change the electron distribution of the metal complex, and lead to various photoluminescent properties, such as a range of emission colours.[30]

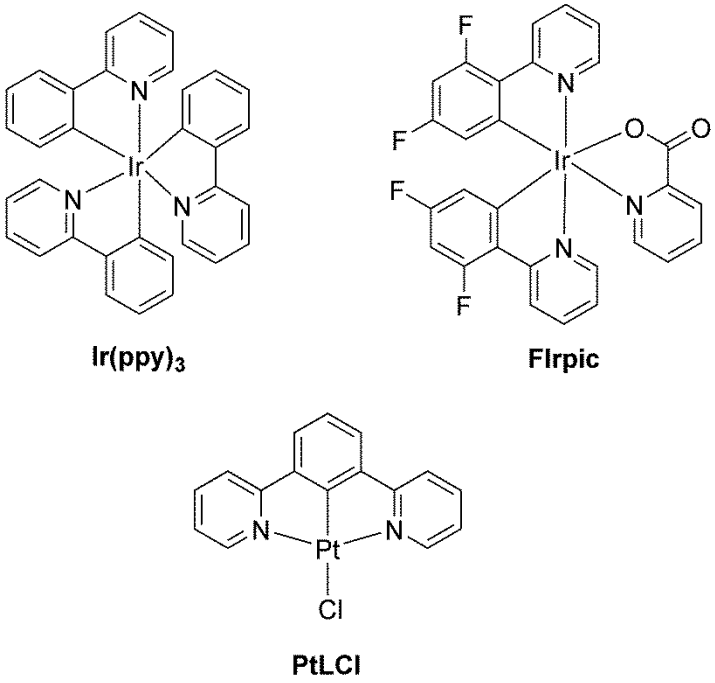

Figure 2.4. Examples of phosphorescent Ir(III) and Pt(II) complexes used in OLED.

Relatively short phosphorescence lifetimes and high PLQY are the factors determining the performance of triplet-harvesting metal complexes in OLEDs and these have been found in Pt(II) and Ir(III) based organic compounds. Their room temperature photophysics is usually very simple, comprising monoexponential triplet decay. However and interestingly, low temperature photophysics of these complexes is very interesting as the lowest triplet state is split (without magnetic field) due to the strong

spin-orbit coupling. This phenomenon is called zero-field splitting (ZFS) and occurs even in non-metal molecules, however the value of ZFS in this case is negligible, $\approx 10^{-5}$ eV. In cases where the lowest triplet state has an admixture of metal d-orbitals the ZFS can reach values up to $\approx 10^{-2}$ eV. Due to ZFS the different phosphorescence lifetimes of the split sub-states can be observed at very low temperatures, where the thermal energy is not enough to allow for fast thermal equilibration between them. In general, the most desired for OLEDs is that the d-orbitals of metal mix with ligand-centred orbitals giving a metal-ligand charge transfer (MLCT) state, while purely ligand centred states have long phosphorescence lifetime and metal-centred states are usually non-emissive.[30,34,35]

In Pt(II) and Ir(III) metal complexes (as well as other metal-containing complexes), the intersystem crossing rate is so fast that the fluorescence rate is not able to compete. Fluorescence, therefore, is usually mostly absent in these molecules and cannot be observed with typical measurement techniques (**Figure 2.5**). Absorption of light typically occurs as an $S_0 \rightarrow S_n$ process, (however $S_0 \rightarrow T_1$ absorption bands are postulated to exist). Upon formation of the singlet excited state, rapid ISC populates the triplet state from where the complexes emits efficient phosphorescence through their ^{3}MLCT states, in the typical lifetime range of 1-10 μs at room temperature. These complexes have found a prominent role as emitters in OLEDs covering nearly the whole visible spectrum from sky blue to deep red and NIR.[14,30,36,37]

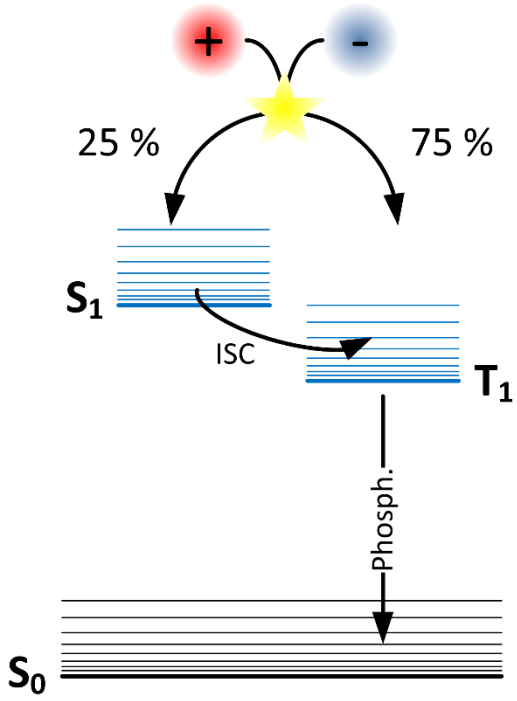

Figure 2.5. Phosphorescent emitters in OLED. 75 % of excited states generated in OLED are harvested as efficient phosphorescence. The 25 % of singlet states intersystem cross and add up with the initial triplet state population. That gives up to 100 % excited states harvesting in such emitter.

2.6.3 Triplet exciton up-conversion through TADF

Delayed fluorescence emitters are a large group of fluorescent molecules that can either be purely organic (metal-free) or contain metals, such as copper or silver in their structures.[38,39] The most useful molecules in this group are thermally-activated delayed fluorescence (TADF) emitters and are those mainly discussed in this work. There is a large variety of design patterns, but the vast majority of metal-free TADF emitters are comprised of a twisted donor-acceptor structure (**Figure 2.6**). Their main design principle is in the use of charge-transfer excited states to reduce singlet-triplet energy splitting, allowing the non-radiative spin-forbidden transitions between singlet and triplet states, due to induced spin-orbit coupling, to be relatively fast. This in turn allows thermally-induced up-conversion and recovery of the triplet excited states through the singlet state – as delayed fluorescence.[5,7,40]

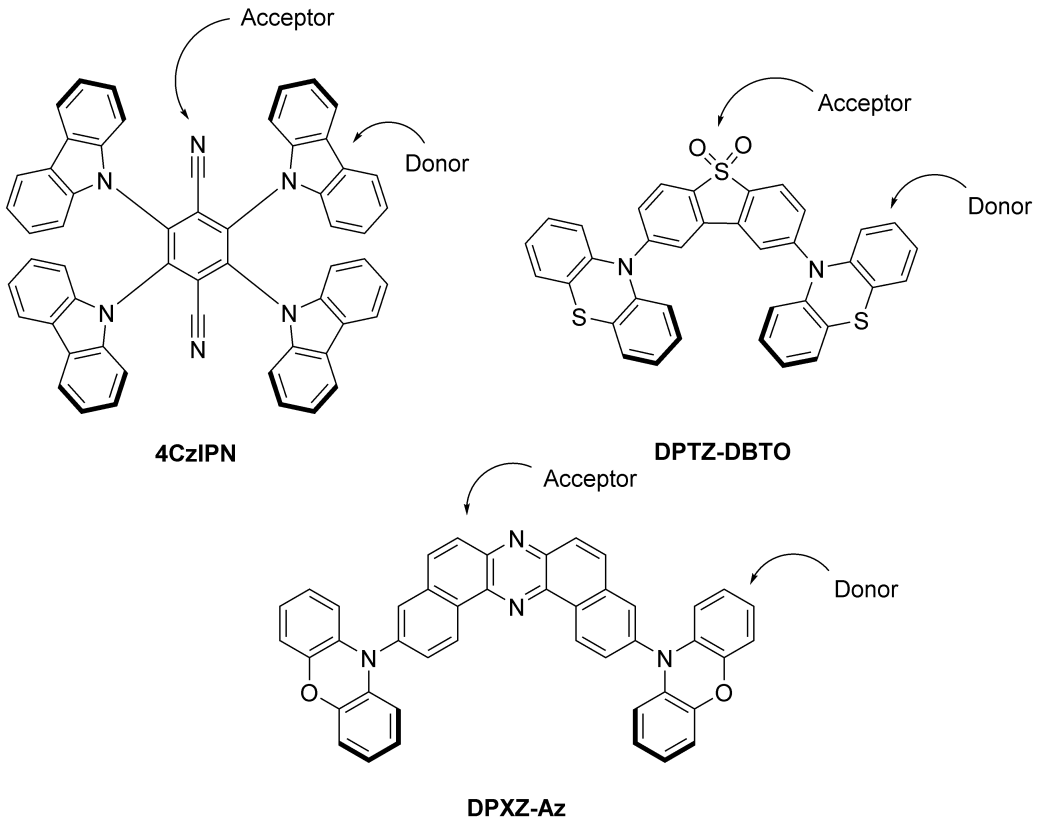

Figure 2.6. Examples of TADF molecules used in OLED. Electron donors and acceptors are indicated with arrows. Note: donors and acceptors never lie in the same plane.

Thermally activated delayed fluorescence molecules have been recognised in recent years as efficient replacements for Pt(II) and Ir(III) complexes. In this case no phosphorescence occurs at room temperature and (typically) no metal is involved. Spin-orbit coupling is obtained by introduction of charge transfer (CT) or (sometimes) nπ* states. However, in this case the aim is not to accelerate phosphorescence lifetime, but to speed-up the exchange between S_1 and T_1 states (**Figure 2.7**). In this case the $T_1 \rightarrow S_1$ transition is always endoenergetic, thus thermal energy will be of vital importance in the process. In fact TADF works accordingly to a Boltzmann process, with the intensity and lifetime of the delayed fluorescence being dependent upon temperature and activation energy. As OLEDs are desired to work at temperatures around 295 K (room temperature), there is a general trend to obtain emitters with negligibly small TADF activation energy as the temperature is generally kept constant.[5,40–42]

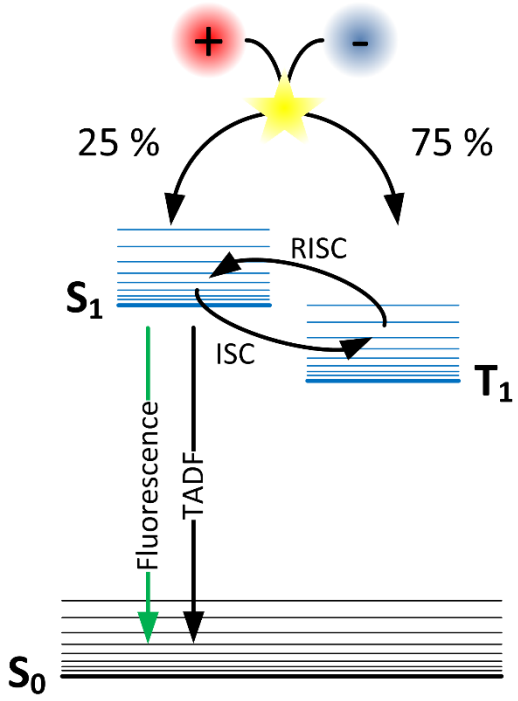

Figure 2.7. TADF emitters in OLED. 25% of initially generated singlet states either directly emit as fluorescence or intersystem cross increasing the triplet population. The whole population of triplet excited states is harvested through endothermic up-conversion to the singlet state (from where the fluorescence emission occurs). This accounts for up to 100 % excited states being harvested in a TADF emitter. Note the cycling between S_1 and T_1 through ISC and RISC may result in a significant population of molecules emitting after up- and down-converting several times.

The harvest of triplet states through the TADF mechanism requires complex processes that are currently described by vibronic spin-orbit coupling (VSOC) model that involves mixing of the CT states with triplet states of localized character, which is responsible for acceleration of the ISC and RISC rates. However, in some conditions hyperfine coupling (HFC) interactions may also be involved in the ISC/RISC mechanism (**Figure 2.8**). It appears the role of HFC interactions are predominant when the local triplet state(s) are energetically too far away from the CT state, and thus are unable to promote LE-CT mixing, thus a direct interaction between ^{1}CT and ^{3}CT through hyperfine coupling is required to promote ISC/RISC. The role of VSOC and HFC are still a matter of debate in the TADF community. In this thesis, the coexistence of the two mechanisms is proposed with HFC and VSOC giving partial contributions to the final effect.[40,41,43]

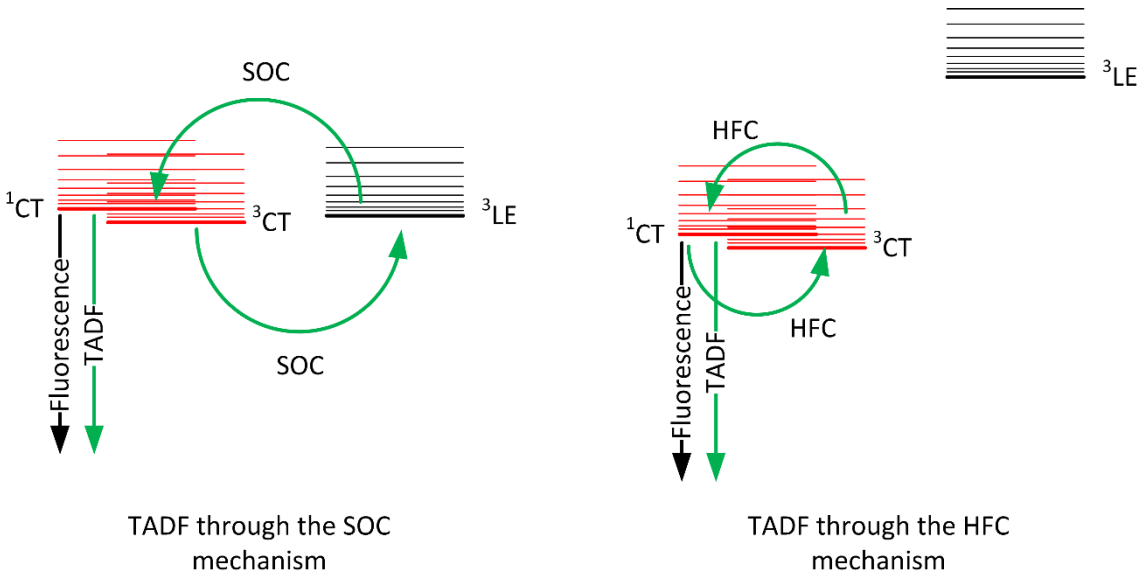

Figure 2.8. Schematic diagram for TADF mechanism: SOC mechanism (left); HFC mechanism (right).

2.7 Types of excited states in π-conjugated molecules and their characteristics

The excited states in organic molecules can be described as mono-(or uni-)molecular and bimolecular. States involving three and more molecules are not typically considered. The unimolecular state, namely *exciton*, can also be described as "*monomer*" in the context of excimer formation, to highlight the fact that an *excimer* involves the interaction between two molecules (excited state dimer). Although the term "*monomer*" is broadly used in literature, author prefers to use the term exciton whenever possible. In excimers, an excited state molecule interacts with an identical molecule existing in the ground state. This leads to molecular orbital mixing, so called "exciton resonance" giving an excited state dimer that does not possess a ground state counterpart.[14,23,44]

Another type of bimolecular excited state is the *exciplex*, sometimes named also "*heteroexcimer*". This is because the principle of *exciplex* formation is identical to formation of excimers. The main difference is that exciplex are formed between two different molecules and involve some degree of charge transfer: one molecule working

as an electron donor and the other as an electron acceptor. The molecules, as typically described in the literature, are bound by electrostatic forces as the donor gives up one electron to the acceptor. Although this seems to be a scientific consensus that donor and acceptor form a sort of an ion pair, the actual degree of charge separation in those excited state complexes remains unclear.[16,18,45]

2.7.1 Exciton

Excitonic states are used commonly in OLEDs and can be observed in virtually all π-conjugated systems. These states can evolve to excimers and exciplexes upon specific conditions as being their precursors. Typically, excitonic emitters are showing narrow photoluminescence spectra as their emission is considered as *local* which relates to the large overlap between the molecular orbitals related to the electron transition. However, for the purpose of this work charge-transfer (CT) emitters based on intramolecular states are also considered as excitonic, even though their behaviour is very often closer related with exciplexes.

In OLEDs, three types of excitonic emitters are used, namely: fluorescent, phosphorescent and delayed fluorescence emitters. These were described in previous sections.[1]

2.7.2 Excimer

Excimeric species are formed as a result of the interaction between two identical molecules of which one is in its electronic excited state. The bond between two molecules (M for the ground state molecule and M* for the excited state molecule) M-M* forms through mixing of the respective frontier molecular orbitals. This is also described using a term excimer resonance. Such behaviour is not limited to organic molecules and is commonly observed in bi-atomic systems, including noble gases were excimers are observed.[46] The bond that is formed is analogous to a covalent bond, but much longer and weaker.[23]

As excimers are bi-molecular species, their occurrence is highly dependent upon molecules' concentration, therefore, in general the exciton and excimer species coexist in varying ratios. Extreme dilutions or high concentrations lead to (nearly) purely excitonic or purely excimeric excited state populations. This leads to a more complicated description of such emitters, not only including quenching phenomena but also excimer/exciton ratios varying as a function of concentration.[47]

Each of the excitonic emitters: fluorescent, TADF or phosphorescent is potentially able to form respective excimers. In general OLED emitters are not based on excimeric species. This due to usually lower photoluminescence quantum yields of excimers when compared with their respective exciton counterparts. However, in the special case of planar metal complexes, such as those formed by Pt(II), the two metal centres of the excimer-forming molecules can couple their orbitals resulting in formation of a MMLCT-like (Metal-Metal-Ligand Charge-Transfer) state that escalates the spin-orbit coupling interaction. This leads to significantly faster radiative rate constants of such excimers making them a very suitable solution for red and NIR emitters, where the non-radiative decay is faster.[30,48] Note that MMLCT state can only exist upon the existence of the metal-metal orbital in the ground state such as it occurs in Pt-Pt dimers. This does not occur in excitons as they do not show any orbital interaction in the ground state. Nevertheless, the excited state of the excimer shows similar experimental characteristics to the excited state dimer which gives grounds to treat both alike.

Phosphorescent excimer emitters are predominantly planar Pt(II) metal complexes (**Figure 2.9**). This is because a flat geometry around the metal centre is necessary for successful metal-metal interactions to occur. On the other hand the metal centres and their electron structure dictate the geometry of a molecule, as described in the Valence Shell Electron Pair Repulsion (VSEPR) model,[49] which makes Ir(III) complexes that show octahedral geometry around the metal centre, unsuitable for MMLCT interaction in the case of excimer formation.

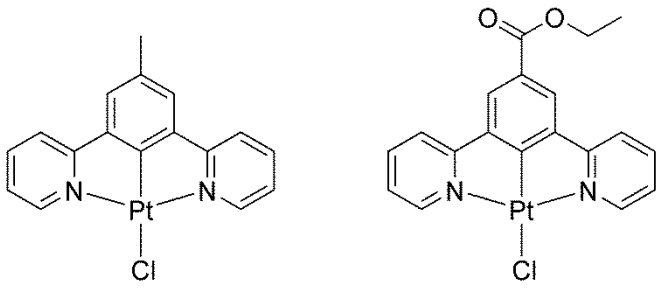

PtL^{1}Cl **PtL^{2}Cl**

Figure 2.9. Excimer-forming planar Pt(II) complexes.[14]

2.7.3 Exciplex

Exciplex emitters are similar to excimer emitters. However, the formation of exciplex states involve some degree of charge transfer between electron donor (D) and electron acceptor (A) species, of which one is in the excited state (does not matter which one). Upon excitation, the donor and acceptor species interact forming a charge transfer state. Although this is usually described as (nearly) complete transfer of the electron, the degree of electron transfer may vary in different donor-acceptor pairs. Exciplexes with small degree of charge transfer are sometimes called heteroexcimers.[16,45,50]

Exciplexes were brought to OLEDs for two main reasons: firstly, they employ electron-rich (usually hole-transporting) and electron-deficient (usually electron-transporting) materials as a blend or bilayer, thus facilitating good charge transport through the device (**Figure 2.10**). Secondly, exciplexes bring charge transfer states into the system, and thus behave similarly to the regular, intramolecular "excitonic" charge transfer molecules, leading to reduced exchange interactions that result on small singlet-triplet energy gaps, which can induce TADF emission. The harvesting of triplet excited states in exciplex forming blends by means of TADF is discussed in this thesis.[51–53]

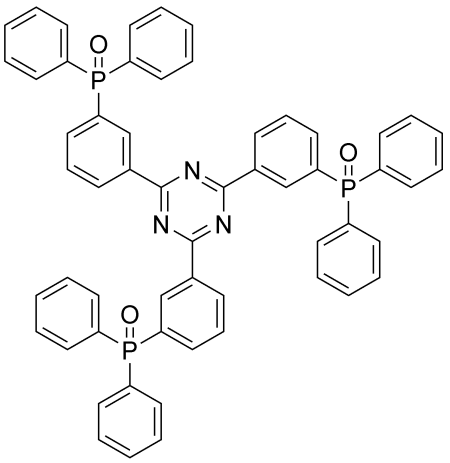

PO-T2T

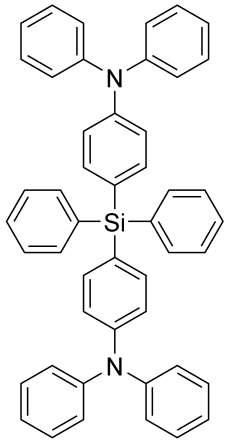

TSBPA

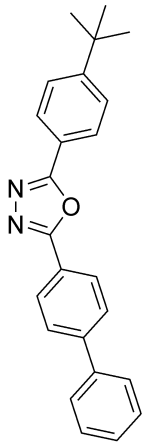

PBD

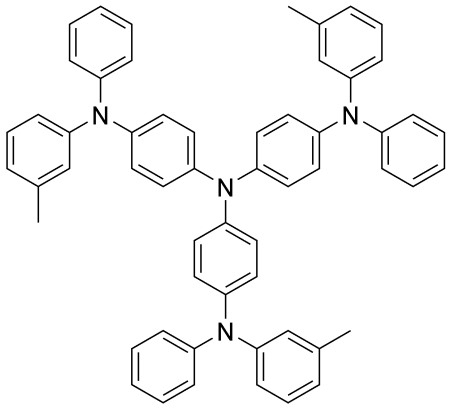

m-MTDATA

Figure 2.10. Examples of exciplex-forming materials: TSBPA:PO-T2T and m-MTDATA:PBD.

3 Experimental

3.1 Sample preparation and storage

3.1.1 Films

Films are prepared either using dropcast/spincoating or vacuum thermal evaporation (VTE). Films obtained with VTE technique are produced in a similar fashion to the OLED devices, see section 3.7. Details on the preparation of thin films by dropcast and spincoating methods are given below.

Dropcast films are prepared by dispensing 100-200 μL of a solution onto a disc substrate placed on a hotplate (optional), where the solvent is left to evaporate in order to obtain a solid film. The solution concentration and temperature at which the solvent is left to evaporate are dependent on the solvent used as depicted in Table 3.1 Note, that the film has to be transparent (amorphous) as opaque films may indicate crystallisation. The films are placed into a vacuum chamber for a period of 1-2 hours to remove residual solvent.

Table 3.1. Summary of conditions of fabrication of dropcast films.

Solvent	**Dissolved solid**	**Hotplate temperature, °C**	**Concentration of main ingredient, mg mL^{-1}**
Toluene	Zeonex 480 (polymer) + dopant	80-90	100
Toluene	Small molecule	80-90	5-10
Chloroform	Small molecule	20-60	5-10

3.1.2 Solutions

Stock solutions in various solvents (i.e. toluene, chloroform, dichloromethane) are prepared at concentrations of 1 mg mL^{-1} or 10^{-3} M and are further diluted to 10^{-5} M for spectroscopic measurements. Note that solutions in solvents that may lead to

degradation, such as chloroform, are considered unstable, thus they are prepared directly before use. In example: easily oxidizing molecules, such as triphenylamine derivatives, may turn brown, green or yellow upon formation of radical/cation radical species. Platinum(II) complexes may react with chloroform upon the presence of oxygen by bonding to the chlorine atoms with formation of platinum(IV) complexes.

3.2 Spectrophotometry

UV-Vis absorption spectra have been obtained using UV-3600 double beam spectrophotometer (Shimadzu). The films for absorption measurements were spin-coated using a similar method as in the OLED fabrication. Always a clean substrate made of the same material (either quartz or sapphire) was used as a blank. Solutions were measured in quartz fluorescence cuvettes using always the same pair of walls throughout all measurements.

3.3 Spectrofluorimetry

Photoluminescence (PL) spectra of films were recorded using FluoroLog fluorescence spectrometer (Jobin Yvon) or a matrix spectrometer QePro (Ocean Optics). The films were produced similarly to the spectrophotometric measurements or by drop cast.

3.4 Time-resolved gated spectroscopy

The working principle of the iCCD cameras is based on the image intensifier, which not only intensifies the incoming light but also works as a shutter (gate). The intensifier consists of a photocathode that is sensitive to a specific spectral range [i.e., ultraviolet (UV), visible, red, and near-infrared (NIR)], a micro-channel plate (MCP), and a phosphor. By changing the photocathode, it is possible to adapt the camera to a specific use. The photocathode converts incoming photons into photoelectrons that are multiplied in the MCP and then hit the phosphor screen generating photons. These photons, through a system of lenses, are focused onto a CCD chip and are converted into an electrical signal.

3.4.1 Control of delay and gate time

To collect time dependent emission spectra throughout the range from 1 ns to 100 ms with sufficient signal-to-noise ratio, the integration (exposure) time increases exponentially along with exponentially increasing the time delay (**Figure 3.1**). This is dictated by the properties of the photoluminescence decay, which follows exponential laws in most systems.

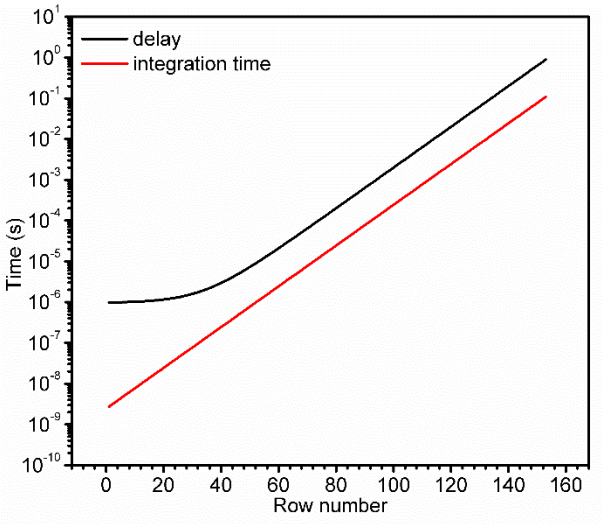

Figure 3.1. Delay and integration time changes in the experimental file used.

3.4.2 Spectral response of the iCCD chip

Spectral response of the iCCD is of vital importance for proper analysis of the recorded emission spectra. In this thesis the spectral response of the camera was investigated in the range from ≈350 – 800 nm using a certified, balanced deuterium-halogen calibration lamp supplied by Avantes. The calibration lamp light has been passed through the optical setup (lenses, spectrograph) to mimic the emission illuminated by a real sample.

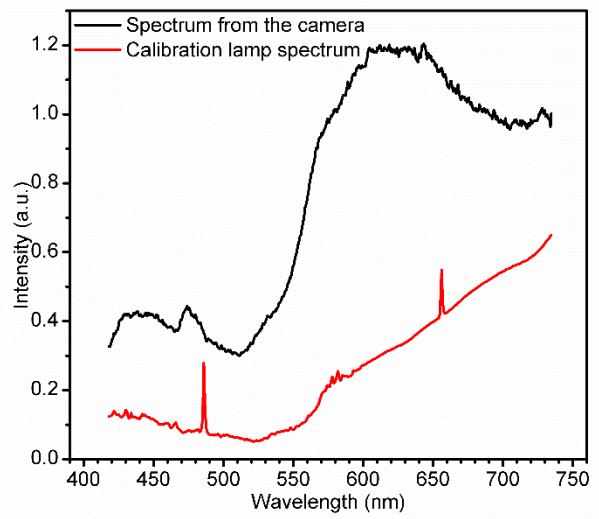

Figure 3.2. Calibration lamp spectrum and iCCD camera spectral response in a selected wavelength range.

The spectral response of the camera is compared with the calibration lamp spectrum (**Figure 3.2**). The ratio between the latter and the former is the calibration curve. Due to the imperfection of the iCCD chip and smaller spectral resolution of the signals than in typical fluorometers, the raw correction curve is affected by high frequency noise. This is unfavourable in practical applications, thus all correction curves are smoothened (**Figure 3.3**).

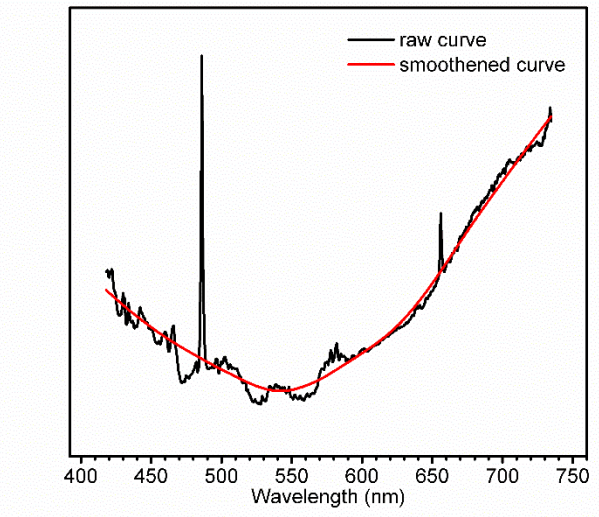

Figure 3.3. Calibration spectrum: before and after smoothing.

3.4.3 Data processing

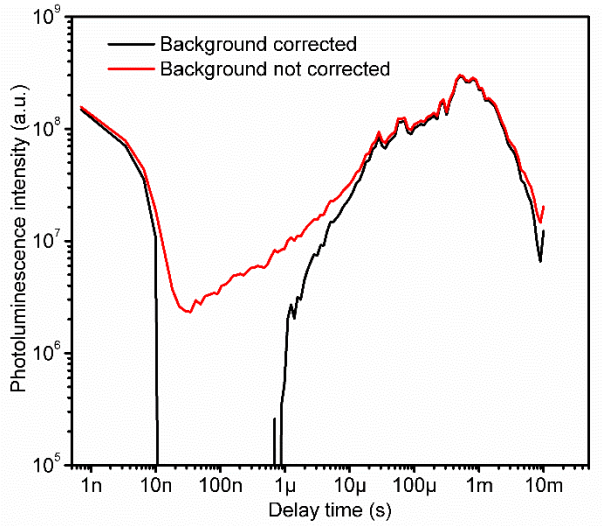

Figure 3.4. Raw photoluminescence spectra integral.

Data processing is of vital importance in the acquisition of "real" time-dependent emission spectra and decays. This is essential to the appropriate interpretation of the results and to obtain good fitting of the decay curves. Data processing involves removing incorrect luminescence background values (Figure 3.4, Figure 3.5), as the underestimation of the background may lead to the appearance of artefacts, such as luminescence decaying as a power law. Other problems that may occur are the occurrence of multiexponential photoluminescence decays that in reality are mono- or biexponential processes. In order to avoid such problems it is advised to manually control the luminescence background when processing spectral data to obtain the photoluminescence transient decays.

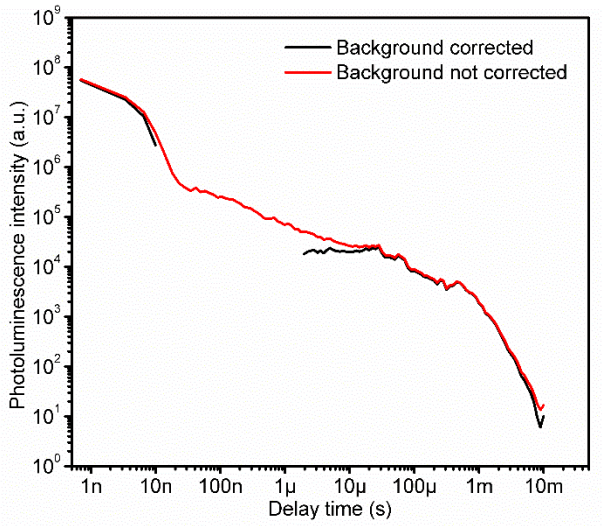

Figure 3.5. Photoluminescence spectra integral divided by the integration time.

3.5 Photoluminescence quantum yield measurements in solid state

The photoluminescence quantum yield (PLQY) of molecules in solid thin films is recorded using an integration sphere, as part of our home-built setup. The sample is placed in a special sample holder suitable for disc samples. Any kind of sample can be characterised: drop cast, spin coat or thermally deposited. The PLQY is estimated from the integral intensities of the sample emission and excitation light that is absorbed by the sample. For strongly emitting samples PLQY can be determined with accuracies close to 5%, however for weaker emissions the accuracy of the measurement may be lower, and the error could be in the order of 10-20% or even larger, depending on the circumstances. In a typical situation it is enough to record the emission spectrum obtained with a blank (empty sphere) and with the sample directly excited (3.1). The measurement can be further corrected for reabsorption of the emitted light, and multi-excitations, which usually gives a correction factor on the order of 2-5%. In this case a third measurement is performed, with a sample inside the sphere but positioned in a way that is not directly in the excitation beam, see (3.2) and (3.3).[54]

Equations used in the PLQY determination are given below:

$$\Phi = \frac{P_1}{L_0 - L_1} \tag{3.1}$$

$$\Phi = \frac{P_1 - (1 - A)P_2}{L_0 A} \tag{3.2}$$

$$\mathrm{A} = 1 - \frac{L_1}{L_2} \tag{3.3}$$

Where: Φ – photoluminescence quantum yield; A – sample absorbance, a.u. ; L_0 – integral excitation intensity (empty sphere), a.u.; L_1 – integral excitation intensity (sample in beam), a.u.; L_2 – integral excitation intensity (sample out of beam), a.u.; P_1 – integral photoluminescence intensity (sample in beam), a.u.; P_2 – integral photoluminescence intensity (sample out of beam), a.u.;

3.6 Photoluminescence quantum yield measurements in a solution

The PLQY determination in solution is made using a gradient method described in the literature.[9,55] It is based on recording fluorescence intensity (defined as the integrated area under the emission spectrum) as a function of the compound's absorbance at the excitation wavelength. This is done for all samples of unknown PLQY and also for a compound of known PLQY (so-called "standard"). The gradients (slope of the intensity-absorbance relation) are then compared, and corrected for differences in refractive indices, when standard and sample are measured in different solvents. The following equation is used:

$$\Phi_x = \Phi_s \frac{Grad_x}{Grad_s} \frac{{\eta_x}^2}{{\eta_s}^2} \quad (3.4)$$

Where: $Grad_x$ – gradient (slope) of the linear fit of the relation between photoluminescence intensity and absorbance of an unknown sample, a.u.; $Grad_s$ – gradient of the linear fit of the relation between photoluminescence intensity and absorbance of a standard, a.u.; η_x, η_s – refractive indices of the solutions of unknown sample and standard, respectively, a.u.

In principle the equation above can be used with any number of experimental data points (including only one point with an assumption that at zero absorbance the integral fluorescence is zero), however the precision rises dramatically with the number of points that are collected and it is recommended to use at least 4-5 of these to allow a good fit. Note the PLQY measurement is only valid in the concentration range where the relation is linear, and the compound's absorbance at the excitation wavelength should be kept below 0.1. Excitation wavelengths for standard and sample must be identical.

In general, the choice of a standard is dictated by the absorption/emission regions of the samples, in a way that the standard absorbs and emits in similar regions. Also, a good practice is to adjust the standard PLQY to the expected PLQY of the sample, i.e. samples with low PLQY should be measured against a low PLQY standard, thus using one, universal standard for all samples is in principle incorrect.

3.7 Fabrication of OLED devices by vacuum thermal evaporation

OLEDs are often fabricated using vacuum thermal evaporation. The principle of this method is based on the sublimation/evaporation of solid substances upon heating them in vacuum, which is used by two main reasons: 1) allows for low evaporation temperature of a given substance, so that even a small partial vapour pressure is achieved at relatively low temperatures, avoiding compound degradation; 2) the mean free path of the molecules is larger than the vertical dimension of the evaporation

chamber – this allows the molecules to travel in straight paths, giving even thickness of the evaporated film.

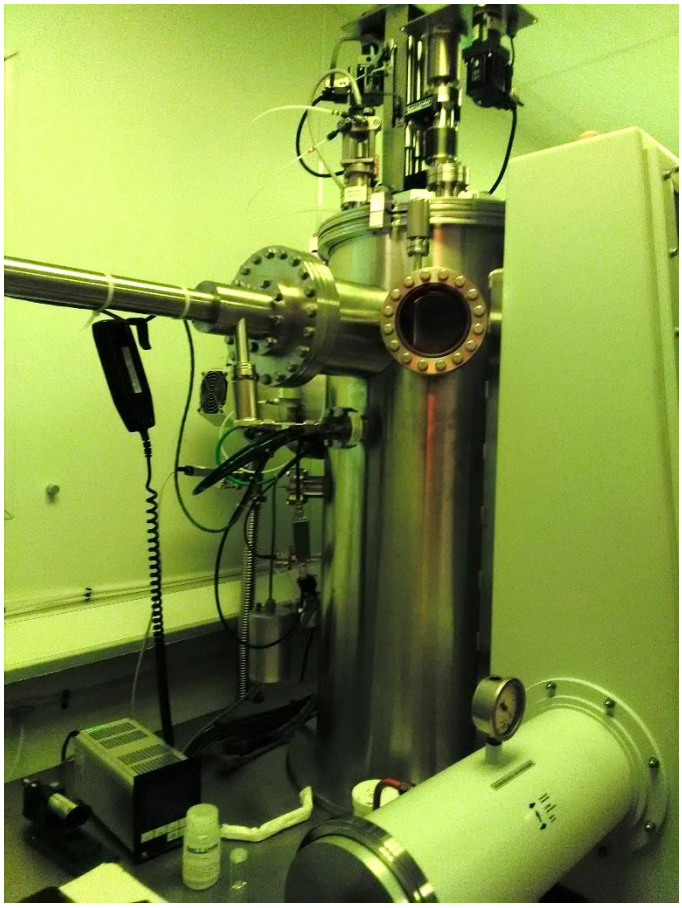

Figure 3.6. Kurt J. Lesker Spectros II evaporator.

The evaporator comprises a number of organic evaporation sources that are heated with electrical coils. The material is placed in tall alumina crucibles. These are called low temperature sources, as they can be heated up to ≈500 °C which is sufficient for most organic materials, but insufficient for most inorganic, such as metal salts, oxides and elemental metals. For this reason special thermal sources that can be heated up to higher temperatures, which are equipped with specialized heaters and use either alumina or boron nitride crucibles, are used to evaporate materials like lithium fluoride, aluminium or molybdenum(VI) oxide.

Figure 3.7. Encapsulated OLED devices.

A typical OLED comprises several organic layers topped with an aluminium layer, deposited on top of an ultrathin (≈1 nm) layer of a good electron injection material, usually a lithium or caesium salt. These two layers are used as the electron injection electrode. The aluminium electrodes are deposited perpendicularly to the Indium Tin Oxide (ITO) stripes that are used as the transparent electrode, therefore the access to the aluminium electrical contacts are available on the left and right side of the device, while the ITO (anode) is accessible from the top and the bottom (**Figure 3.7**, **Figure 3.8**).

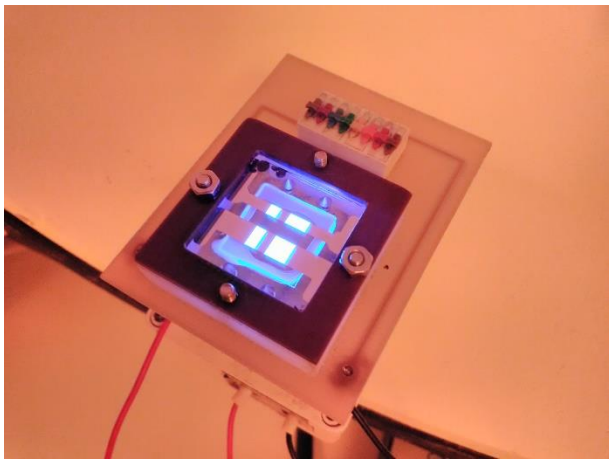

Figure 3.8. Blue OLED device at work.

3.7.1 Hybrid dry and wet technique

The principal difference between this and the vacuum thermal evaporation method is that here the device is fabricated using (several) solution-processed layers (typically spin coated). These include the PEDOT:PSS (hole injection), hole transport/electron blocking, and emissive layers. More sophisticated methods can also use a solution processed electron transport layer, but commonly the top electrode is evaporated. In this work the electron transport and electron injection materials, and the aluminium cathode are thermally evaporated while other layers are solution-processed.

The films are spin coated at various speeds and from different solution concentrations. Three basic formulations were used in this work for the solution-processed layers: toluene-based, chloroform-based, and chlorobenzene-based. The first is used as default, and the latter are used only if the molecules used for OLED fabrication are insufficiently soluble in toluene.

Toluene-based formulation comprises the host molecule(s) at concentration of 10 mg mL^{-1} with 5-10% w/w emissive molecule doped into it. The solubility of the dopant molecule required for fabrication of a device is in the range of 0.5-1 mg mL^{-1} (or higher) in toluene. The solution is then spun at 2500 RPM to give a 25-35 nm film. The film is annealed at 50°C for 10 min.

Chloroform-based formulation based on a mixture of 95% chloroform (v/v) and 5% (v/v) chlorobenzene. In this case a 20 mg mL^{-1} solution of the host molecule(s) is used with 1-30% (w/w) doping, giving a solubility range of 0.2-6 mg mL^{-1} in chloroform + chlorobenzene (95:5 v/v). The solution is then spun at 5000 RPM to give a 55-75 nm film. The film is annealed at 50°C for 10 min.

Chlorobenzene-based formulation based on pure chlorobenzene. In this case a 20 mg mL^{-1} solution of the host molecule(s) is used with 1-5% (w/w) doping, giving a solubility range of 0.2-1 mg mL^{-1} in chlorobenzene. The solution is then spun at 2000 RPM to give 60-80 nm film. The film is annealed at 120°C for 20 min.

In addition a hole transport/electron blocking layer that is spun from a 3 mg mL^{-1} high molecular weight poly(*N*-vinylcarbazole) ($M=10^6$ Da) solution in a chloroform-based formulation is also used. The solution is spun at 8000 RPM to give a 10 nm film. The film is annealed at 50°C for 10 min.

PEDOT:PSS (HIL 1.3N) is spun at 10000 RPM to give a 45 nm film. The film is annealed at 200°C for 3 min.

3.8 Cyclic voltammetry measurements

Cyclic voltammetry measurements were performed according to previously established procedures,[56,57] using a platinum (Pt) working disc with 1 mm^2 area as the working electrode, a Pt wire as an auxiliary electrode and a silver (Ag) wire as the pseudo-reference electrode. Preparation of the silver pseudo-reference electrode requires formation of a thin layer of silver salts on the surface of the electrode. In order to do this a silver wire is polished with sandpaper and then placed into concentrated hydrochloric acid with access to air for few days. Then the electrode is washed with water and acetone and is ready to use after drying. The pseudo-reference electrode is calibrated against ferrocene which is performed every time a new sample is analysed. Typical value of the half wave oxidation potential of ferrocene should be 0.4-0.6V and strongly depends upon geometry of the cell.

The cyclic voltammetry analysis is performed in dichloromethane solution, using tetrabutylammonium tetrafluoroborate as a supporting electrolyte. The measurement is performed in nitrogen-purged solutions at 0.05 V s^{-1} scan rate. Exemplary results can be found in the figure below (**Figure 3.9**).

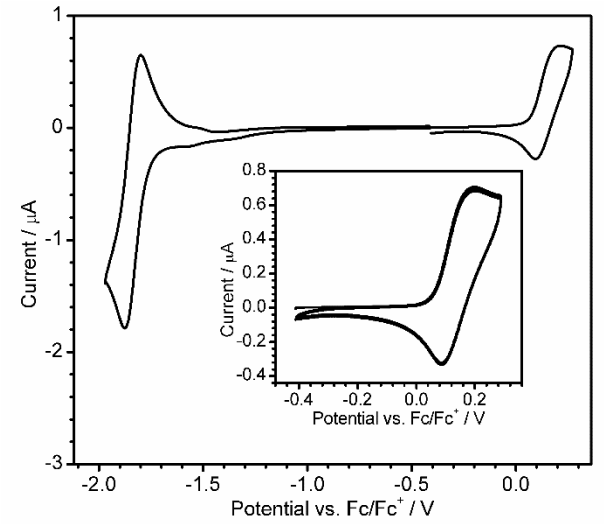

Figure 3.9. Example of a cyclic voltammogram of an organic molecule recorded in 0.1 M BuN_4BF_4 in dichloromethane.

4 Investigation of triplet harvesting in excitonic states of purely organic materials

The material contained within this chapter has been published as:

P. Pander, A. Swist, R. Motyka, J. Soloducho, F. B. Dias and P. Data, *J. Mater. Chem. C*, 2018, **6**, 5434–5443.

4.1 Introduction

Acridones have been known as biologically active compounds[58–61], however recently they were used as electron-accepting units in several donor-acceptor and donor-acceptor-donor systems.[62–64] The acridone moiety is particularly interesting because it contains an electron-accepting carbonyl group (>C=O) along with an electron-donating nitrogen atom bearing lone pair electrons. Acridone is also a commercially available[65] building block, and thus a good candidate to use as a cheap and commonly available acceptor in OLED emitters.[66] On the other hand, phenothiazine which is very popular in drug applications, i.e. in chlorpromazine[67] and carbazole, among others, have recently become popular as donors in donor-acceptor molecules for the design of TADF emitters.[40,68–70]

Thermally activated delayed fluorescent (TADF) OLED materials have been widely investigated in recent years by several groups around the globe.[7,41,45,71–81] A typical TADF emitter does not contain rare precious metals, however metal-based TADF emitters, such as copper complexes have also been widely investigated in recent years.[34,38,82,83]

Almost all TADF emitters are donor-acceptor type structures showing broad charge transfer (CT) emission. TADF by itself does not require the formation of CT states. However, the use of CT states is a very simple way to decrease the singlet-triplet energy gap and thus promote efficient triplet harvesting. While TADF emitters are excellent in their triplet harvesting properties, the presence of CT states negatively impacts on the colour purity of most TADF-OLEDs. Basically the electroluminescence of TADF molecules is broad, with a large full width at half maximum (FWHM). TADF molecules formed with donor-acceptor units with weak CT character are interesting as they may result in materials showing narrow, resolved emission even in OLED host, but still being able to harvest triplets.

It is also worth to point out that not only TADF emitters may supersede metal complexes in OLED applications, as also metal-free organic room temperature phosphors show a promising perspective for their future application in the field.[84–87] Metal-free organic phosphors show a substantial triplet formation yield along with a relatively fast triplet radiative decay, similarly to metal complexes, but without heavy metal content. If non-radiative decay is successfully suppressed, the organic phosphors can exhibit long-lived emission.[87,88]

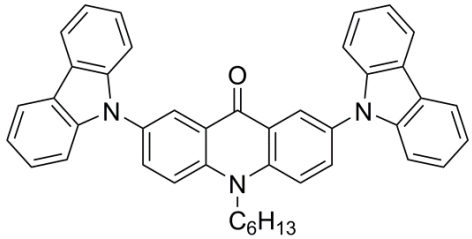

1

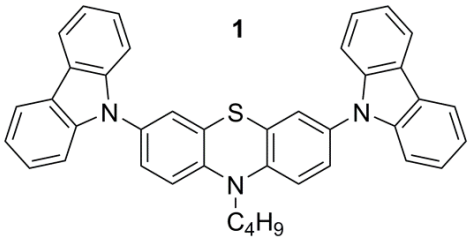

2

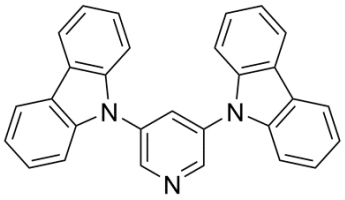

BCbmPy

Figure 4.1. Investigated molecules. Note: the molecules have been synthesized by A. Świst and R. Motyka.

This chapter is focused on the investigation of the photophysical properties of a novel TADF emitter carrying acridone as the electron-acceptor unit, and two carbazole donors in a D-A-D configuration. A molecule with high triplet energy **BCbmPy** is used as the host material. The TADF properties of the acridone D-A-D molecule **1** are compared with molecule **2**, an RTP emitter designed with no CT states, i.e. in a D-D-D configuration (**Figure 4.1**). Prototype OLED devices with these compounds are fabricated and characterized. By comparing the photophysics and device performance of these molecules the similarities and dissimilarities between the TADF and RTP mechanisms are highlighted, helping to better understand how these two mechanisms can be optimized to maximize luminescence efficiency.

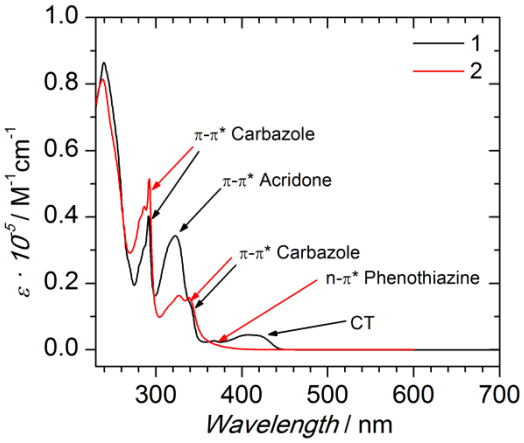

*Figure 4.2. Absorption spectra of **1** and **2** in methylcyclohexane (MCH).*

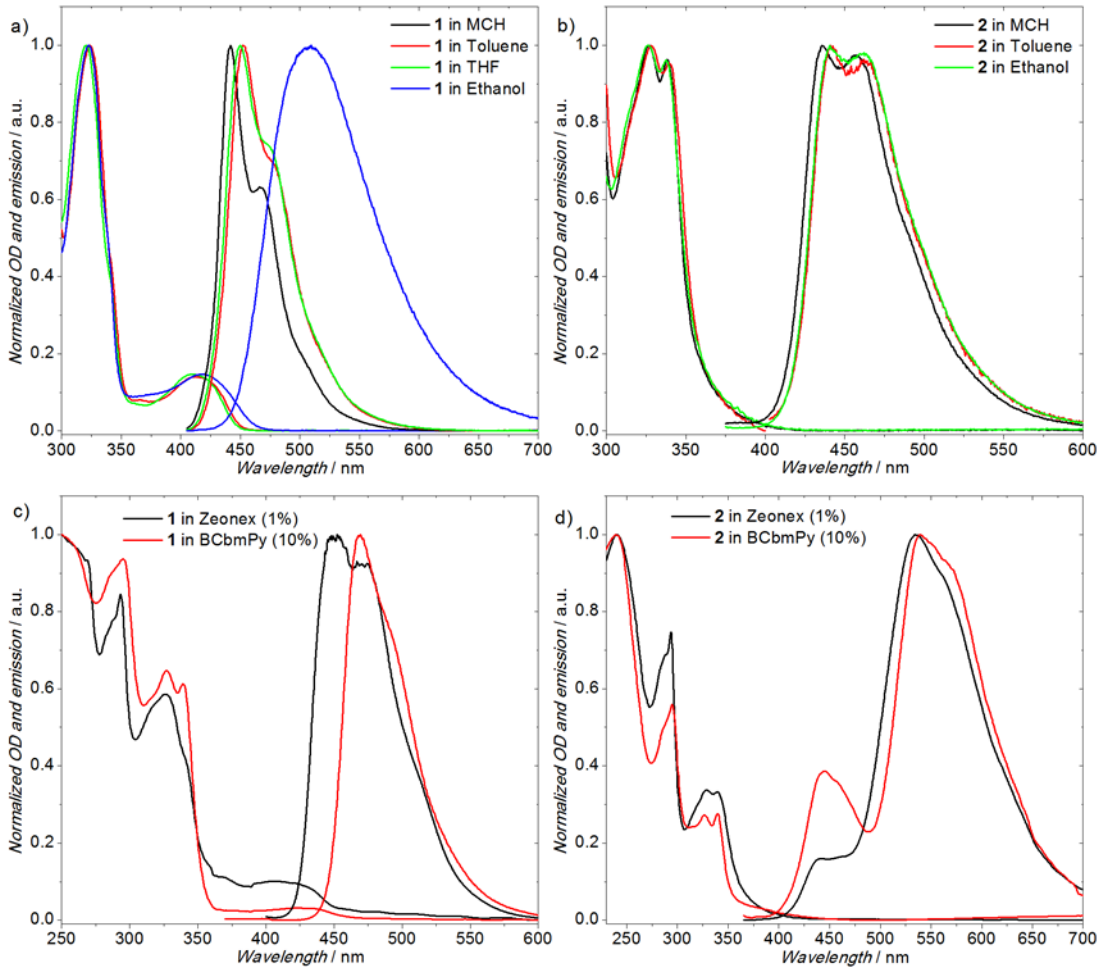

Figure 4.3. Photoluminescence and absorption spectra of 1 and 2 in various solvents and matrices: a), b) UV-Vis and fluorescence spectra in solution; c), d) UV-Vis and fluorescence spectra in solid films. λ_{ex} = 355 nm.

4.2 Results and discussion

4.2.1 Steady state photophysics

Starting from the basic photophysical behaviour of molecules **1** and **2**, the presented systems are first investigated in solution. In **1** four absorption bands can be observed in methylcyclohexane (MCH) solution (**Figure 4.2**): λ_{max} = 239 nm ($\varepsilon \approx 9 \times 10^4$ M^{-1} cm^{-1}), λ_{max} = 291 nm ($\varepsilon \approx 4 \times 10^4$ M^{-1} cm^{-1}), λ_{max} = 322 nm ($\varepsilon \approx 3 \times 10^4$ M^{-1} cm^{-1}), λ_{max} = 407 nm ($\varepsilon \approx 5 \times 10^3$ M^{-1} cm^{-1}). The three first absorption bands are associated with π-π* transitions due to their high absorption coefficients. The fourth λ_{max} = 407 nm is associated with a transition forbidden by geometry, such as CT, due to a small absorption coefficient. A series of absorption spectra recorded in solvents of different polarity show that this low-energy absorption band red-shifts upon increasing dielectric constant of the solvent (**Figure 4.3**). The band maximum shifts from 407 nm in MCH to 418 nm in ethanol, whereas the *onset* shifts from 445 nm to 465 nm, respectively. This is a typical behaviour for a charge-transfer absorption band, where excited state with large dipole moment is stabilized by the molecules of the polar solvent. Interestingly, only one absorption band, λ_{max} = 291 nm can clearly be attributed to the carbazole moiety, whereas none of the unsubstituted acridone[64] absorption bands can be directly found in the absorption of **1**. However, the absorption bands related to each subunit of **1** can be indicated using literature data[89] and by comparison with the absorption spectrum of compound **2** (**Figure 4.2**).

The emission of **1** is clearly well resolved in methylcyclohexane, toluene, and tetrahydrofuran, but in ethanol the fluorescence spectrum is broad and featureless (**Figure 4.3**). The lowest singlet excited state in **1** has a weak charge transfer character. Therefore, the fluorescence spectrum remains resolved in non-polar or moderately-polar solvents, where no large displacements have to occur when adjusting the molecular structure of the compound in the excited state, due to the interactions between the excited state dipole moment and the weak dipole moment of solvent molecules. This

results in a hybrid local and charge transfer state, CT + LE, or so-called weak CT state. In highly polar solvents, such as ethanol, the interactions between the excited state dipole moment and the dipole moment of the solvent molecules are stronger, resulting in larger structural changes giving rise to a typical broad CT emission. This is consistent with previous, calculation-based observations of a hybrid local and charge transfer character of HOMO-LUMO transition in **1**.[90]

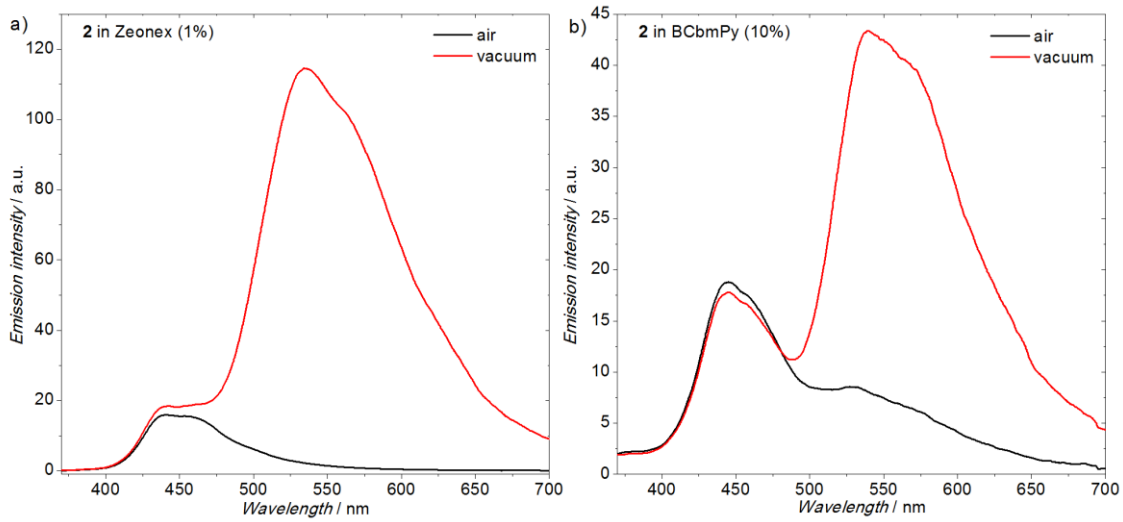

Figure 4.4 Steady-state photoluminescence spectra of 2 doped in Zeonex (drop-cast) and BCbmPy (co-evaporation) recorded in air and in a vacuum. λ_{ex} = 355 nm.

Absorption bands of **2** in MCH (**Figure 4.2**) are: λ_{max} = 238 nm ($\varepsilon \approx 8 \cdot 10^4$ M^{-1} cm^{-1}), λ_{max} = 292 nm ($\varepsilon \approx 5 \cdot 10^4$ M^{-1} cm^{-1}), characteristic absorption band of carbazole with two maxima λ_{max} = 326, 338 nm ($\varepsilon \approx 1.5 \cdot 10^4$ M^{-1} cm^{-1}), and a shoulder λ_{sh} = 345-407 nm ($\varepsilon < 8 \cdot 10^3$ M^{-1} cm^{-1}). The first two absorption bands have the same origin as respective absorption bands in **1** and should therefore be attributed to π-π* transitions, whereas the latter is a shoulder of the n-π* transition in phenothiazine. The emission spectrum of **2**, which shows blue fluorescence, hardly changes with solvent polarity, suggesting no involvement of charge transfer states. Such a behaviour is a result of its D-D-D structure where neither carbazole nor phenothiazine show pronounced acceptor properties.

In fact, both compounds show blue fluorescence in diluted toluene solution. Interestingly, they show significantly different photoluminescence quantum yield (PLQY). PLQY in a degassed toluene solution of **1** (Φ_{PL} = 0.79) is much larger than the value obtained for **2** (Φ_{PL} = 0.05). Phenothiazine moiety induces high triplet formation yield in **2** which therefore leads to a low Φ_{PL} in solution. Interestingly, photoluminescence of **2** when doped in polymer films (Φ_{PL} = 0.05) in the presence of air is very similar to toluene solution. However, in vacuum the emission spectrum reveals additional band which in turn causes a rise in the photoluminescence quantum yield (Φ_{PL} = 0.58) (**Figure 4.4**). Oxygen normally quenches long-lived triplet states, therefore, the difference in photoluminescence between air and vacuum is due to long-lived phosphorescence emission from the triplet state.

A typical TADF emitter with a D-A-D structure usually shows featureless, pure CT emission when dispersed in OLED matrix[7,41,73–77]. However, **1** shows a narrow, resolved photoluminescence in OLED host (**Figure 4.3c**), suggesting a mixed CT + LE nature of the emissive state. The full width at half maximum FWHM = 54 nm, is among the smallest values for TADF molecules. Identical FWHM and spectrum is observed in electroluminescence (see below **Figure 4.10a**, Dev 1). It is worth of notice that comparably small FWHM values are only observed for deep blue emission, i.e. FWHM = 46 nm.[91] The appearance of narrower spectra in deep blue emitters are due to their wavelength scale representation, instead of being presented in cm^{-1}, this causes the spectra in the blue to appear narrower and being broader in red. To avoid this effect the emission spectra should be presented in cm^{-1} or eV which would be more correct in comparing different colour emissions (such as blue and red). Unfortunately, FWHM values are usually reported in nanometers, and this convention is followed here. In the light of that conclusion it is stated that FWHM of 54 nm is extremely low in comparison with typical values observed in the range of sky-blue TADF emitters (100-150 nm[92–95]). The low FWHM value is important for luminescence colour purity in practical

applications, such as in Samsung Galaxy cell phones.[17] It is worth to note that some recently developed TADF emitters, exploiting B-N multiple resonance effect[17] show much narrower emission with FWHM = 28 nm. However, those emitters are based in a completely different molecular design, and present no CT properties. Unfortunately, although the devices showed high EQE of 20.2% the maximum device brightness was extremely low, and the OLEDs have also shown a pronounced efficiency roll-off.

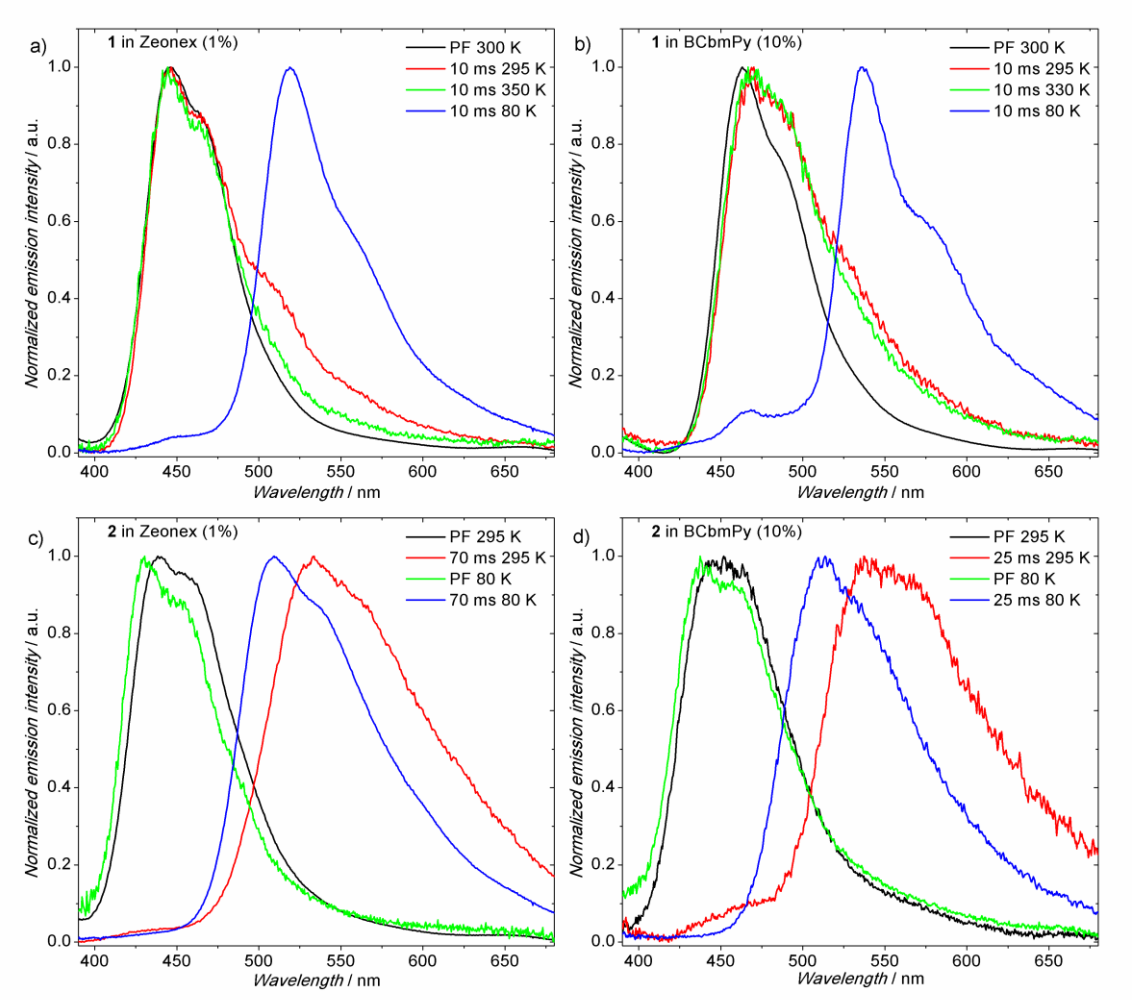

Figure 4.5 Time-resolved photoluminescence spectra of the molecules doped into Zeonex and BCbmPy. All spectra recorded either in vacuum (at 295 K and above) or in nitrogen (at 80 K). λ_{ex} *= 355 nm.*

Compound **1** shows similarly narrow photoluminescence spectrum in toluene, Zeonex and in the OLED host. This means **1** is not significantly susceptible to the polarity/polarizability of the environment as a result of its weak CT nature. However, **1**

shows a batochromic shift in the OLED host respective to toluene and Zeonex. In toluene solution or in Zeonex **1** shows blue fluorescence with a maximum at ≈ 450 nm, while the emission in **BCbmPy** is red shifted with a maximum at ≈ 470 nm. The reasons for the red shift are given later in the text. Therefore, only in a strong polar medium, such as ethanol, the charge transfer state in **1** gives a broad, featureless emission spectrum.

As mentioned previously, molecule **2** is a room temperature phosphor (**Figure 4.4**, **Figure 4.5**). The phosphorescence of molecule **2** is so strong that it constitutes 91 % of the total emission in Zeonex and over 60 % in **BCbmPy**, at room temperature in a vacuum. This suggests that the triplet formation yield of **2** is very high as for a metal-free molecule. Due to the relatively low oxygen permeability of **BCbmPy** a trace of phosphorescence is visible even in air (**Figure 4.4**). However, more intense phosphorescence is observed in Zeonex than in **BCbmPy** due to a better suppression of non-radiative decay in the polymer film.

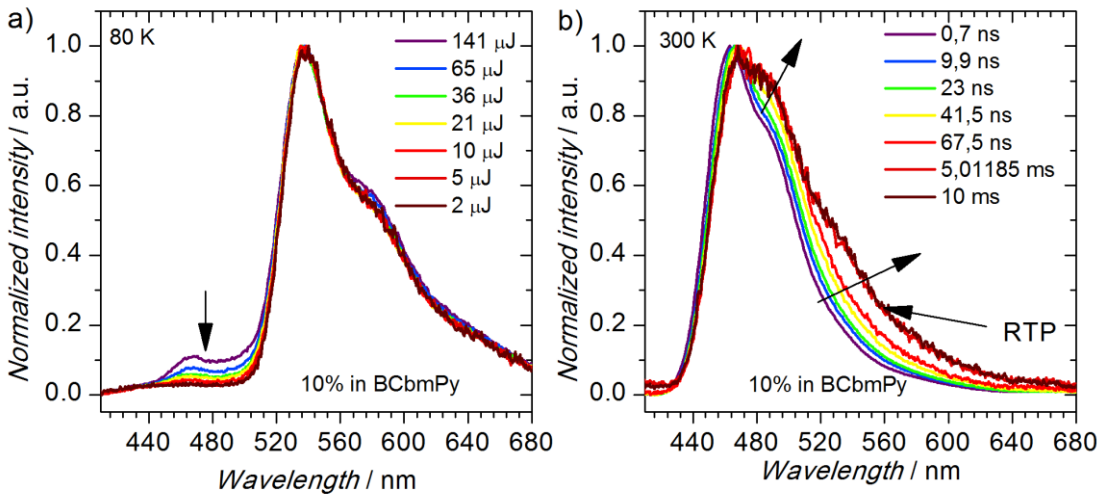

*Figure 4.6. a) Phosphorescence spectra of **1** at 80 K recorded using various laser pulse energy (delay 10 ms). Delayed fluorescence shows supralinear laser pulse dependence which indicates triplet-triplet annihilation; b) Time-resolved spectra of **1** recorded at 295 K. The emission spectrum gradually loses the vibronic structure with time delay. RTP – room temperature phosphorescence. λ_{ex} = 355 nm.*

4.2.2 Time-resolved photoluminescence study

Time-resolved spectra of **1** in solid state (**Figure 4.5 a** and **b**) stay in agreement with the steady-state spectra presented above. Prompt and delayed fluorescence in Zeonex do overlap. Not only TADF is observed, but RTP is present also and forms a shoulder on the red edge of the spectrum. No changes to the prompt and delayed fluorescence spectra can be observed over time, therefore, the system is rather not complicated to describe. Singlet S_1 = 2.96 eV and triplet T_1 = 2.54 eV energy can be derived from prompt fluorescence and phosphorescence *onsets*. From these values a large singlet-triplet splitting $\Delta E_{S\text{-}T}$ = 0.42 eV is calculated. Interestingly, **1** doped in **BCbmPy** exhibits more complicated photophysical behaviour. As the prompt and delayed fluorescence spectra do not overlap perfectly. This suggests that prompt and delayed fluorescence originate from molecules with different surrounding or conformation. Most probably, delayed fluorescence originates mostly from molecules with more relaxed conformation, whereas prompt fluorescence originates from molecules prior to their conformational relaxation **(Figure 4.6b)**. Other observations are rather similar to the features seen in Zeonex films. Also here an insignificant contribution of room

temperature phosphorescence can be observed. Interestingly, even at temperatures as low as 80 K, there is still a small portion of delayed fluorescence present as a shoulder between 450-500 nm (**Figure 4.5b**). Laser fluence experiment (**Figure 4.6a**) indicates clearly a supralinear power dependence, therefore, this emission can be attributed mostly to triplet-triplet annihilation (TTA). It is clear that at higher doping concentrations (such as 10% in solid film) molecules are relatively close to each other and are able to diffuse and collide even at low temperature. Such interaction of two molecules in triplet state leads to triplet fusion.

Phosphorescence spectra of **1** observed in Zeonex and in **BCbmPy** show identical vibronic structure (**Figure 4.5 a** and **b**). Interestingly, the triplet emission in the OLED host is visibly red-shifted, consistent with a lower triplet energy of **1** in **BCbmPy** than in Zeonex. Both singlet S_1 = 2.83 eV and triplet T_1 = 2.43 eV energy in **BCbmPy** doped film are shifted by almost the same value, relative to Zeonex, resulting in nearly identical $\Delta E_{S\text{-}T}$ = 0.40 eV as in the polymer. Simultaneous decrease in S_1 and T_1 energy in **BCbmPy** is related most likely with a π-π interaction between the host and the dopant. It affects both the triplet and the singlet as both bear a partially delocalized character. This interaction is not present in Zeonex as this polymer is fully aliphatic. Taking into account experimental errors in the determination of singlet-triplet energy gaps, usually in a range of ± 0.03-0.05 eV, the two singlet-triplet energy gaps (in Zeonex and **BCbmPy**) can be considered as identical within the margin of error. The presence of both RTP and TADF is due to a large singlet-triplet energy gap in this material $\Delta E_{ST} \approx 0.4$ eV. Basically, the reverse intersystem crossing rate (RISC) is not fast enough to efficiently compete with the decay rates of the triplet state, hence harvest all triplet states by the way of TADF, therefore, a small population of molecules are able to decay radiatively from the triplet state by emitting phosphorescence.

The time-resolved spectra of **2** when dispersed in Zeonex (**Figure 4.5 c** and **d**) show the energy of singlet S_1 = 3.02 eV and triplet T_1 = 2.56 eV states to be close to the

respective values observed in **1**. Moreover, the singlet-triplet energy splitting is also similar, $\Delta E_{S\text{-}T}$ = 0.46 eV. It is worth to note that in both hosts (Zeonex and **BCbmPy**) the phosphorescence of **2** is blue-shifted at low temperature. This suggests that **2** shows some kind of rigidochromism. The molecular motion causing this effect is considered to be related to fast interconversion between *H*-intra and *H*-extra like conformers of phenothiazine or with thermal oscillation of the most stable conformer.[41,43,69,96,97] It has been observed that the existence of these two conformers may affect the photophysics of phenothiazine based molecules,[41,69,97] however in non-substituted phenothiazines, where the barrier for conformer interconversion is relatively small, this is unlikely.[96] In **2**, the *N*-n-butyl group causes insignificant steric hindrance, thus insufficient to pose any energy barrier large enough to obstruct the *H*-intra / *H*-extra interconversion. In such a situation the high energy conformer is quickly interconverted to the most stable counterpart and thus only one ground state conformer is observed in the photophysics.

By comparing **1** and **2** it is not entirely clear why **1** shows TADF emission whereas **2** does not. Why in **1** the phosphorescence at room temperature is very weak, but in **2** it is much stronger than fluorescence? Why is there any TADF in **1** at all? One can argue that the reason is the difference between the nature of the respective emissive states: In **1** this is a CT+LE state, whereas in **2** it is a nπ* state. In **1** the CT+LE singlet is coupled to a partially delocalized $^3\pi\pi^*$ state located on acridone, giving optimal conditions for RISC, except for the large $\Delta E_{S\text{-}T}$. In **2**, however, the triplet state is located on the phenothiazine moiety. This is confirmed by previous literature data (i.e. the carbazole triplet is located at ca. 3 eV),[98,99] and the phosphorescence of **2** is also very similar in energy and spectrum shape to the phosphorescence of phenothiazine itself[40], however slightly red-shifted, probably due to the effect of substitution with carbazole units, which causes partial delocalization of the triplet state, as in molecule **1** (described below).

It can be concluded from the steady-state spectra (**Figure 4.3 b** and **d**) that the singlet state in **2** has major nπ* character. On the other hand the triplet state is short-lived, and thus indicates nπ* character too. Obviously, a direct transition between ^{1}nπ* and ^{3}nπ* should be very slow due to their similar orbital geometry, therefore there must be at least one upper ^{3}ππ* state which acts as an intermediate energy level to explain fast intersystem crossing in **2**. A potential candidate for such a state is a carbazole ^{3}ππ* local triplet state. This is not a typical configuration for a TADF emitter (i.e. no CT states), however, high phosphorescence intensity and low fluorescence quantum yield suggest a moderate spin-orbit coupling and relatively fast intersystem crossing (ISC). RISC and ISC represent in fact the same spin flip process occurring between the low S_1 level and higher energy levels of the triplet state, which only proceed in different directions. Therefore, if ISC is fast, RISC should be too. However, the total RISC rate should include an endothermic step where the low energy triplet states are first upconverted to higher energy vibrational levels, from where they are converted in singlet states. The entire rate may thus be limited by a significant energy barrier, and follows an Arrhenius relation. For this reason RISC is slower than ISC.

In terms of their possible TADF properties the molecule general structural concept, such as D-A-D or D-D-D, is almost irrelevant. It is much easier to design a donor-acceptor TADF emitter than a non-CT TADF emitter. However, TADF properties have been found in numerous molecules with no D-A or D-A-D structures and with no CT states, including D-D-D systems.[78,100–102]

The prompt fluorescence of **1** is very strong and relatively long-lived which suggests slow ISC. Large singlet-triplet splitting on the other hand implies also a slow RISC rate, in fact the delayed fluorescence lifetime reaches 26 ms in Zeonex (**Table 1**). This is surprisingly comparable with the RTP lifetime of **2** which is 23 ± 1 ms. Speaking about RTP and TADF lifetimes at room temperature it is important to consider also the phosphorescence lifetime at low temperature (i.e. 80 K), to observe the effects of

reduced thermal energy and suppression of non-radiative decay. The long phosphorescence lifetime of **1** at 80 K 0.5 ± 0.2 s, indicates a slow non-radiative deactivation rate of the triplet state at low temperature and that the T_1 radiative rate is also slow. On the other hand, the phosphorescence lifetime of **2** at 80 K is only 38 ± 2 ms. From these observations we conclude that the slow deactivation of the triplet state directly to the ground state in **1** is the main cause for the observation of TADF in this compound. This is because a long-lived triplet state gives enough time for RISC to compete and being able to harvest triplet states. On the other hand, **2** shows a short phosphorescence lifetime, even at 80 K, which indicates the triplet state is significantly affected by a fast radiative rate, and probably also by a faster non-radiative rate. This fast deactivation of the triplet state directly to ground state in 2 quenches TADF as the slow RISC rate (due to a large ΔE_{S-T} = 0.46 eV) is not able to compete and very little (if any) triplets are harvested through TADF. Therefore, these results show that a lowest $^3\pi\pi^*$ triplet state is more suitable for a TADF emitter than a $^3n\pi^*$ if the ΔE_{S-T} is large.

It is therefore concluded that TADF emitters with wide energy gap, like **1**, must exhibit long phosphorescence lifetime, which is significantly longer than the TADF lifetime at room temperature. On the other hand, short phosphorescence lifetime at room temperature kills TADF as efficient RISC in these conditions is impossible. These observations, however may seem obvious, are rarely taken into account. As TADF and RTP are in fact two sides of the same coin it is not only the ΔE_{S-T} which makes the material a TADF emitter or not. The lifetime of the triplet state at room temperature is also very important.

What in fact really decides whether a molecule is suitable to be a TADF or a RTP emitter is the competition between the RISC rate constant and the rate constants that control the deactivation of the lowest triplet state directly to the ground state (including both radiative and non-radiative decay). A long triplet state lifetime allows TADF while a short lifetime quenches the triplet population and stops TADF. In most situations, a

short triplet lifetime is caused by a fast non-radiative decay and in this situation, the molecule will show only fluorescence. However, if the short triplet lifetime is due to a fast radiative decay, RTP is observed as it is in **2**. All emitters with sufficiently long phosphorescence lifetime in relation to the RISC rate have potential to show TADF, regardless of their structure.

It has been also observed that the phosphorescence spectra of D-A or D-A-D molecules with limited D-A conjugation are identical or very similar to the phosphorescence spectrum of their donor or acceptor units.[40,77,103] However, in some cases the phosphorescence of such molecules is red-shifted or distorted in relation to the phosphorescence of the donor or acceptor units due to the effect of partial conjugation.[77,104] Carbazole phosphorescence has already been described in literature[98,99] and its triplet level energy is roughly equal to 3 eV. Moreover, the vibronic structure of the carbazole phosphorescence spectrum is different from that observed in **1** (**Figure 4.5 a** and **b**). On the other hand, the phosphorescence of *N*-substituted acridone-containing molecules[63] has a similar vibronic structure to the spectrum reported in this work. The triplet energy of those molecules is also higher (2.8 eV) than in the case presented here (2.54 eV). It appears therefore that the electron-donating carbazole moieties in **1** red-shift the acridone phosphorescence spectrum (i.e. decrease the triplet state energy) by conjugating with the central acridone unit. The impact of *C*-substitution, so extended conjugation, on acridone is also observed in the absorption spectrum. Absorption bands of 2,6-substituted[64] acridone derivatives are completely different from the characteristic absorption bands seen in the unsubstituted acridone, which are not visible in the spectra of the derivatives. This shows that 2,6-substituted acridone (with carbazole, in this work, or diphenylamine[64]) is partially conjugated with its attached donor moieties.

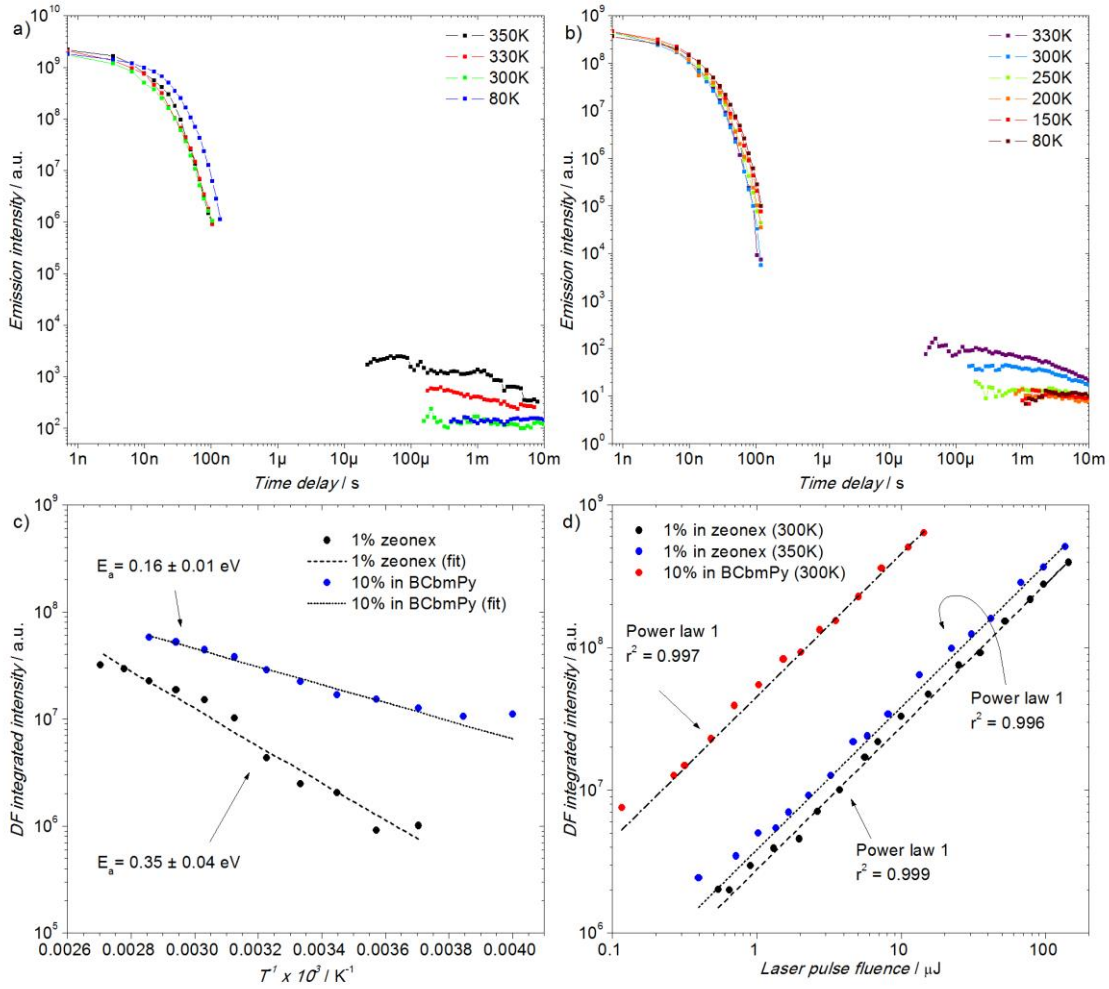

Figure 4.7 a), b) Photoluminescence decay of 1 at various temperatures; c) d) Temperature and power dependence of 1 emission in Zeonex and BCbmPy. λ_{ex} = 355 nm.

Delayed fluorescence of **1** shows clear temperature dependence in both Zeonex and **BCbmPy** matrices (**Figure 4.7 a**, **b**, **c**). Interestingly, the effect of temperature on the decay profile seems to be negligible below 250K. This behaviour is caused by the phosphorescence emission, which increases in intensity at low temperatures. As expected, the prompt fluorescence in either host is almost not affected by the temperature change, and shows similar lifetime, close to 10 ns, in all hosts. On the other hand, the lifetime of the delayed fluorescence is remarkably long: 26.8 ± 0.7 ms in Zeonex and 10.2 ± 0.5 ms in the OLED host. This is also a result of the large singlet-triplet energy splitting which results in a slow RISC rate. The power dependence of the

delayed fluorescence in both matrices is shown in **Figure 4.7d**. A linear dependence is clearly observed in both cases, indicating that the TADF mechanism is dominant at room temperature. Additionally, the power dependence experiment was performed also at 350 K in Zeonex matrix, showing that the mechanism remains unchanged.

The temperature dependence of the delayed fluorescence in **1** is especially interesting (**Figure 4.7 a**, **b**, **c**). **1** in Zeonex shows TADF activation energy E_a = 0.35 ± 0.04 eV which is within the experimental error identical to the value of ΔE_{ST}. Interestingly, **1** behaves differently in **BCbmPy** host as the activation energy is reduced to only 0.16±0.01 eV which is much lower than the ΔE_{ST} = 0.40 eV recorded in this case. The reduced activation energy of **1** in **BCbmPy** explains the high OLED EQE (**Figure 4.10**). The divergence between E_a and ΔE_{ST}, however typical, has not been fully explained yet. One possible explanation is a specific alignment of upper triplet states, which couple with both T_1 and S_1, reducing the actual size of the energy barrier.[74]

*Table 4.1 Spectroscopic properties of **1** and **2** in zeonex and toluene.*

Comp.	**Matrix / solvent**	**λ_{abs}, nm[a]**	**λ_{em}, nm[b]**	**Φ_{PL} [c]**	**τ_{PF}, ns[d]**	**τ_{DF}, ms[e]**	**τ_{PH}, ms[f]**	**S_1 / T_1, eV[g]**	**ΔE_{ST}, eV[h]**
1	toluene	323, 413	469	0.79	14 ± 2	-	-	-	-
	Zeonex	293, 326, 407	451	0.95	9.1 ± 0.6	26.8 ± 0.7	500 ± 200 (80 K)	2.96 / 2.54	0.42
2	toluene	327, 338	441, 462	0.05	1.81 ± 0.02	-	-	-	-
	Zeonex	241, 294, 328, 340	439, 532	0.58	1.96 ± 0.02	-	23 ± 1 (295 K) 38 ± 2 (80 K)	3.02 / 2.56	0.46

[a] absorption maxima; [b] photoluminescence maxima; [c] Φ_{PL} photoluminescence quantum yield in specified solvent/matrix in oxygen-free conditions; [d] prompt fluorescence lifetime; [e] delayed fluorescence lifetime; [f] phosphorescence lifetime; [g] singlet and triplet energy; [h] singlet-triplet energy splitting.

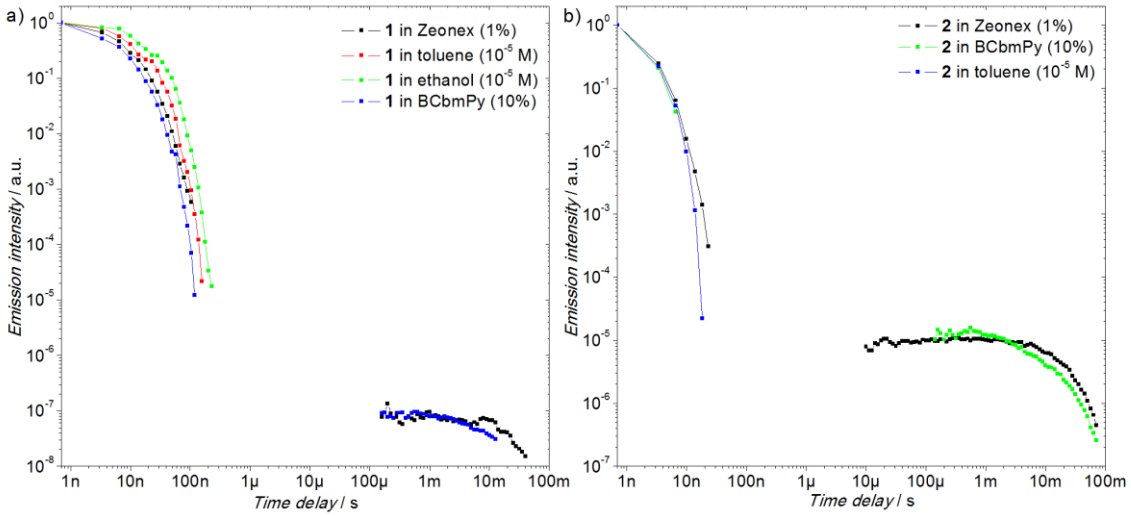

Figure 4.8 Photoluminescence decay of 1 and 2 in various matrices and solvents at room temperature. λ_{ex} = 355 nm.

The photoluminescence decays of **1** and **2** are very similar in both Zeonex and **BCbmPy**. However, in **BCbmPy** the E_a is reduced for **1**, so this improves its performance in the OLED host relative to Zeonex. Both hosts are relatively rigid, thus they effectively suppress non-radiative decay. As expected, the delayed fluorescence in **1** and RTP in **2** can only be observed in solid films (**Figure 4.8**). In solutions, the emitter-solvent interactions, such as collisions, deactivate the triplet excited state, therefore no TADF, or RTP, can be observed. This is because the radiative lifetime of these molecules is very long, thus intermolecular collisions are able to quench long-lived triplet states well before they undergo a radiative transition or RISC.

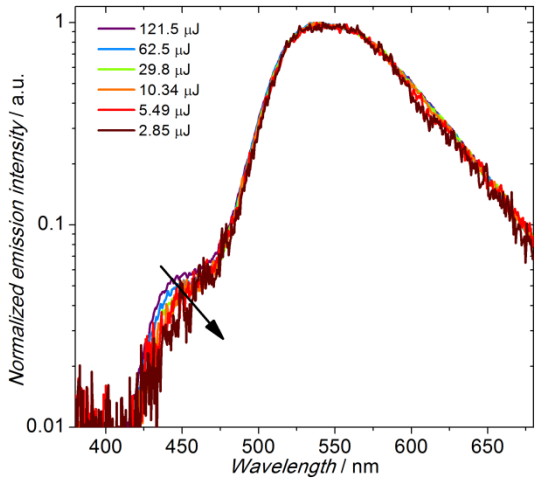

Figure 4.9. Phosphorescence spectra of 2 10% in BCbmPy recorded at various laser pulse energy. A tail at ca. 450 nm decreases at small powers indicating supralinear power dependence, which suggests triplet-triplet annihilation. λ_{ex} *= 355 nm.*

The prompt fluorescence lifetime of **1** in toluene solution (τ = 14 ± 2 ns) is slightly larger than in the solid state (τ = 9.1 ± 0.6 ns in Zeonex, τ = 9.3 ± 0.4 ns in BCbmPy). Even longer lifetime τ = 18 ± 2 ns is observed in ethanol solution, where the emission has purely CT character.

On the other hand, **2** shows short-lived fluorescence both in Zeonex and toluene (1.81 ± 0.02 ns and 1.96 ± 0.02 ns, respectively), which is due to a fast intersystem crossing. Phosphorescence of **2** in Zeonex has a lifetime of only 23 ± 1 ms, which increases at 80 K to 38 ± 2 ms. Such a short phosphorescence lifetime confirms a strong nπ* character to the triplet state and moderate spin-orbit coupling.

In both doped **BCbmPy** films weak triplet-triplet annihilation (TTA) is observed (**Figure 4.9**). This is likely associated with the higher doping concentration used in **BCbmPy** (10 %) compared to Zeonex (1 %) where this phenomenon does not appear. In **BCbmPy** films doped with **1** the TTA emission is observed only at low temperatures (**Figure 4.6a**) as at RT, the TADF dominates.

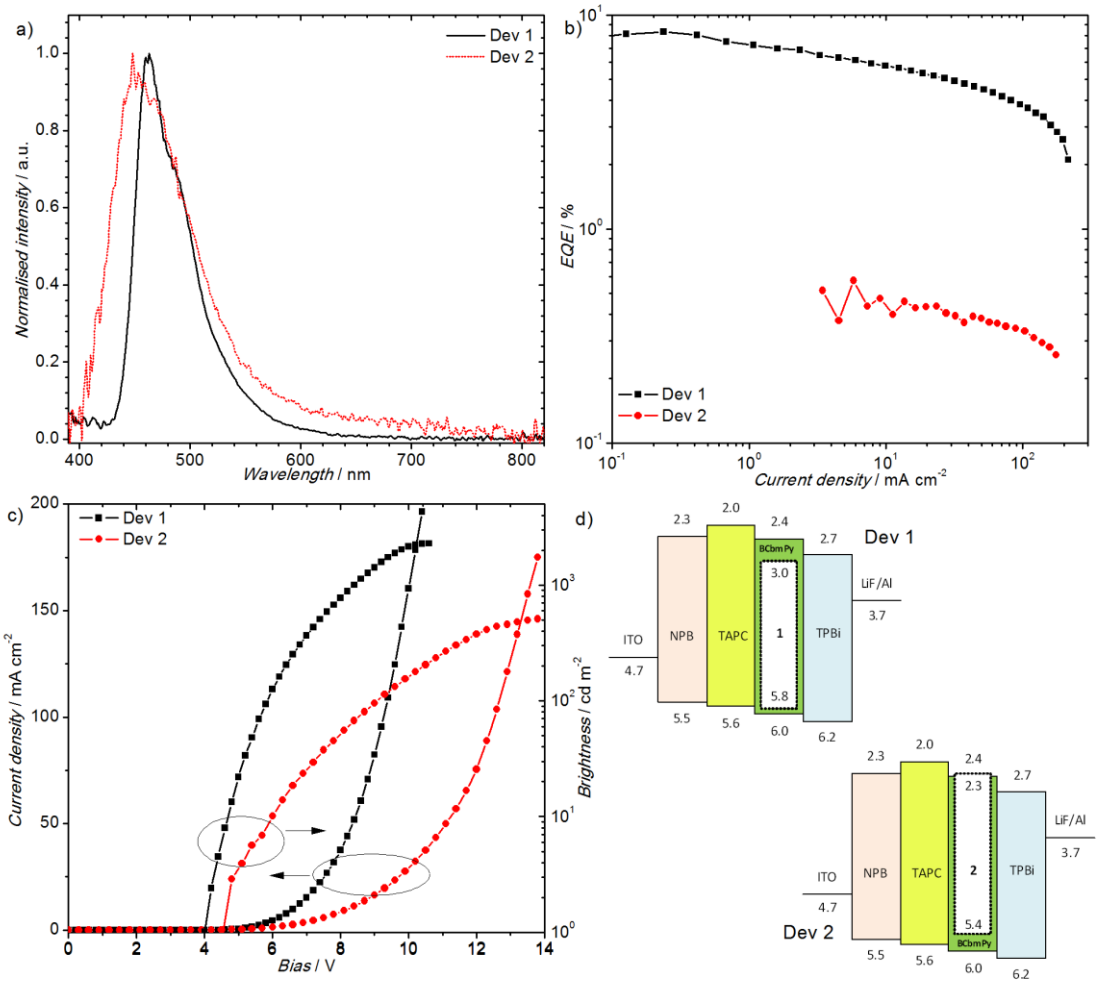

Figure 4.10 Characteristics of OLED devices fabricated using emitters and host presented in this work: a) electroluminescence spectra; b) EQE – current density characteristics; c) current density / brightness – voltage characteristics; d) schematic of device structures. Note: device 1 has been fabricated and characterised by P. Data.

4.2.3 OLED devices

OLED devices were fabricated with **1** and **2** as dopants (**Figure 4.10**). In order to confine the hole and electron in the emitting layer, thus maximizing the chances for charge recombination, a structure of ITO/NPB (40 nm)/TAPC (10 nm)/BCbmPy co 10% dopant (20 nm)/TPBi (60 nm)/LiF (1 nm)/Al(100 nm) was used. The devices show turn on voltage of 4 V (dopant **1**) and 4.6 V (dopant **2**) at 1 cd m^{-2}. The efficiency of devices is dictated by the Φ_{PL} of the respective dopant. High EQE of 8.2 % in Dev 1 is due to triplet harvesting due to TADF. It is worth to note the narrow electroluminescence spectrum of Dev 1 with small FWHM = 53 nm, one of the smallest

values among D-A or D-A-D TADF emitters. Dev 2, in fact, should also benefit from triplet harvesting in molecule **2**, at least by TTA or by emission of phosphorescence. Unfortunately phosphorescence is not observed, likely due to operative triplet-quenching processes, i.e. TTA or triplet-polaron annihilation, that are promoted by the long-lived phosphorescence. As a result the maximal EQE of the device reaches only 0.5 %. High triplet formation yield of **2** in the presence of triplet quenching processes results in small EQE as all of the triplet states remain non-emissive.

4.3 Conclusions

Two molecules with very similar and large ΔE_{ST} but absolutely different properties have been investigated. It was found that the reason for molecule **1** to be a TADF emitter and the **2** a RTP emitter lies in the difference of their triplet lifetime due to their different radiative rate constants. Therefore, the triplet state lifetime determines the performance of the TADF emitter, as well as the ΔE_{ST}. A good TADF emitter must show a triplet lifetime that is long enough to allow the RISC rate to compete with the rate of triplet decay to the ground-state. Molecule **2** shows prominent phosphorescent properties, with very high (90 %) phosphorescence contribution at room temperature due to its high triplet radiative rate constant.

The phosphorescent molecule **2** performs in a device with just 0.5 % EQE and with only the fluorescence band being visible in the electroluminescence spectrum. On the other hand, the TADF emitter **1** gave an efficient device with 8.2 % EQE and well-resolved, narrow electroluminescence with FWHM = 53 nm, which is an exceptionally low value for a TADF emitter. The device was also much brighter than the previously reported by Hatakeyama,[17] with FWHM = 28 nm, established by using multiple resonance effects in a TADF emitter. The design of new, efficient TADF emitters with narrow emission spectrum is an inevitable development pathway in the field, especially if the materials are meant to be used for display applications. This work presents a novel blue emitter

with narrow electroluminescence spectrum based on an acridone acceptor used in D-A-D configuration for the first time to obtain TADF.

5 Investigation of triplet harvesting in excitonic states of platinum metal complexes

The material contained within this chapter has been published as:

P. Pander, R. Bulmer, R. Martinscroft, S. Thompson, F. W. Lewis, T. J. Penfold, F. B. Dias and V. N. Kozhevnikov, *Inorg. Chem.*, 2018, **57**, 3825–3832.

5.1 Introduction

Upon discovery of the new class of OLED emitters – TADF's – the fate of the metal complexes seemed to be determined.[5] However, as they remain a very promising option for orange, red and NIR emission they are still being intensively researched.[14,37,105–107] Platinum(II) and iridium(III) metal complexes have found a profound role in vacuum-deposited and solution-processed OLEDs due to short phosphorescence lifetimes and high PLQY. Although Pt(II) and Ir(III) are the most common, the luminescent complexes are not only limited to them as metals such as copper, gold or silver can also be used.[39,108,109] Due to mixing of the *d* orbital of the metal centre with π-orbital(s) of the ligand(s) a strong spin-orbit coupling effect is produced and therefore the direct transition from the T_1 state to the ground S_0 state, which is forbidden by spin, becomes partially allowed. Similarly it does happen to the $S_1 \rightarrow T_1$ transition, thus upon light excitation intersystem crossing in such systems is usually virtually 100% efficient and very fast (<1 ns). Finally, such metal complexes typically show short phosphorescence lifetimes and any fluorescence emission arising from the system is highly unlikely.[105,106] These properties make them suitable for OLEDs as, firstly, they are able to harvest both the 25% of singlets and 75% of triplets effectively as electrophosphorescence, and secondly, they do it showing a short-lived phosphorescence (usually ~ μs lifetime).

Short-lived phosphorescence allows reducing effects of electroluminescence-quenching processes that affect efficiency and roll-off.

In this chapter newly synthesized ONNO (indication of coordinating centres, O-oxygen, N-nitrogen) tetradentate (so that one ligand bounds the metal centre with four coordinating centres altogether) complexes are studied. Small modifications affecting their solubility and emission colour have been made to the structure of the ligands. In this chapter platinum(II) complexes are investigated as exciton yellow-green/orange OLED emitters. The work shows how potentially insignificant changes to the structure of the molecules affect their solubility and luminescent properties.

In order to aim for low-cost OLED fabrication methods, techniques such as inkjet or slot-die printing are preferred. Optimization of these methods for a specific material is usually very complicated, therefore preliminary tests and research is performed using spin-coated devices. Owing to the good solubility of these complexes in chlorinated solvents, they can be used to produce cost-efficient solution-processed OLEDs.

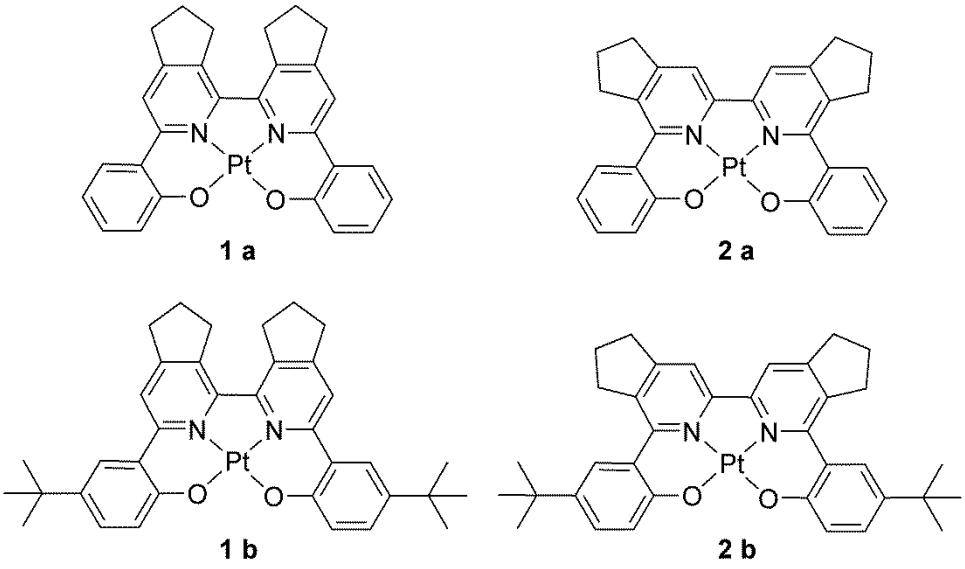

Figure 5.1. Structures of Pt(II) complexes characterised in this work. Note: the molecules have been synthesized by the group of V. N. Kozhevnikov.

5.2 Results and discussion

5.2.1 Solution state photophysics

Small changes in the ligand structure between **1** and **2** cause noticeable differences in the properties of the complexes. For example, in toluene solution, **2a,** which is an isomer of **1a** differing only by the position of the cyclopentene ring, has a more blue-shifted emission spectrum relative to **1a**. A similar trend is observed in **1b** and **2b**.

The photoluminescence spectra in solution (**Figure 5.2a**) are nearly featureless and relatively broad, but when dispersed in a rigid and non-polar polymer (Zeonex), the spectra show more resolved vibronic structure (**Figure 5.2c**). Interestingly, the phosphorescence spectra of each pair of analogues in Zeonex (**1a** and **1b**, **2a** and **2b**) are nearly identical, although they differ in solution. This indicates that the difference in the emission colour of *tert*-butylated and non-substituted analogues is mostly a result of additional vibrational/rotational modes in *tert*-butylated molecules and the electron-donating effect of this group is less important.

At 77 K all four complexes display well resolved, blue-shifted emission (relatively to their room temperature emissions). In all cases the 0-0 transition is the strongest in the spectrum. Within each group of complexes (**1a** and **1b**, **2a** and **2b**), the low temperature phosphorescence spectra show a very similar shape with identical vibronic structure, but the analogues with *tert*-butyl groups (**1b**, **2b**) give more red-shifted spectra in comparison with their counterparts **1a** and **2a**. This is in fact an indication that the electronic effect of the *tert*-butyl group is significative. In general, a notable rigidochromism is observed in these complexes showing that the molecules are susceptible to intramolecular motion and interactions at room temperature. In both series, the introduction of the *tert*-butyl group reduces the luminescence quantum yield, Φ_{PL}, which is probably due to the larger number of vibrational/rotational modes present. Molecules with cyclopentene rings on the outer periphery of the bipyridine moiety (**2a**, **2b**) show larger Φ_{PL} than that of the corresponding isomers (**1a, 1b**).

This argument is supported by the phosphorescence lifetime measurements. In toluene solution, **2a** shows the longest phosphorescence lifetime, whereas **1b** shows the shortest. Smaller phosphorescence time constants in **1b** and **2b** are also found compared to their corresponding analogues **1a** and **2a**. We attribute the shorter phosphorescence lifetime of **1b** and **2b** relative to their analogues **1a** and **2b** to the increased non-radiative decay. All decay profiles recorded in toluene are perfectly monoexponential as shown in **Figure 5.2b**. The photophysical properties of the complexes **1a**, **1b**, **2a** and **2b** are summarized in **Table 5.1**.

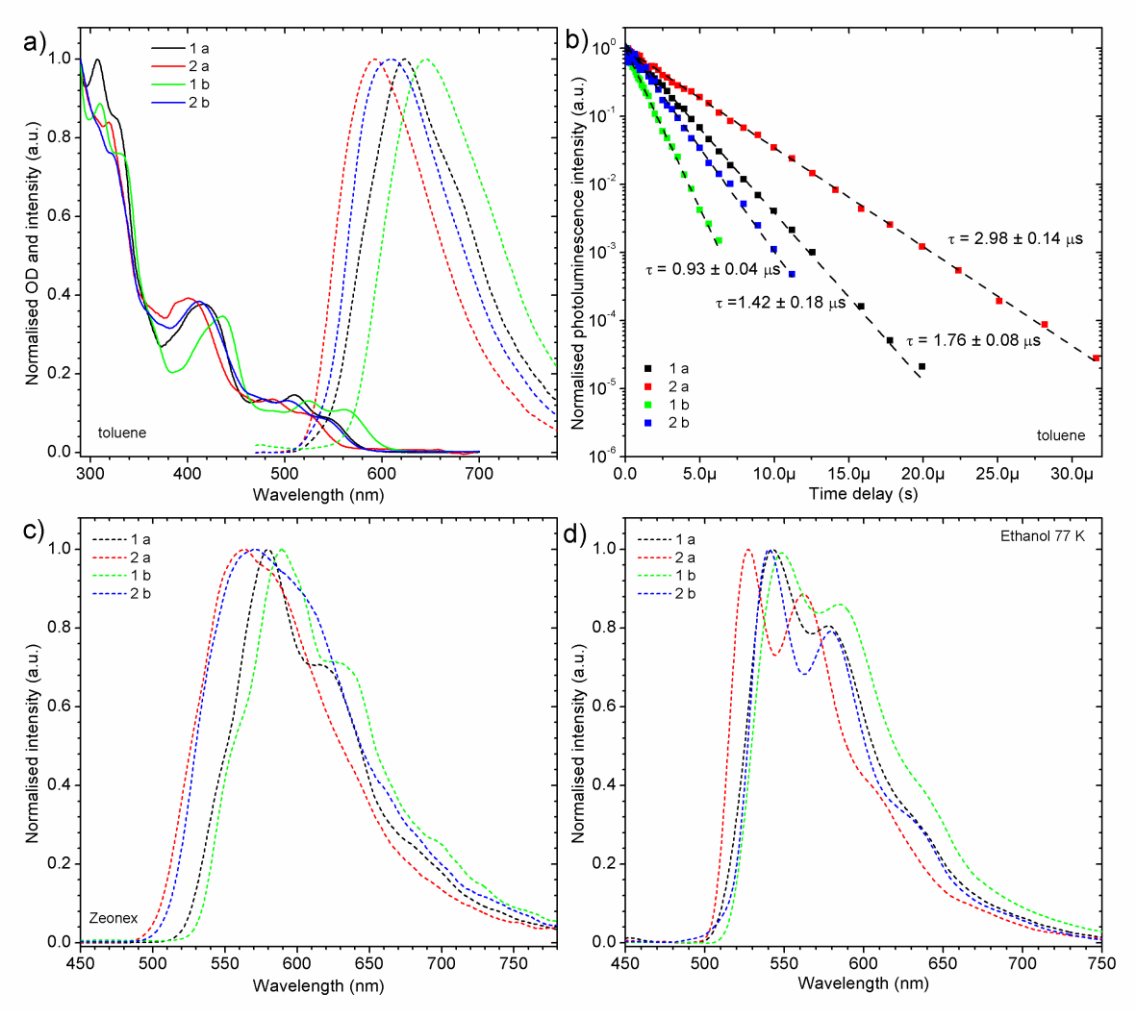

Figure 5.2 Photophysical characterisation of Pt-complexes: a) absorption and phosphorescence spectra in toluene at room temperature, λ_{exc} = 400 nm; b) phosphorescence decay in toluene at room temperature, λ_{exc} = 355 nm; c) Phosphorescence spectra in Zeonex 480 at room temperature, λ_{exc} = 400 nm; d) phosphorescence spectra in ethanol glass at 77 K, λ_{exc} = 400 nm.

Table 5.1 Summary of the photophysical properties of the complexes.

	Absorption	**Emission**				
	λ_{abs}, nm ($\varepsilon \times 10^{-4}$, M^{-1} cm^{-1})[a]	λ_{em}, nm[b]	τ, µs[c]	Φ_{PL}[d]	λ_{em}, nm[e]	τ, µs[f]
Solvent	Toluene	Toluene			Zeonex® 480	
1a	541 (0.22), 509 (0.31), 478 (0.27), 417 (0.80), 329 (1.85), 308 (2.12)	624	1.76 ± 0.08	0.24	580	7.6 ± 0.4
2a	527 (0.17), 489 (0.27), 399 (0.85), 320 (1.80)	593	2.98 ± 0.14	0.34	564	5.5 ± 0.4
1b	564 (0.30), 523 (0.38), 488 (0.30), 436 (1.02), 335 (2.20), 310 (2.61)	646	0.93 ± 0.04	0.12	589	5.4 ± 0.2
2b	547 (0.15), 506 (0.26), 470 (0.30), 410 (0.80), 323 (1.57)	610	1.42 ± 0.18	0.25	572	4.8 ± 0.4

[a] Absorption band wavelength and absorption coefficient with ±15% error; [b] Emission maxima in toluene; [c] Phosphorescence lifetime at room temperature in degassed solution; [d] Photoluminescence quantum yield in degassed solution with ±15% error; [e] Emission maxima in Zeonex polymer; [f] Phosphorescence lifetime in Zeonex in vacuum.

5.2.2 Solid state photophysics

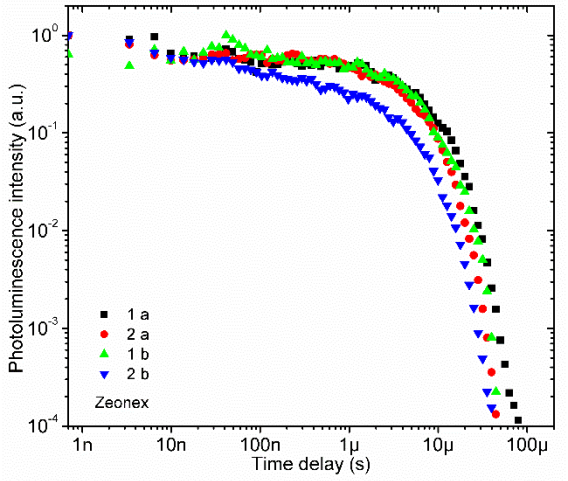

Figure 5.3. Photoluminescence decay of 0.1 % Zeonex films at 295 K, λ_{exc} = 355 nm.

The photoluminescence decay of 0.1 % loaded Zeonex films is very simple (**Figure 5.3**). Zeonex as a neutral matrix does not complicate any luminescence processes thus phosphorescence of these metal complexes decays monoexponentially in this host. Behaviour of phosphor-doped PVK:PBD blends is more complicated than Zeonex films

(**Figure 5.4**). It is worth noting that the 355 nm excitation is absorbed mostly by the host, so the effects observed in there, are complicated by the energy transfer processes between host and guest. The behaviour of 5% **1a**, **1b** films is relatively simple (**Figure 5.5**) as due to the higher doping concentration almost all excitons from the host are transferred to the dopant by FRET, leaving almost no triplet excitons in the host (ISC in the host is slower than FRET). Only a weak host fluorescence can be observed in **1b** : PVK:PBD blend. In this case a short-lived fluorescence decay of the host, and the dopant phosphorescence with a monoexponential decay is observed. The photoluminescence decay of these blends at 80K is slightly more complicated than at 295K. The Phosphor's luminescence exponential decay is slower and more host fluorescence is observed at early (<100 ns) times. Additionally, a weak, long-lived emission which does not clearly fit to an exponential expression becomes observable. It is likely that the same phenomenon is observed in **2a**, and **2b** blends with PVK:PBD with much lower amplitude (see text below for details).

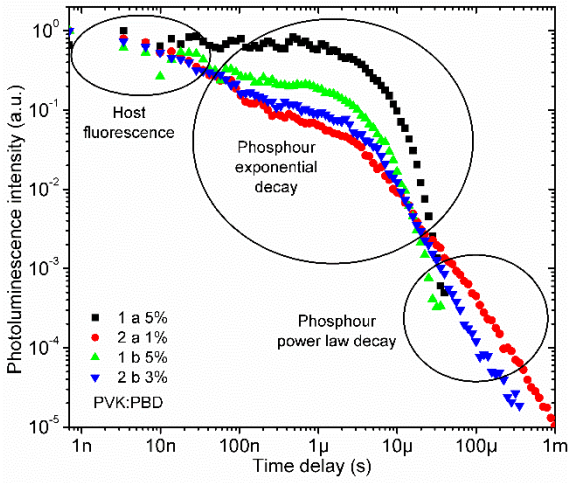

Figure 5.4. Photoluminescence decay of doped PVK:PBD (60:40) films at 295 K, λ_{exc} = 355 nm.

The host fluorescence is more intense in blends of PVK:PBD doped with **2a**, and **2b** due to the low doping concentration. Moreover, due to ineffective quenching of hosts' singlet states, intersystem crossing (ISC) occurs, giving rise to formation of long-lived triplet states in the host matrix. Short-lived host fluorescence (exponential decay) is

recorded in short time regime (<100 ns), followed by the exponential decay of the phosphor luminescence in the microsecond time range. This exponential regime is then followed by a power law decay region with the same emission pattern as in the exponential part of the decay. The power law decay is assigned to an effect of the excited states being stored by the host and slowly being transferred to the dopant, therefore, creating a distance-distribution of the energy transfer rate constant that induces the power law regime. This is because dopant molecules are too far away from each other and so the triplet states of host molecules must migrate to be quenched by the emitter. This process is dependent upon molecular motion, therefore becomes slower at low temperature. The exponential decay of the dopant also becomes slower at lower temperature. A power law decay that is identical to the case reported here was earlier observed in electroluminescence.[3] Further studies in exciplexes (see Chapter 7) have shown this phenomenon to be universal and likely to be due to the presence of bimolecular charge recombination of free charge carriers appearing as a result of exciton/exciplex dissociation.

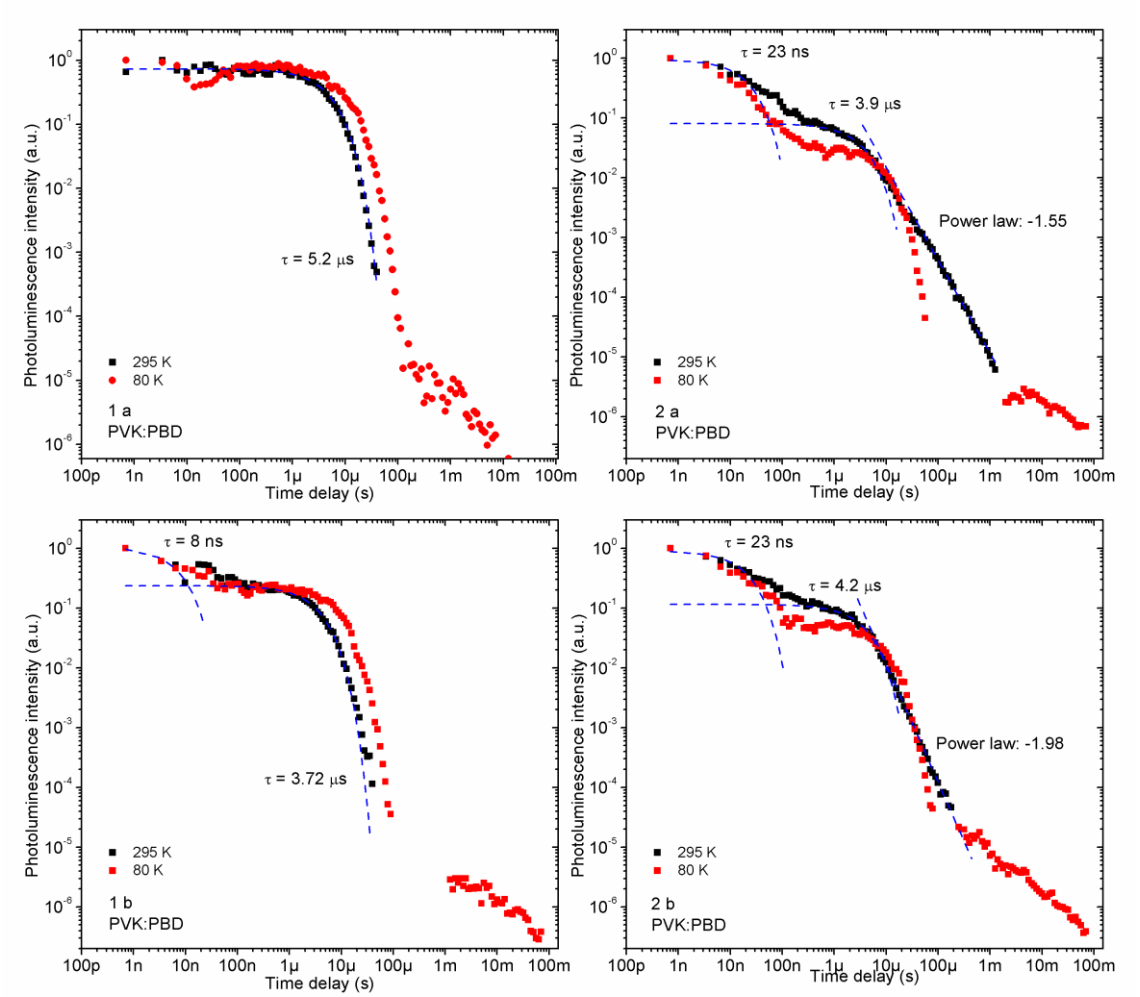

Figure 5.5. Photoluminescence decay of PVK:PBD (60:40) doped films at 295 and 80 K, λ_{exc} = 355 nm. Decay at 295 K is fitted with monoexponential and power law expressions. Power law expression used for fitting: $y = ax^b$, where a and b are fitting parameters, while x is time and y is photoluminescence intensity. "Power law:" denotes the exponent b of the fit. Note: error limits not available.

5.2.3 Electrochemistry

Cyclic voltammetry studies on the complexes **1a**, **1b**, **2a** and **2b** show that all compounds behave similarly and show a reversible reduction that involves the N^N (bipyridine) ligands. Oxidation of the complexes is however irreversible. In this case the behaviour of **1a** and **2a** is nearly identical, this is also observed for their *tert*-butylated analogues **1b** and **2b** (**Figure 3**). This proves that oxidation of these complexes involves the phenyl rings of the O^O ligand, as the alkyl substitution of this moiety changes the

electro-oxidation signal pattern, meaning that the alkyl-substituted and non-alkyl-substituted complexes undergo different chemical reactions upon oxidation. The complexes show very similar oxidation and reduction potentials. However, **2a** and **2b** show larger electrochemical energy gap (0.05-0.07 eV), which explains the observed blue shift of their emission in comparison to the other two molecules. The results are summarised in **Table 5.2**.

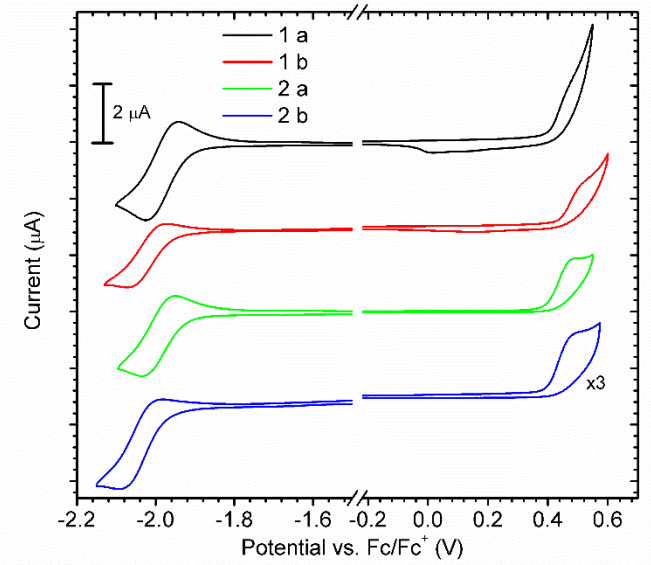

Figure 5.6 Electrochemical oxidation and reduction cycles of the investigated complexes recorded with cyclic voltammetry at 0.05 V s^{-1} scan rate in 0.1 M Bu_4NBF_4/DCM supporting electrolyte. Note the results for 2b were recorded at lower concentration due to its limited solubility.

Table 5.2 Electrochemical properties of the investigated complexes. Note all potentials are relative to the standard potential of ferrocene/ferrocenium redox couple.

Complex	**E_{ox}^{CV}, V[a]**	**E_{red}^{CV}, V[b]**	**IP, eV[c]**	**EA, eV[d]**	**E_g^{el}, eV[e]**
1 a	0.40	-1.92	5.50	3.18	2.32
2 a	0.44	-1.95	5.54	3.15	2.39
1 b	0.40	-1.92	5.50	3.18	2.32
2 b	0.40	-1.97	5.50	3.13	2.37

[a]*Onset* oxidation potential recorded with cyclic voltammetry; [b]*Onset* reduction potential recorded with cyclic voltammetry; [c]Ionization potential IP = E_{ox}^{CV} + 5.1[11]; [d]Electron affinity EA = E_{red}^{CV} + 5.1; [e]Electrochemical energy gap E_g^{el} = IP – EA. IP, EA correspond to HOMO and LUMO energy, respectively, and are used as their estimates.

5.3 OLED Fabrication and Characterization

Solution-processed devices were fabricated from the complexes **1a**, **1b**, **2a** and **2b** using chlorobenzene solutions of mixed host (PVK + PBD) and dopant. The dopant concentration was limited in some cases due to the poor solubility of some of the complexes in chlorobenzene, for this reason, toluene could not be used as a solvent; except for **1a** which was dissolved in toluene to produce a device with 5% dopant concentration. Devices of **1a** in toluene have shown similar performances to the presented chlorobenzene-based OLEDs. The poor solubility of complexes **2a** and **2b** resulted in a limited dopant concentration (1% and 3%, respectively). This is likely to decrease the efficiency of host to dopant energy transfer (due to limited Förster & Dexter radius) and cause problems with direct charge injection to the dopant, which in turn decreases the efficiency of the device. This is clearly the problem in devices containing **2a**, and it is also shown in the photophysical study where in the case of PVK:PBD films with low doping concentration (complexes **2a** and **2b**) another (see **Figure 5.4**), slower mechanism for energy transfer is observed (i.e. limited by hole-electron pair recombination[110]). When the photophysical data are compared with the electroluminescence spectra it becomes clear that in OLEDs direct charge injection to the dopant is the dominating process, while the energy transfer from the host to the guest is less predominant. On the other hand, energy transfer governs the photoluminescence in PVK:PBD mixed host. It is important to note that for this reason the efficiency of the OLED devices is slightly larger than it would be expected from the photophysics.

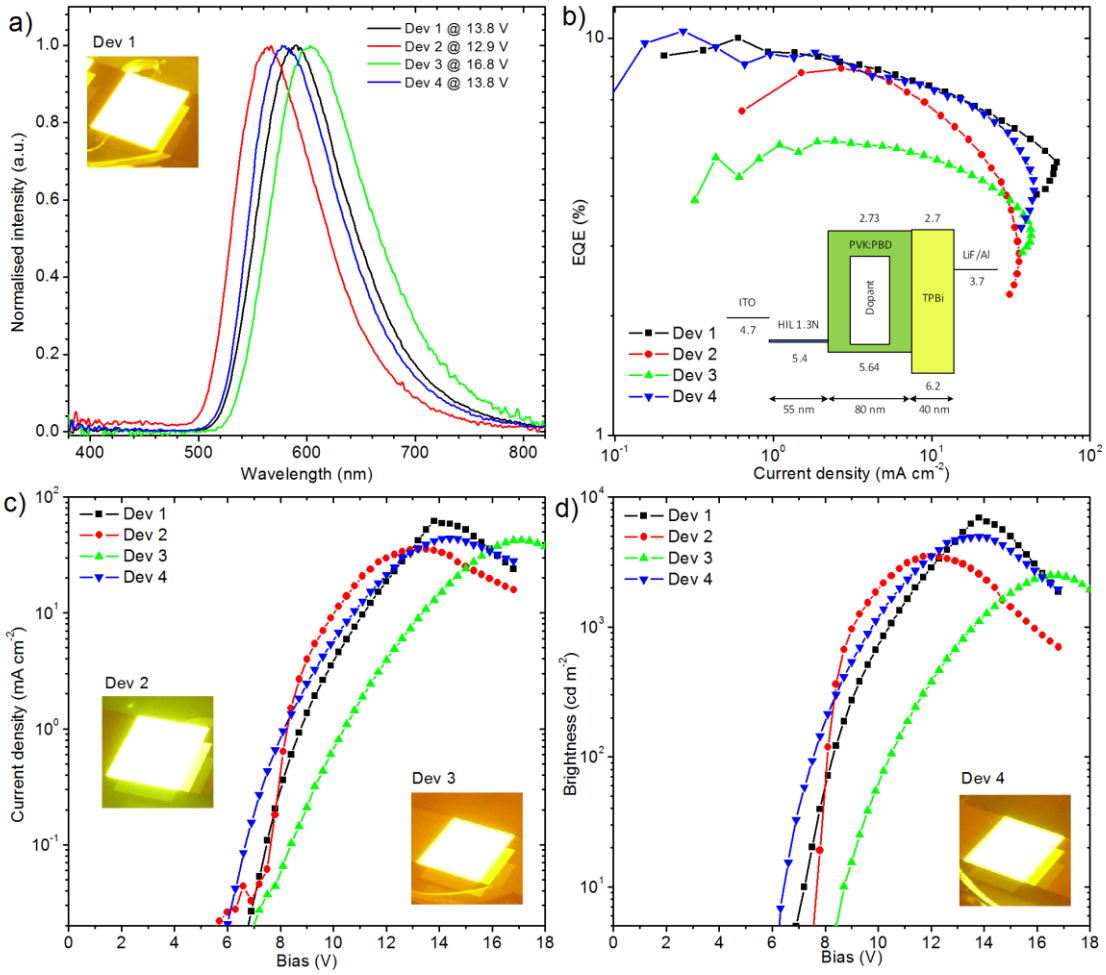

*Figure 5.7 Characteristics of the OLED devices produced from **1a**, **1b**, **2a** and **2b**: a) electroluminescence spectra; b) external quantum efficiency (EQE) vs. current density; c) J-V curves; d) brightness vs. bias. The insets are photographs of the working devices. The inset in figure b) shows the device architecture.*

All the compounds perform well as dopants in OLEDs (**Figure 5.7**) giving electroluminescence from yellow-green to orange that is in full agreement with the photophysical results. All dopants except **1b** give efficient devices with EQE of 8.4-10.4% and satisfactory current efficiency of 22.3-24.9 cd A^{-1}. The brightness of these devices reached up to 7000 cd m^{-2} in the case of **1a**, while the device derived from **1b** shows the lowest brightness of 2500 cd m^{-2}. The turn-on voltage is in the typical range for the OLED structure used with a PVK:PBD host.[18] The OLEDs based on **1b** perform worse than the others, including lower efficiency and visibly higher optical turn-on voltage.

Due to the higher photoluminescence quantum yield both in doped film and in solution, the **2a**-based OLED was expected to have a higher maximum EQE and in general to outperform the **1a**-based OLED. However, the low solubility of the complex imposed limitations in doping concentration, and the device with **2a** as the dopant (1%) is therefore less efficient than the device incorporating **1a** (5%). The yellowish electroluminescence of devices 1 and 3 is close to that of candlelight, while device 2 has a more green and device 4 a more red electroluminescence. The colorimetric coordinates in the CIE 1931 colour space of a typical candle (0.52, 0.42)[111] and those of the presented devices 1 and 3 are close to these values (see **Table 5.3**). Interestingly, the candlelight colour has been achieved with the use of only one emitter whereas other solutions use 2-3 of them.[111,112]

Table 5.3 Summary of the characteristics of the OLED devices.

Device	**Dopant**	**Turn on at 10 cd m^{-2}, V**	**EQE, %**			**Max. Current efficiency, cd A^{-1}**	**Max. brightness, cd m^{-2}**	**EL max., nm**	**CIE (x,y) at max. brightness**
			max.	**at 100 cd m^{-2}**	**at 1000 cd m^{-2}**				
Dev 1	1 a	7.2	10.0	9.7	8.2	23.2	7000	590	0.54, 0.46
Dev 2	2 a	7.6	8.4	6.6*	8.2	24.9	3500	567	0.46, 0.51
Dev 3	1 b	8.7	5.5	5.3	4.9	9.9	2500	603	0.57, 0.42
Dev 4	2 b	6.4	10.4	9.3	8.0	22.3	5000	577	0.52, 0.47

Device architecture: ITO | HIL 1.3N (55 nm) | dopant (1-5%) co PVK:PBD (60:40) (80 nm) | TPBi (40 nm) | LiF (0.8 nm) | Al (100 nm); Doping concentration: Dev 1: **1 a** (5%), Dev 2: **2 a** (1%), Dev 3: **1 b** (5%), Dev 4: **2 b** (3%). * Value recorded at 118 cd m^{-2}.

5.4 Conclusions

Four tetradentate ONNO Pt(II) complexes have been characterised and simple solution-processed OLED devices produced. These devices exhibit yellow-green to orange electroluminescence with EQE up to 10.4%. Fabrication of solution-processed devices was made possible due to good solubility of these complexes in chlorobenzene, however, not all the molecules dissolved equally well. In fact the molecules with the cyclopentene ring in the outer periphery dissolve better than the isomeric counterparts.

Also, the additional *tert*-butyl group added in molecules **1 b** and **2 b** did not improve their solubility. In fact **1a** is more soluble than the *tert*-butylated counterpart.

These Pt(II) complexes show a strong rigidochromic effect, and their photoluminescence is significantly red shifted in solution (i.e. orange-red) and blue shifted in ethanol glass at 77 K (i.e. green). This suggests a relatively flexible molecular structure that can allow for a number of molecular motions at room temperature, but are suppressed at 77 K.

Finally, due to the small load of the emitter in some cases (1-3% w/w) dictated by low solubility, the energy transfer from OLED host to guest, as seen in the photophysics, was found to be slow and more complex. It was revealed that the host stores the energy gained upon photoexcitation in long-lived states that are slowly transported to the emitter molecules. This leads to relatively long-lived power-law decaying phosphorescence that is strongly temperature-dependent. This type of emission is later discussed in Chapter 7.

6 Triplet harvesting in excimeric states of platinum metal complexes

The material contained within this chapter has been published as:

M. T. Walden, **P. Pander**, D. S. Yufit, F. B. Dias and J. A. G. Williams, *J. Mater. Chem. C*, 2019 DOI: 10.1039/C9TC00768G.

6.1 Introduction

Phosphorescent Pt metal complexes have proven their usefulness in OLED devices due to their high photoluminescence quantum yields and short phosphorescence lifetimes.[113–115] Platinum(II) and iridium(III) are the most common metal centres used in luminescent metal complexes.[37,116,117] Platinum(II) however due to their square planar geometry around the metal centre allows for face-to-face alignment of molecules, leading to metal-metal-ligand charge-transfer (MMLCT) interactions.[11,14,106] Thus, these Pt(II) complexes are likely to form excimer excited states and aggregates with high radiative rate constants. Pt(II) excimer-forming complexes have shown promising properties in OLED applications, especially in generation of orange-red to NIR light.[48] A lot of research has been done in this field by J. Kalinowski, M. Cocchi and J.A.G. Williams.[11,14,20,106]

The low solubility of metal complexes is usually a limitation for their use in solution-processed devices. This is especially true for excimer-forming molecules that require high concentrations of emitter in the blend. The molecules used in this work are equipped with *tert*-butyl groups that apparently do improve their solubility allowing for loads as large as 30% in a solution-processed layer.

Excimer-forming metal complexes are not only interesting through their useful properties, but they also show interesting and not fully explained photophysical characteristics. As excimers are formed predominately at high concentrations, there is also the possibility that intermolecular ground state interactions, such as aggregates are formed. The interplay of excimer and aggregate emissions is one of the issues discussed in this chapter.

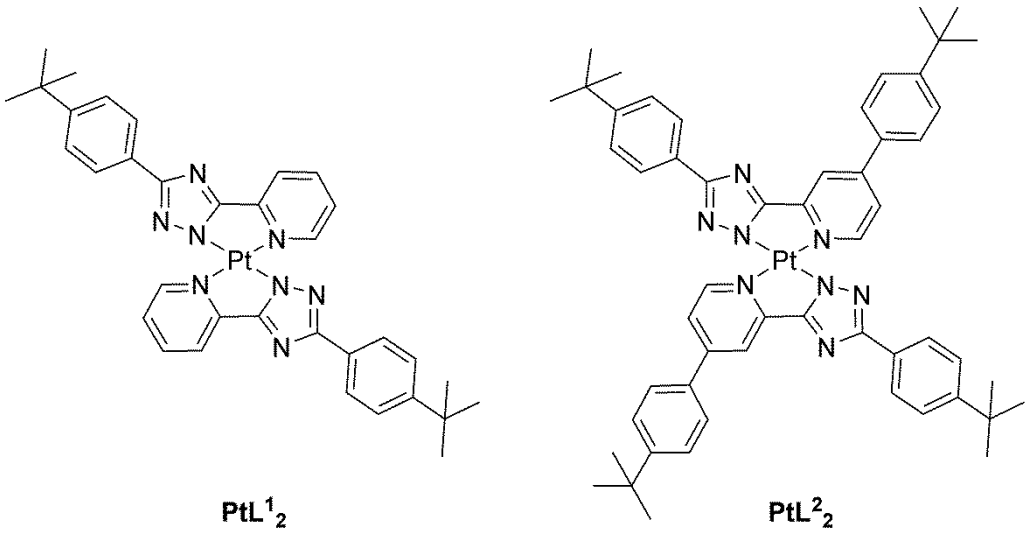

Figure 6.1. Structures of excimer-forming Pt(II) complexes characterised in this work. Note: the molecules were synthesized by M. Walden.

6.2 Solid-state Measurements

PtL$^1_2$ and **PtL$^2_2$** similarly to solutions, also show excimer-forming properties in the solid state (**Figure 6.2**). This is especially true in **PtL$^1_2$** which has to be diluted in polystyrene to a very low concentration in order to observe exciton-dominated photoluminescence, λ_{max} = 501 nm (λ_{max} = 510 nm for **PtL$^2_2$**). Interestingly, and differently from solutions, there is clearly a red-shift of the emission maximum at $\lambda >$ 550 nm upon increasing the percentage load of the metal complex. This leads to emission from neat films (λ_{max} = 599 nm in **PtL$^1_2$**, λ_{max} = 645 nm in **PtL$^2_2$**) to be

significantly red-shifted in relation to the 30%-doped OLED host (λ_{max} = 582 nm in **PtL$^1_2$**, λ_{max} = 608 nm in **PtL$^2_2$**). This suggests formation of new species which most likely are related to aggregates.

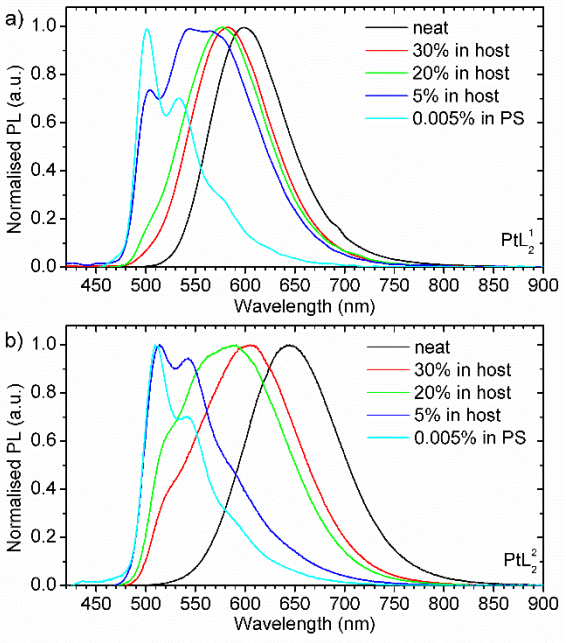

Figure 6.2. Photoluminescence spectra of the investigated metal complexes in OLED host (mCP:OXD7 80:20), polystyrene matrix (PS) and neat film. The percentage represents weight concentration of the emitter in the chosen matrix. λ_{exc} = 365 nm

To further understand the behaviour of the metal complexes in solid films, time-resolved photoluminescence experiments have been performed in a series of concentrations, from 0.005% w/w in polystyrene to neat film at 295 K and 80 K. The films were investigated using a gated iCCD camera and the photoluminescence has been analysed as a sum of the emissions from a range of wavelengths (i.e. sum of exciton, excimer and aggregate emissions, not specific wavelengths, see respective time-resolved spectra, i.e. **Figure 6.4** and **Figure 6.5**). First of all, it is clear in either case (**Figure 6.3**) that the photoluminescence lifetime reduces upon increasing the concentration of the metal complex. This effect is related to the formation of excimer and aggregate species being favoured, which results on significantly shorter luminescence lifetimes than in the respective exciton emission. Interestingly, only in the polystyrene matrix in high diluted conditions, the photoluminescence decay is clearly

monoexponential, reflecting the radiative decay of the exciton species. The lifetimes (at 295 K) are 6.0 ± 0.2 μs for **PtL$^1_2$** and 3.3 ± 0.1 μs for **PtL$^2_2$**. Upon increasing the concentration in the host-guest systems the photoluminescence decay lifetime shortens and apparently becomes predominantly biexponential. This is mainly due to the coexistence of either the exciton, excimer and the aggregate emissions. In fact the photoluminescence decay should be fitted in this case with a triexponential expression to reflect all the luminescent components, however the radiative lifetimes of the excimer and the aggregate are relatively similar, and cannot be distinguished as two separate exponential terms. In the cases where the decays were fitted with biexponential expressions, an average lifetime is used in the discussion below, as described in an earlier work.[118] In general the (average) photoluminescence lifetimes of **PtL$^1_2$** and **PtL$^2_2$** decrease to 0.15 μs and 0.35 μs in neat film at 295 K, respectively. The same trend is observed at 80K, at which the lifetimes change from 8.0 ± 0.3 μs in **PtL$^1_2$** and 3.8 ± 0.1 μs in **PtL$^2_2$** in polystyrene to 1.1 μs in **PtL$^1_2$** and 1.37 μs in **PtL$^2_2$** when in neat films. These values are longer than the lifetimes recorded at 295K, which is typically due to the suppression of the molecular vibrations at lower temperatures. Interestingly, the increase in the radiative lifetime at 80K, relatively to the lifetime at 295K is larger in **PtL$^1_2$** than in the **PtL$^2_2$** at all concentrations. This suggest a much faster non-radiative decay rate in the former compound, especially for the excimer/aggregate emissions, despite the more red shifted emission of these species in **PtL$^2_2$**.

PtL$^1_2$ and **PtL$^2_2$** excimers thus seem not to follow the energy gap law which is related with the fact that the excimer does not have a ground state form. The excited state of **PtL$^2_2$** is more resistant to vibrational deactivation, likely due to its more rigid structure.

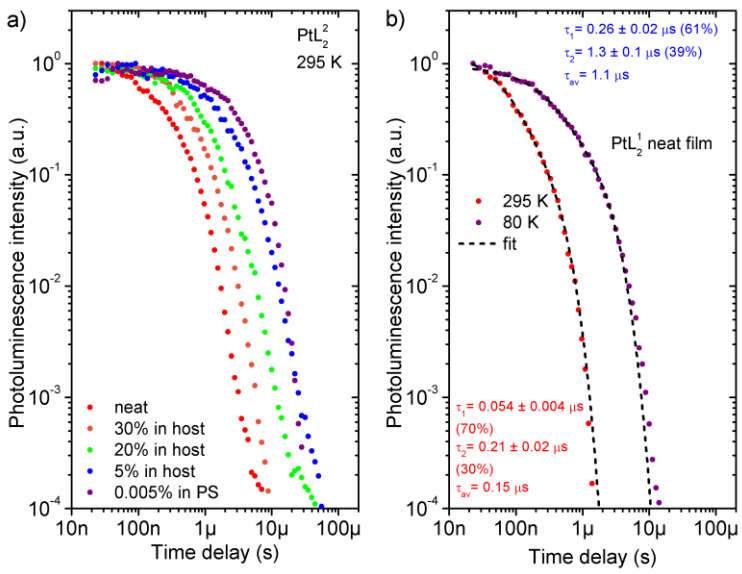

Figure 6.3. a) Photoluminescence decay of ***PtL²₂*** *in OLED host (mCP:OXD7 80:20), polystyrene matrix (PS) and neat film at 295 K. The percentage represents weight concentration of the emitter in the chosen matrix. b) Photoluminescence decay of a neat film of* ***PtL¹₂*** *at 295 K and 80 K.* λ_{exc} *= 355 nm*

The abovementioned emissions can be observed in the time-resolved spectra (i.e. **Figure 6.5**). First of all, the exciton emission ($\lambda \approx$ 500-550 nm) can clearly be distinguished from the excimer/aggregate emissions ($\lambda \approx$ 550-750 nm) due to its different wavelength range and clear vibronic structure (also see steady state emissions, **Figure 6.2**). In contrast, the excimer and aggregate emissions, both broad and with Gaussian shape, overlap strongly, thus giving no clear distinction between one and the other. However, the excimer/aggregate emissions clearly red-shift over time in all cases, giving a clear sign that the contribution of these two Gaussian components is changing in favour of the more red shifted species at longer delay times. It is thus assumed that the more red shifted emission is originated from the aggregate, therefore, the excimer photoluminescence decay has to be slightly faster than that of the aggregate. Further inspection of excitation spectra (**Figure 6.6**, **Figure 6.7**) reveals the aggregates to be present in case of both emitters at higher concentration. Similar findings have been shown earlier by Kalinowski *et al.*[20]. Interestingly, a closer look at the excitation spectra of PtL^1_2 suggests inhomogeneity of the films as aggregates seem to be visible also at

lower concentrations. This is reasonable due to the lower solubility of the **PtL$^1_2$** complex.

Interestingly, a different behaviour of the exciton emissions is noticed at low concentration, as for example 5% in OLED host, but also at other concentrations. In general, at 5% concentration, clearly in **PtL$^1_2$** but still visibly in **PtL$^2_2$**, the exciton emission lives longer than the excimer photoluminescence (i.e. see **Figure 6.4**). This behaviour indicates that there are two distinct populations of excited states: those forming excimers and those that never form excimers (emitting solely as excitons). On the contrary, at higher metal complex load dispersed in the OLED host, the situation is exactly the opposite, showing that the exciton emission in fact lives shorter than the excimer/aggregate emission. This indicates that the majority of the excited state population is related with excimer/aggregate formation and that the exciton species are quenched by the formation of excimers or by aggregates.

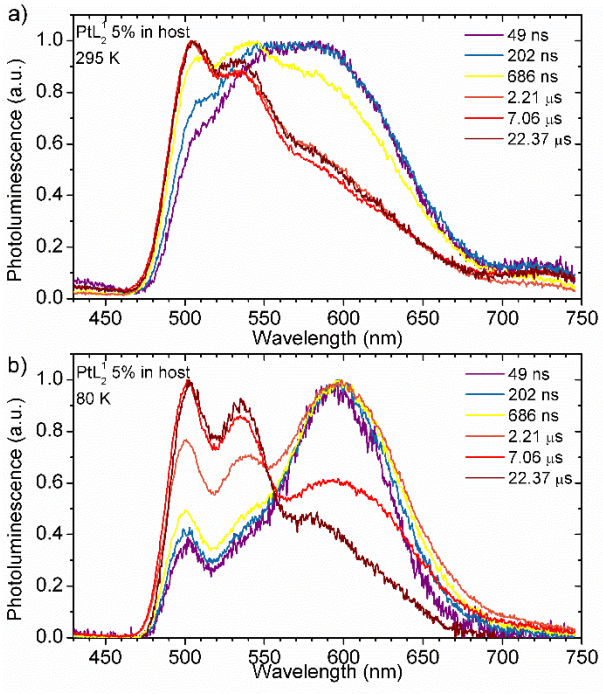

Figure 6.4. Time-resolved photoluminescence spectra of PtL$^1_2$ 5% (w/w) doped in OLED host (mCP:OXD7 80:20). λ_{exc} = 355 nm

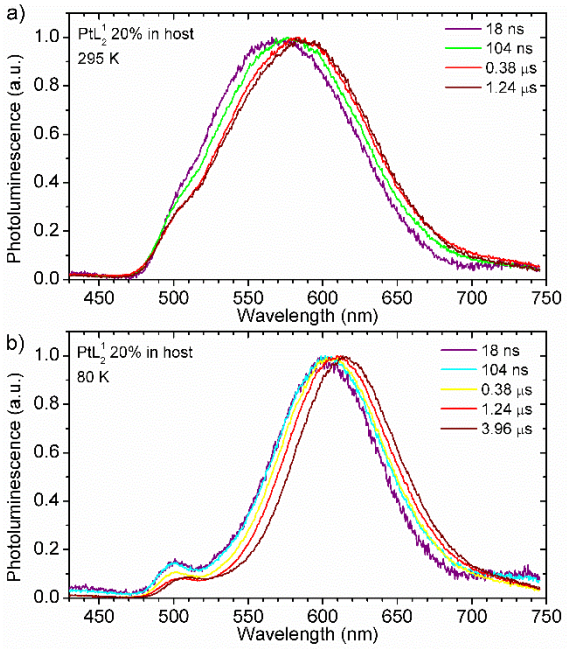

Figure 6.5. Time-resolved photoluminescence spectra of the ***PtL$^1_2$*** *metal complex in OLED host (mCP:OXD7 80:20) at 20% (w/w) load.* λ_{exc} *= 355 nm*

Finally, the exciton emission is more clearly visible at 80 K than at 295 K, which is partially due to the better resolved vibronic structure of the exciton emission spectrum and partially due to the red shift of the excimer/aggregate emission at 80 K in relation to the 295 K. This causes the exciton emission that does not shift with temperature to be more clearly distinguished from the Gaussian excimer/aggregate emissions. There is also no clear indication that the exciton – excimer/aggregate emission ratio changes with temperature – if so, the change is insignificant in the discussed temperature range.

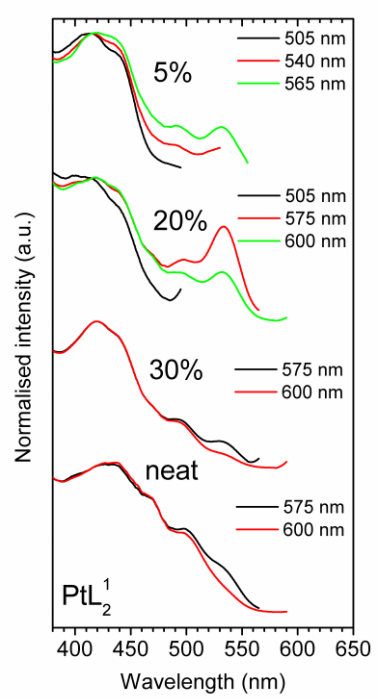

Figure 6.6. Excitation spectra of PtL^1_2 thin films: percentage represents weight concentration of the emitter in mCP:OXD7 (80:20) host. Collected emission wavelength is given in the figure legend.

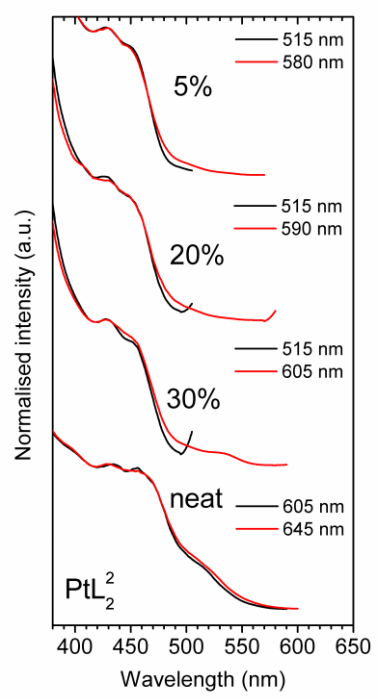

Figure 6.7. Excitation spectra of PtL^2_2 thin films: percentage represents weight concentration of the emitter in mCP:OXD7 (80:20) host. Collected emission wavelength is given in the figure legend.

6.3 Electrochemistry

Both complexes clearly undergo irreversible oxidation at a similar *onset* potential (0.65-0.71 V) as shown in **Figure 6.8**. Interestingly, the $\mathbf{PtL^2_2}$ complex clearly shows a higher reduction *onset* potential (-1.85 V) in comparison to the $\mathbf{PtL^1_2}$ (-2.01 V) and also a *quasi*-reversible reduction process, whilst in the respective $\mathbf{PtL^1_2}$ the reduction is irreversible. Using the electrochemical reduction and oxidation *onset* potentials and commonly accepted relations[119–121] (1) and (2) the ionization potential (IP) and electron affinity (EA) values can be estimated. IP and EA for $\mathbf{PtL^1_2}$ are 5.75 eV and 3.09 eV while the respective values for $\mathbf{PtL^2_2}$ equal 5.81 eV and 3.25 eV. This means the former has larger (2.66 eV) electrochemical energy gap than the latter (2.56 eV). The findings are thus consistent with the photophysical results and the optical energy gaps. IP and EA correspond to the HOMO and LUMO energy, respectively. Interestingly, these results show that extension of ligand conjugation in $\mathbf{PtL^2_2}$ affects rather LUMO than HOMO.

$$\mathrm{IP} = \mathrm{E}^{\mathrm{ox}}_{\mathrm{onset}} + 5.1 \qquad (6.1)$$

$$\mathrm{EA} = \mathrm{E}^{\mathrm{red}}_{\mathrm{onset}} + 5.1 \qquad (6.2)$$

Where E^{ox}_{onset} – *onset* oxidation potential, E^{red}_{onset} – *onset* reduction potential. Both potentials are relative to the standard potential of the Fc/Fc^+ redox pair.

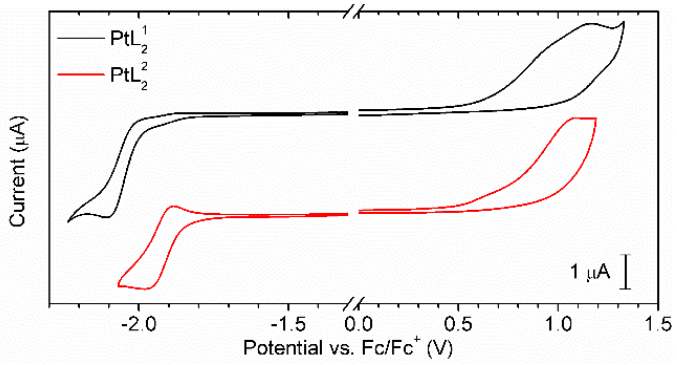

Figure 6.8. Cyclic voltammetry in 0.1 M Bu_4NBF_4 / DCM showing electrochemical processes: oxidation (right) and reduction (left) of both investigated metal complexes.

6.4 OLED devices

Owing to the good solubility (5-10 mg mL^{-1} of the chloroform:chlorobenzene 95:5 mixture) of the newly synthesized metal complexes, their use in solution-processed devices is demonstrated. The main aim of the work was to show devices with exciton-dominated and excimer-dominated emissions to reveal the tunability effect of the electroluminescence colour due to the formation of excimers. To achieve this goal a set of OLED devices was prepared with various doping concentrations (5%, 20%, 30%). Lower than 5% doping was not used due to energy transfer issues reducing the efficiency of devices at lower load. On the other hand, the maximum load was limited to 30% due to unfavourable charge mobility of the dopants, again reducing the device efficiency at high percent content of the emitter. A blend of mCP and OXD-7 in a mass ratio of 80:20 was found to give the best device efficiency and was chosen for fabrication of the devices. Using this approach devices Dev 1-3 (**PtL^1_2** as a dopant) and Dev 4-6 (**PtL^2_2** as a dopant) were fabricated (see **Figure 6.9**). Dev 1-6 are all based on the same architecture: ITO | HIL 1.3N (45 nm) | mCP:OXD-7 (80:20) co x% dopant (60±5 nm) | TPBi (50 nm) | LiF (0.8 nm) | Al (100 nm). Due to the superior excimer-forming properties of **PtL^1_2** in solid state Dev 1-3 show all similar yellowish EL colour, CIE coordinates from (0.50,0.49) in Dev 1 to (0.41,0.55) in Dev 3, due to a dominating role of excimer emission. On the other hand, Dev 6 shows almost purely excitonic electroluminescence with green colour and CIE (0.35,0.58) while upon increasing the

doping concentration this shifts to yellow-orange in Dev 5, CIE (0.47,0.51), and orange-red in Dev 4, CIE (0.52,0.47). This shows versatility of this class of emitters to realise multicolour emissions from a single molecule. In general, the EL of Dev 1-6 are identical with PL spectra of the respective blends (see **Figure 6.2**). These devices have shown superior maximum external quantum efficiency (EQE) in the range of 8.8-12.5% very low roll-off and high maximum luminance of up to 28700 cd m^{-2} (Dev 2). Dev 1-6 however show high turn-on voltage of ca. ≈9-11 V suggesting existence of an energy barrier in the device. The modification of the device structure using a host/hole transport material with lower HOMO than mCP was not successful and this strategy did not improve the device turn-on voltage. However, using a different electron transport material with a higher LUMO it was possible to reduce the device turn-on voltage significantly. A new set of devices has been produced using an optimised mixture mCP:PO-T2T (70:30). The 70:30 mass ratio was optimised for the lowest turn-on voltage as a primary parameter. Dev 8-13 (**Figure 6.10** and **Figure 6.11**) with an architecture ITO | HIL 1.3N (45 nm) | mCP:PO-T2T (70:30) co x% dopant (70±5 nm) | PO-T2T (50 nm) | LiF (0.8 nm) | Al (100 nm) have been produced. Dev 8-13 show a turn-on voltage of 7-8 V, but their efficiency has dropped visibly. This is likely due to improved electron mobility in the emitting layer causing current leakage to the HIL. Finally, to demonstrate the versatility of the metal complex emitters a vacuum evaporated device Dev 7 has been fabricated. The device structure: ITO | NPB (35 nm) | TSBPA (10 nm) | mCP (5 nm) | mCP co 30% **PtL^1_2** (20 nm) | TPBi (50 nm) | LiF (0.8 nm) | Al (100 nm) allowed a low turn-on voltage 3.8 V and superior external quantum efficiency of 15.0% and maximum brightness of 39000 cd m^{-2}. The EL spectrum of Dev 7 is in principle similar to Dev 2 and Dev 3. The relatively small differences are assigned to different packing in the vacuum deposited layer than in the solution-processed film.

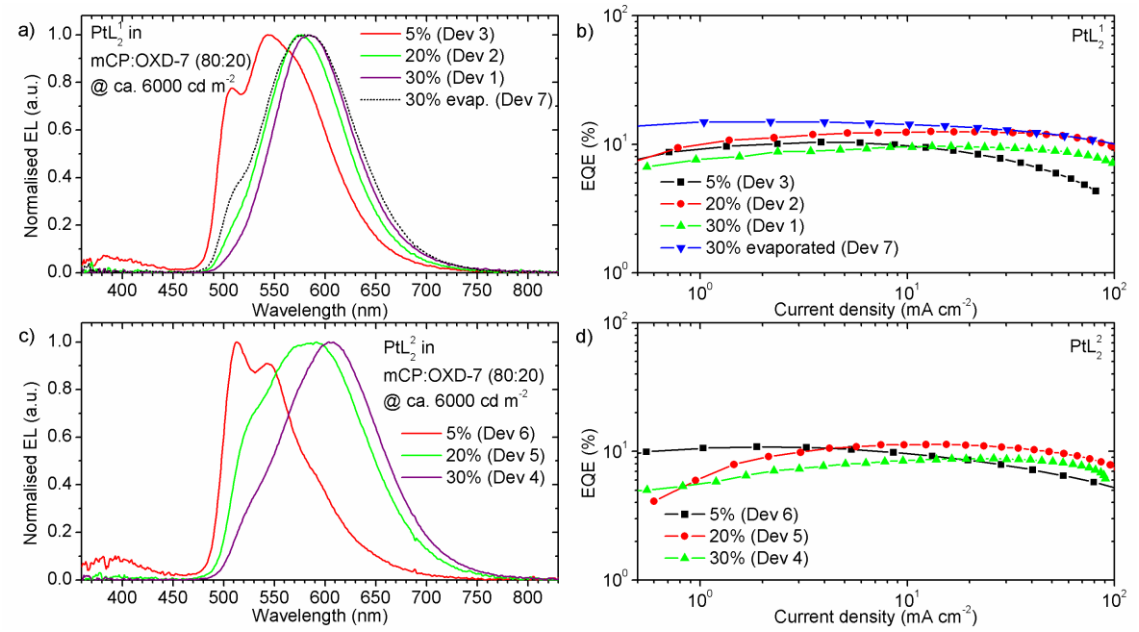

Figure 6.9. Characteristics of OLED devices: a), c) – electroluminescence spectra; b), d) – EQE – current density characteristics. Note the percent values in devices Dev 1-6 represent weight concentration of the emitter, while in evaporated Dev 7 this value represents a percent evaporation rate contribution in co-evaporation.

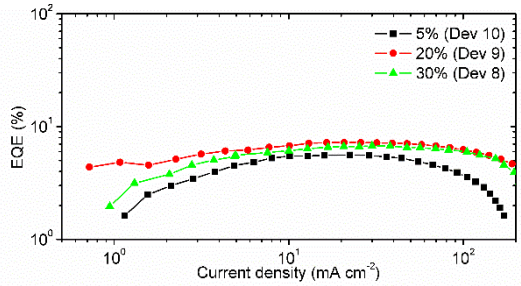

Figure 6.10. External quantum efficiency (EQE)-current density characteristics of devices 8-10.

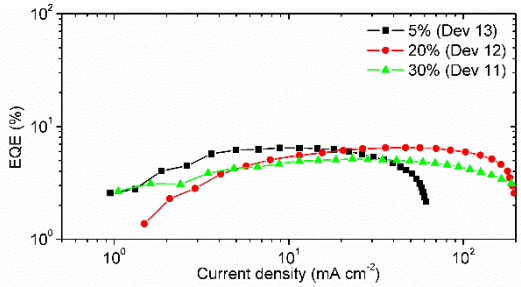

Figure 6.11. External quantum efficiency (EQE)-current density characteristics of devices 11-13.

Table 6.1. Summary of OLED device characteristics.

Device	**Dopant**	**Dopant conc. %**	**Φ_{PL} in film**	**V_{ON} @ 10 cd m^{-2} / V**	**EQE, %: max / at 1 mA cm^{-2} / at 10 mA m^{-2}**	**CE, cd A^{-1}: max / at 1 mA cm^{-2} / at 10 mA m^{-2}**	**L_{max}, cd m^{-2}**	**CIE (x,y) at L_{max}**
Dev 1	PtL^1_2	30	0.55 ±0.06	12.0	9.6 / 7.6 / 9.7	27.2 / 22.5 / 26.5	19800	0.50, 0.49
Dev 2	PtL^1_2	20	0.61 ±0.06	11.9	12.5 / 10.1 / 12.3	38.2 / 30.9 / 37.9	28700	0.47, 0.51
Dev 3	PtL^1_2	5	0.63 ±0.06	11.1	10.4 / 9.2 / 9.7	34.3 / 30.9 / 32.4	26100	0.41, 0.55
Dev 4	PtL^2_2	30	0.58 ±0.06	9.5	8.8 / 5.2 / 8.3	19.2 / 11.2 / 18.1	13400	0.52, 0.47
Dev 5	PtL^2_2	20	0.57 ±0.06	10.1	11.4 / 6.2 / 11.4	30.8 / 20.3 / 30.3	21000	0.47, 0.51
Dev 6	PtL^2_2	5	0.85 ±0.09	10.4	10.9 / 10.4 / 9.7	35.8 / 34.1 / 30.3	26900	0.35, 0.58
Dev 7*	PtL^1_2	30*	-	3.8	15.0 / 15.0 / 14.5	42.7 / 41.8 / 40.3	38800	0.45, 0.51
Dev 8	PtL^1_2	30	-	8.4	6.8 / 2.1 / 6.1	21.4 / 10.4 / 20.2	25900	0.45, 0.53
Dev 9	PtL^1_2	20	-	7.3	7.3 / 4.7 / 6.9	24.1 / 11.2 / 22.8	30300	0.42, 0.55
Dev 10	PtL^1_2	5	-	7.8	5.6 / - / 5.5	17.6 / - / 17.0	12000	0.29, 0.54
Dev 11	PtL^2_2	30	-	7.7	5.1 / 2.6 / 4.8	12.6 / 6.1 / 11.8	15300	0.49, 0.49
Dev 12	PtL^2_2	20	-	8.3	6.5 / - / 5.4	18.2 / - / 15.0	21800	0.45, 0.52
Dev 13	PtL^2_2	5	-	7.9	6.5 / 2.6 / 6.3	21.4 / 7.7 / 21.4	8300	0.30, 0.57

* This device was prepared by vacuum thermal evaporation. The 30% concentration relates to the 30% evaporation rate contribution of dopant during co-evaporation of the emissive layer.

Device structures were as follows:

Dev 1-6: ITO | HIL 1.3N (45 nm) | mCP:OXD7 (80:20) co x% dopant (60±5 nm) | TPBi (50 nm) | LiF (0.8 nm) | Al (100 nm)

Dev 7: ITO | NPB (35 nm) | TSBPA (10 nm) | mCP (5 nm) | mCP co 30% PtL^1_2 (20 nm) | TPBi (50 nm) | LiF (0.8 nm) | Al (100 nm)

Dev 8-13: ITO | HIL 1.3N (45 nm) | mCP:PO-T2T (70:30) co x% dopant (70±5 nm) | PO-T2T (50 nm) | LiF (0.8 nm) | Al (100 nm)

6.5 Conclusions

The two investigated Pt(II) complexes exhibit mixed, concentration-dependent exciton-excimer emission in solid state. A closer investigation of their photoluminescence revealed the coexistence of excimer and aggregate emissions at higher concentrations. The high solubility of these metal complexes in chlorinated solvents enabled the fabrication of simple, efficient (EQE up to 12.5 %) solution-processed OLED devices with variable contributions of excimer-aggregate and exciton emissions in the electroluminescence spectrum. One of the investigated molecules has also been used in vacuum deposited OLED device, giving 15 % EQE. These results were made possible by triplet-harvesting provided by the metal complex emitter.

Interestingly, the analysis of the time-resolved spectra and excitation spectra has revealed coexistence of excimer and aggregate emissions in solid films of the presented phosphorescent molecules. This is an indication that ground state interactions at high concentrations in solid state cannot be neglected. It is not yet clear however whether the aggregates are beneficial or not to the photoluminescence quantum yield of the solid film. Some earlier reports suggested that aggregated forms of planar Pt(II) complexes show superior PLQY even for deep red/NIR emissions.[48] Surely, the presence of such aggregates red-shifts the complexes photoluminescence further than the excimers do, making them a potentially useful tool to obtain efficient NIR electroluminescence in OLEDs.

7 Triplet harvesting in exciplex states by the way of thermally activated delayed fluorescence

The material contained within this chapter has been published as:

P. Pander, S. Gogoc, M. Colella, P. Data and F. B. Dias, *ACS Appl. Mater. Interfaces*, 2018, **10**, 28796–28802.

7.1 Introduction

Since the fabrication of the first organic light emitting diodes (OLED) by Tang and VanSlyke[4] OLEDs have shown strong potential for application in lighting and display technologies.[1,31] The use of vacuum thermal evaporation (VTE)[7,13,77] is currently the method of choice on the fabrication of the most efficient OLEDs, already in use in smart phones and television displays. However, due to the large material consumption, cost, and the need for spacious high-vacuum chambers and complicated shadow masks, VTE is likely to be used only in high-end applications, where high quality is favoured over the production cost. Therefore, the aim to fabricate OLEDs at low cost directly from solution in large area continues alive. Techniques such as roll-to-roll, slot die or inkjet printing can reduce material usage and costs associated with the long standing aim of printing luminaires and displays. However, these techniques require preferably well-soluble materials with high molecular weight. Burroughes and co-authors[122,123] made the first polymer-based OLEDs. Since then many polymers and dendrimers have shown their usefulness for application in OLEDs and the development of such emitters is still ongoing.[80,124–128]

From the historical point of view OLEDs started to be fabricated with purely-fluorescent organic compounds, which were then superseded by more efficient organic metal complex emitters.[5] This breakthrough opened a pathway to increase exciton harvesting efficiency from 25 up to 100%. Nowadays, the metal complex emitters are being challenged by novel thermally-activated delayed fluorescent (TADF) molecules and polymers which also allow for 100% triplet harvesting,[42,129] without using platinum or iridium. Several TADF emitters have been reported in the literature, showing triplet-harvesting yields close to 100%,[5,68] including D-A_3 molecular structures (one star-shaped donor with three acceptors attached to it) with multiple singlet–triplet state pairs.[130] TADFs have also been used as hosts for phosphorescent metal-complexes.[131] Moreover, by using purely hydrocarbon hosts Cui et al.[132] achieved nearly 100% exciton harvesting for both phosphorescent and TADF dopants. However, still no exciplex-based device realizing 100% exciton harvesting has been shown.[16]

Small-molecule TADF materials have been widely investigated to understand their photophysical and physicochemical properties, however, polymer-based and dendrimer materials, which are more suitable for cost-efficient solution-processing methods have been neglected and solution processed TADF devices remain elusive.

An interesting concept is to use commercially-available or easy to synthesize donor and acceptor materials, which are not TADF, but may form TADF exciplexes.[51,52,133–138] Such exciplex systems may show TADF properties, providing that proper energy alignment between the intermolecular charge-transfer state (^{1}CT) and the local triplet state (^{3}LE) is met.[13,134] In particular, we aim to find blends with high photoluminescence yield (PLQY) and good TADF properties, and this requires solving a trade-off between the energy alignment of the singlet CT and the local triplet ^{3}LE states to maximize reverse intersystem crossing (RISC), and suppressing the efficiency of the non-radiative decay rates.

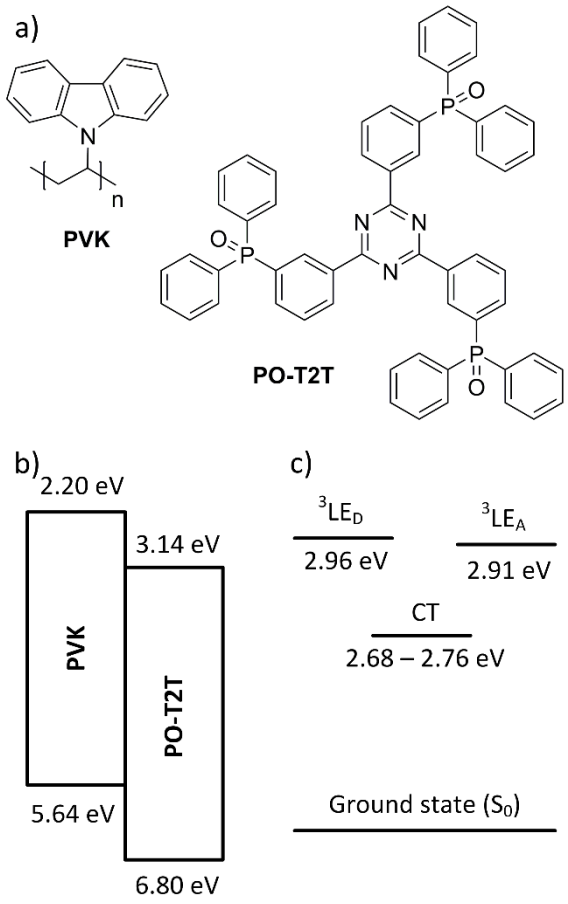

Figure 7.1 a) Structures of donor (PVK) and acceptor materials (PO-T2T) used in this work; b) schematic diagram of electronic energy levels of the donor and acceptor molecules in ground state[36,133]; c) excited state energy diagram of the exciplex blend. ^3LE_D and ^3LE_A denote the triplet states localized on the donor and the acceptor, respectively.

Exciplex systems have been investigated mainly between small molecule-based emitters, which are suitable for vacuum thermal evaporation or similar techniques, but not for solution processing methods, as typically the fabrication of high quality films with small molecules is very challenging from solution processing methods. In contrast, TADF polymer-based exciplex systems allow for efficient triplet harvesting and are suitable for inkjet and slot die printing. In this work, we explore a polymer-small molecule blend to obtain efficient TADF due to the formation of intermolecular exciplex states between the polymer PVK, acting as the electron donor, and the small molecules PO-T2T, acting as the electron acceptor unit, see **Figure 7.1**. This blend can easily be solution-processed and to the best of our knowledge is the first attempt to

produce a polymer-small molecule exciplex aiming strong TADF emission. Due to the prominent film-forming properties of poly(*N*-vinylcarbazole)[37,139] the blend can potentially be used in inkjet or slot-die printing. 2,4,6-Tris[3-(diphenylphosphinyl)phenyl]-1,3,5-triazine (PO-T2T)[133] used as an acceptor shows excellent solubility in toluene, which helps in the formation of high quality films.

7.2 Results and discussion

Excited state intermolecular charge transfer (CT) complexes (exciplexes) are formed between electron donor and acceptor species only in the excited state.[18,50,140] Therefore, no ground state interaction between the donor and acceptor species exist and the absorption spectrum of the blend is thus the sum of the donor's and acceptor's absorption (**Figure 7.2**).

The energy of the intermolecular CT state is roughly a function of the donor's ionization potential (IP_D) and the acceptor's electron affinity (EA_A).[18,50] These are usually identified as the $HOMO_D$ and $LUMO_A$ energies, respectively.[62,141] The formation of the exciplex leads to an emission spectrum that is significantly red-shifted in relation to donor and acceptor species. In the case of poly(*N*-vinylcarbazole) (PVK), IP_D = 5.64 eV,[36] and PO-T2T, EA_A = 3.14 eV,[133] this can clearly be seen in **Figure 7.2**. PVK shows weak blue emission, and the PO-T2T emission is too weak to be recorded. However, the blend of these two materials shows strong green CT photoluminescence ($\Phi_{PL} = 0.12 \pm 0.02$ in air and $\Phi_{PL} = 0.20 \pm 0.03$ in nitrogen).

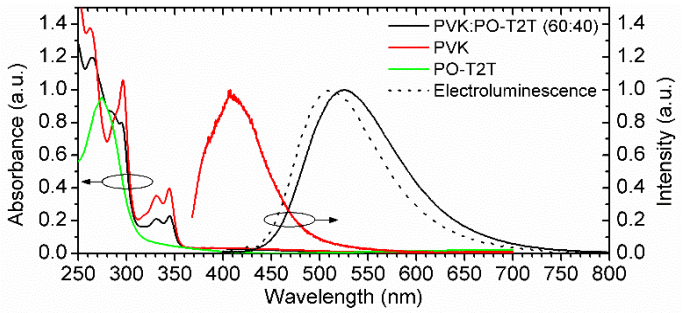

Figure 7.2 Absorption and photoluminescence spectra of donor, acceptor and the blend compared with device electroluminescence (for photoluminescence λ_{exc} = 355 nm). Note that PO-T2T shows no clearly detectable photoluminescence in neat film. Previous works show a very weak photoluminescence from PO-T2T film.[142]

As the PVK : PO-T2T blend possess prominent luminescent properties and shows TADF, it is thus an ideal candidate for use in OLEDs as the emitting layer. These two materials are well soluble in toluene. In particular, when PVK with low molecular weight is used in the blend, high molecular weight PVK (PVKH) can then be used as the hole-transport/electron-blocking layer, which helps to improve device peformance.[104,143] PO-T2T is also used as an electron-transport/hole-blocking layer. However, electron transport and injection layers and cathode are evaporated, but all other layers are solution-processed. This leads to a device structure: ITO | HIL 1.3N (45 nm) | PVKH (10 nm) | PVK : PO-T2T (60:40) (x nm) | PO-T2T (50 nm) | LiF (0.8 nm) | Al (100 nm) where x = 0 (Dev 4), 6 ± 1 (Dev 3), 16 ± 2 (Dev 2), 27 ± 2 nm (Dev 1) (see **Figure 7.7a**, **Figure 7.5, Figure 7.6**, and **Table 7.1**).

A PVK : PO-T2T ratio of 60:40 was used to allow for sufficient hole and electron transport properties of the emissive layer and also to reduce the recombination at the PVKH interface. It is later presented that a variation in the PVK : PO-T2T ratio does not affect the CT state and only a large disproportion between donor and acceptor (such as 1:99) can cause a significant local state emission (**Figure 7.3**, **Figure 7.4**).

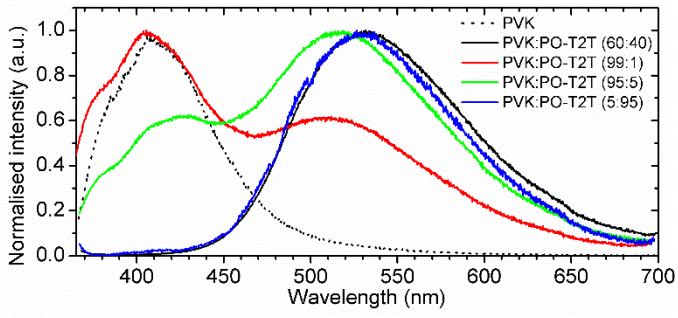

Figure 7.3. Steady state photoluminescence spectra of PVK:PO-T2T blends with various mass ratios and emission spectrum of PVK. All recorded in ambient conditions using λexc = 355 nm.

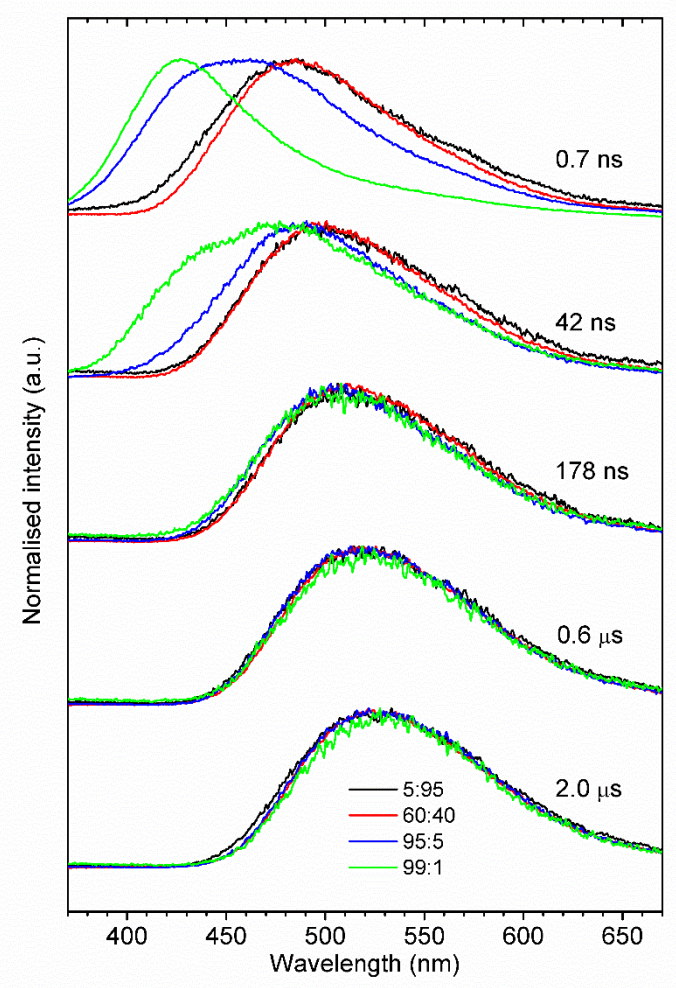

Figure 7.4. Time-resolved photoluminescence spectra of PVK:PO-T2T blends with various mass ratios (black line, 5:95; red line, 60:40; blue line, 95:5; green line, 99:1). Recorded in vacuum at 295 K using λ_{exc} = 355 nm.

Variation of the emissive layer thickness allows for control of the current density and turn-on voltage. The device with the thickest emissive layer (Dev 1) shows the highest EQE = 4.5 %. On the contrary, the lowest turn-on voltage (2.6 V) and the highest maximum brightness is observed in the Dev 4 that uses no blend donor-acceptor emissive layer (x = 0 nm). In this case the recombination occurs at the PVKH | PO-T2T interface. Interestingly, the electroluminescence spectrum is not affected by the emissive layer thickness or by the molecular weight of the donor material, and all devices, Dev 1-4, show similar electroluminescence spectrum at maximum brightness (**Figure 7.4**). Generally speaking, thinner devices provide better charge conductivity, thus the observed current densities increase significantly from Dev 1 to Dev 4. This is caused by the relatively low conductivity of the PVK:PO-T2T blend (more likely due to the low hole mobility of PVK itself), thus a thinner layer provides less resistance. As a result, devices with thicker PVK:PO-T2T layer show lower brightness than devices with thinner or no PVK:PO-T2T layer (Dev 4). Reducing the thickness slightly affects the charge balance, decreasing the maximum EQE of Dev 2-4 relative to Dev 1, but in contrast, the change in current density is much more pronounced. The variation in the optical turn-on voltage between Dev 1-4 is again caused by the low conductivity of PVK. Thinner PVK:PO-T2T layer provides larger current density at lower driving voltage, thus the 1 cd m^{-2} brightness threshold is achieved at lower V_{ON}.

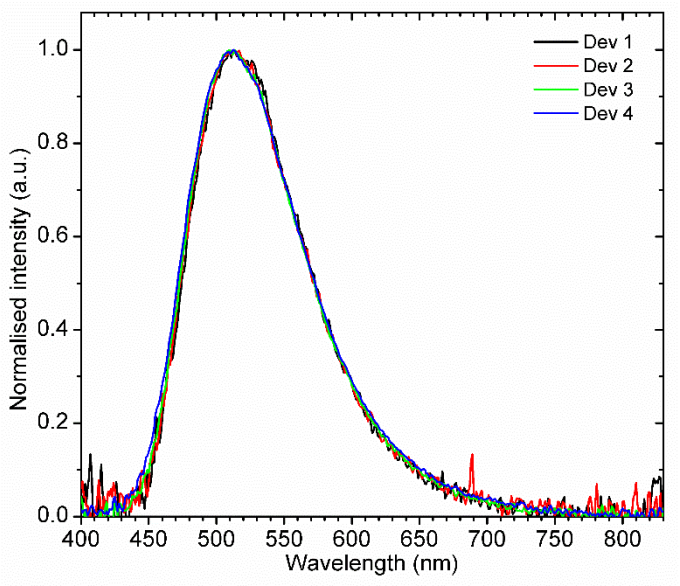

Figure 7.5. Electroluminescence spectra of devices Dev 1-4 at maximum brightness.

The EL spectrum is slightly blue-shifted in relation to the photoluminescence (**Figure 7.2**). Further examination of the electroluminescence spectra under various driving voltages (i.e. see **Figure 7.6**) shows that a small blue-shift in the spectrum (affecting both peak and *onset*) upon rising voltage can be observed. This is more clearly seen in the thinnest Dev 4 than in the other cases, while in the thickest Dev 1 this can hardly be observed. This effect is very likely to be caused by the electric field, changing the CT energy of the emissive species as reported previously by Al-Attar *et al.*[144] While the blue-shift caused by the electric field shows maximum amplitude of ≈ 7 nm (at peak) the shift between EL and PL equals ≈ 13 nm (at peak). This shows the electric field may be an important, but not the only cause of the shift between PL and EL. This suggests that the photo- and electroluminescence may show different contributions of the time-resolved emissive components, i.e. the contribution of the most red-shifted power law emission in photoluminescence may not be present in the electroluminescence.

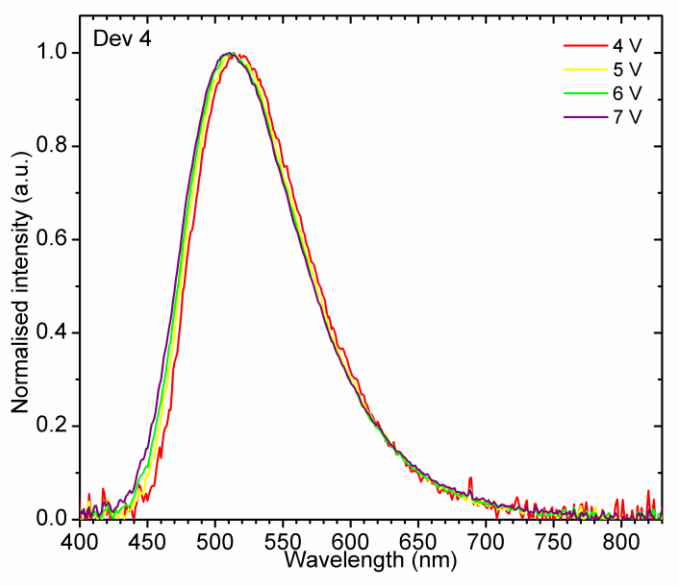

Figure 7.6. Electroluminescence spectra of device Dev 4 at various driving voltages.

Less device efficiency roll-off is observed on devices with thinner or no PVK:PO-T2T layer (Dev 3-4) than in those with thicker EML (Dev 1-2), see **Figure 7.7a**. The actual mechanism causing the roll-off on device efficiency is still not clear and can be caused by a superposition of many different processes. This is thus a very complex issue.[145] However, basing on some of our observations possible major mechanisms can be proposed to explain the behaviour of Dev 1-4. Firstly, the thicker EML provides more space for the recombination zone which is more likely to move upon changing the applied voltage. This may lead to unfavourable charge balance at higher driving voltage leading to a drop in EQE. In thinner devices (Dev 3-4) the recombination zone is either tightly localized between the PVKH and PO-T2T layers or is basically related to the PVKH/PO-T2T interface and is not likely to shift easily. In consequence there is little or no change to the charge balance in those devices at higher applied voltage. Secondly, triplet-triplet annihilation (TTA) and charge trapping phenomena are less likely to appear in thinner layers or at the interface. Thus TTA-related roll-off is more pronounced in Dev 1-2 than in Dev 3-4.

The EQE = 4.5 % achieved in Dev 1 is a result of triplet harvesting by the TADF mechanism. Considering the $\Phi_{PL} = 0.20 \pm 0.03$ the EQE achieved in Dev 1 is close to

the physical limit. Therefore, if TADF was not involved in the electroluminescence produced in this OLED, the EQE would only reach ≈1-1.5 %, assuming ≈0.2-0.3 out coupling factor. Although the EQE remains below the values reported for vacuum deposited small molecule TADF emitters, these devices are at proof of concept level that opens a pathway for future research. PVK has been found to possess many trapping sites, which may in fact quench some of the emissive excitons[146], therefore new exciplex-forming polymers must be developed to possibly improve the EQE.

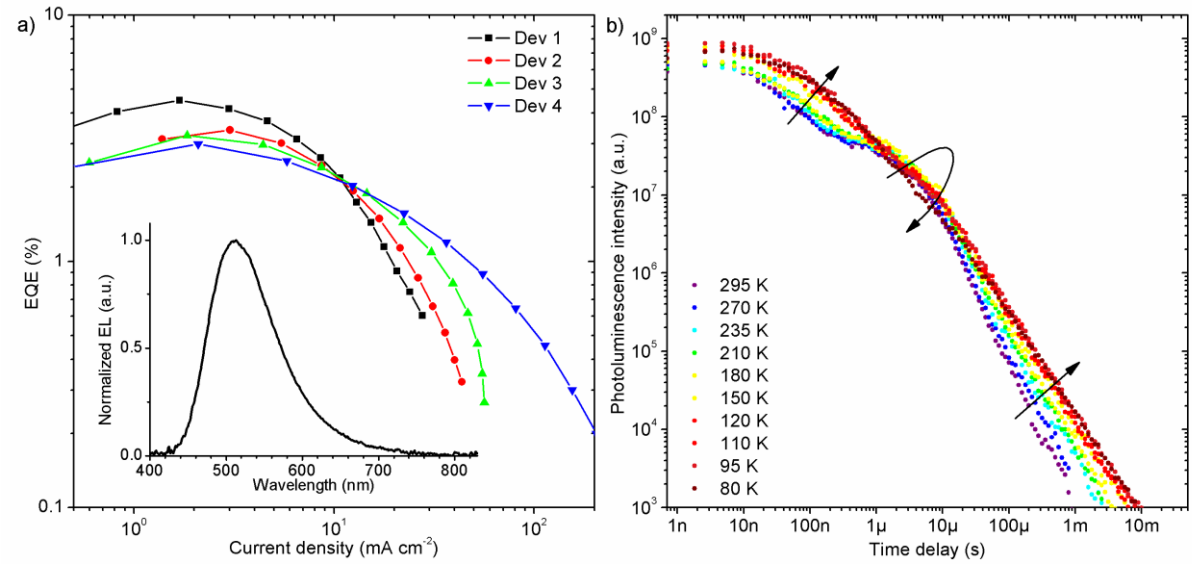

Figure 7.7 a) EQE vs. current density characteristics of OLEDs, inset shows electroluminescence spectrum of Dev 4; b) photoluminescence decay of PVK:PO-T2T exciplex at various temperatures (λ_{ex} = 355 nm).

Time-resolved photophysical analysis of the PVK : PO-T2T luminescence reveals that the exciplex emission shows two exponential components, followed by a power law emission (**Figure 7.7b**, **Figure 7.8**). The first exponential component is the short-lived prompt fluorescence (τ = 32 ± 1 ns), and the second exponential decay is the long-lived delayed fluorescence (τ = 2.9 ± 0.2 μs). The power law emission is likely originated from non-geminate charge recombination of free carriers produced in the blend, as described in previous work.[147] Interestingly, the photoluminescence of the exciplex is significantly affected by non-radiative decay. This is visible as an increase of prompt and delayed fluorescence emissions, between 295 and 150 K, with decreasing

temperature. However, in the temperature range from 150 to 180 K, the delayed fluorescence intensity switches away from the trend observed at higher temperatures and starts decreasing with temperature, as it is normally expected for a thermally-activated process. This behaviour is related to the suppression of the RISC rate due to decreasing the available thermal energy. The temperature dependence in this region down to 80 K is very small, suggesting a negligible (close to zero) singlet-triplet gap of the exciplex.

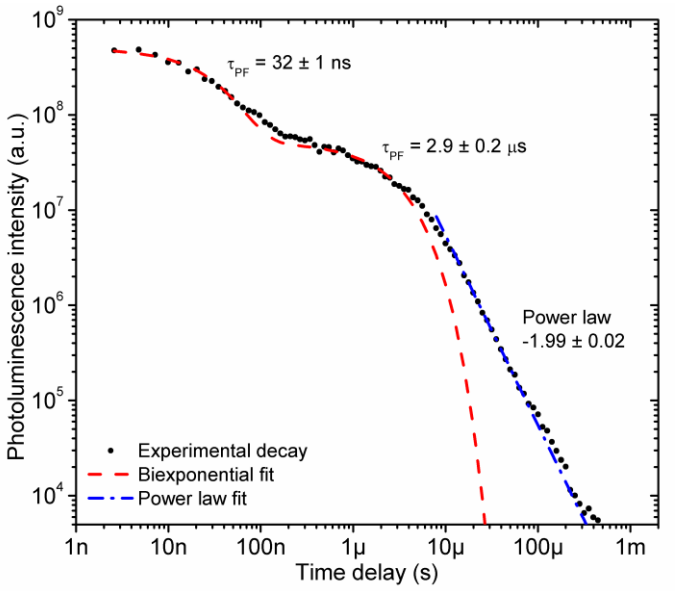

Figure 7.8. Photoluminescence decay at 295 K with fitting exponential and power law curves. Power law expression used for fitting: $y = ax^b$, where a and b are fitting parameters, while x is time and y is photoluminescence intensity. "Power law:" denotes the exponent b of the fit.

Table 7.1 Characteristics of OLED devices.

Device	**x, nm***	**Turn on at 1 cd m^{-2}, V**	**EQE, %**	**Current efficiency, cd A^{-1}**
			max. / at 10 mA cm^{-2}	**max. / at 10 mA cm^{-2}**
Dev 1	27 ± 2	4.9	4.5 / 2.3	13.3 / 6.8
Dev 2	16 ± 2	4.4	3.4 / 2.2	10.0 / 6.5
Dev 3	6 ± 1	3.7	3.3 / 2.2	9.8 / 6.5
Dev 4	0	2.6	3.0 / 2.1	9.3 / 6.3

* Device structure: ITO | HIL 1.3N (45 nm) | PVKH (10 nm) | PVK : PO-T2T (60:40) (x nm) | PO-T2T (50 nm) | LiF (0.8 nm) | Al (100 nm)

The exciplex time-resolved emission, collected using a gated iCCD camera, reveals the whole complexity of the excited state dynamics in this system. The exciplex emission gradually red-shifts over time (**Figure 7.11a**), showing a rapid change between 0.7 ns and 270 ns, of both the *onset* and emission peak. This is an intermediate region between prompt and delayed fluorescence, and shows the most significant spectral changes. The changes observed on the spectrum can be related to the relaxation of the exciplex geometry, i.e. due to changing the distance of the donor and acceptor molecules, which affects CT character through the coulombic factor. Further changes in the spectrum occur between 270 ns and 5 μs, and are probably due to the emission appearing from multiple CT states, with slightly different energies. It appears that different CT states are formed between PO-T2T molecules and various polymer sites as function of their distance. This effect induces the energy distribution associated with the exciplex state that involves PVK and PO-T2T molecules located at different distances, as well as PVK states that involve different number of *N*-vinylcarbazole repeating units. Although a variation on the exciplex energy clearly exists, a dominant state is present as the TADF decay component can easily be fitted using a single exponential equation. This occurs probably because the RISC rate is slower than the energy relaxation of the CT state in the exciplex, i.e. the RISC occurs predominately from the most stable CT states. Therefore, we use the emission spectra from this region to estimate the relaxed CT

energy, which is further discussed in the context of TADF. Note that the emission intensity in this time range shows a linear dependence with excitation power, which is indicative of the TADF mechanism (**Figure 7.9**).

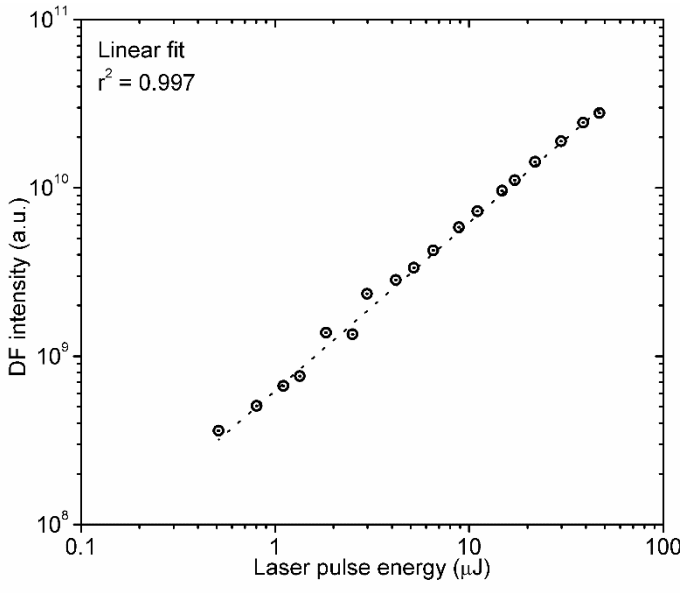

Figure 7.9. Power dependence of delayed fluorescence of PVK:PO-T2T (60:40) exciplex blend in vacuum at 295 K.

The power law decay that is observed from 5 to 10 μs onwards, follows the TADF emission (**Figure 7.7b**, **Figure 7.8**). Within this region no significant changes are observed on the emission spectrum, however, the emission is different from the spectra observed during the TADF exponential regime. Therefore, the origin of the power-law delayed emission is clearly different from that of the TADF regime. We believe this power law emission decay is not created by direct up-conversion of triplet states, but rather from non-geminate charge recombination. This has been observed previously in exciplex blends, [36,147] and is caused by the dissociation of some of the CT states formed in the exciplex, which upon dissociation migrate through the blend as free charge carriers, until recombination later occurs. Polymer-based exciplex blends may be even more likely to undergo this process than small molecules as the charges, i.e. holes or electrons, may be transported not only by hopping between the molecules (or between polymer chains), but also along the polymer backbone (via hopping between grafted

carbazole units, not through the backbone itself). This power law emission intensifies at lower temperatures as the longer CT state lifetime in these conditions promotes charge dissociation. Moreover, the free carriers migrate slower and are less prone to non-radiative deactivation processes.

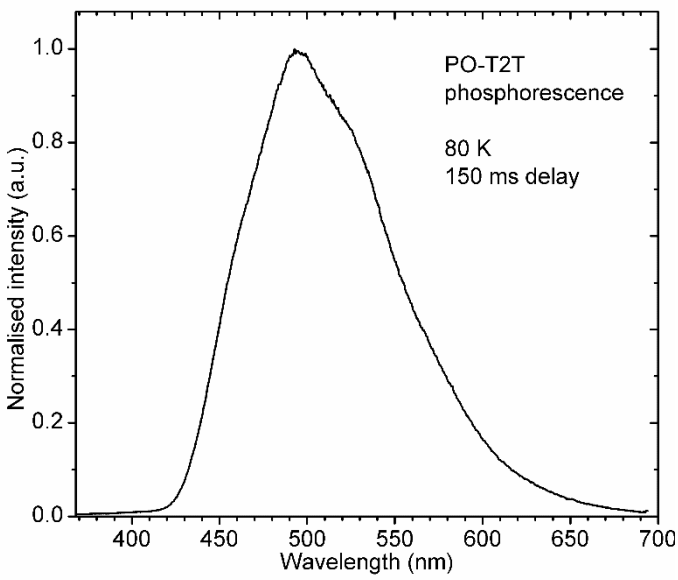

Figure 7.10. Phosphorescence spectrum of PO-T2T in neat film.

Interestingly, the local triplet levels of the molecules forming the exciplex: PVK (T_1 = 2.96 eV)[146] and PO-T2T (T_1 = 2.91 eV, see **Figure 7.10**) are clearly above the CT energy, determined from the delayed fluorescence spectra in **Figure 7.11a**, ^{1}CT = 2.68 - 2.76 eV. In contrast with intramolecular CT states, where a good energy alignment between CT and local triplets has been proposed to be key for efficient triplet harvesting,[13,15,28,43,148] in the case of intermolecular exciplexes we find that an energy alignment where the ^{3}LE is above or isoenergetic with the CT facilitates efficient TADF emission.[12,52,118,133,135,149–151] Recently it has been suggested that the ^{3}LE state plays a crucial role in the reverse intersystem crossing (RISC) mechanism when the ^{1}CT lies above or is isoenergetic with it.[13,41–43,134,152,153] It appears clear that the RISC mechanism in small TADF molecules involves mixing of local and CT triplet states (^{3}LE and ^{3}CT), as it has been observed from the temperature dependent studies of TADF in various intramolecular exciplexes. However, the situation in intermolecular exciplexes appears

to be different. Here, the ^{3}LE state lies clearly above the ^{1}CT state by 0.15-0.23 eV, and it is unlikely for the local triplets to be involved in the RISC process, at least in the way that is suggested by the current theory models. Especially, the ^{3}CT→^{3}LE→^{1}CT involving an endothermic ^{3}CT→^{3}LE up-conversion to a higher local triplet state appears to be questionable in this case. The exciplex described here shows an energy difference between the ^{1}CT and the ^{3}LE of PO-T2T larger than 0.15 eV. This would clearly quench the TADF at 80 K if this gap was relevant. Instead, TADF is only slowed down at this temperature, but can still be easily observed. Moreover, a vast majority of recently studied efficient TADF intermolecular exciplexes show that the CT states are located well below the triplets of the donor and acceptor moieties.[16,133,142] Therefore, we conclude that for intermolecular exciplex systems the most common energy layout is the one where the ^{3}LE state lies above the ^{1}CT, and where the involvement of the local triplet state in the RISC is unlikely. Previous studies suggested that the ISC and RISC processes due to spin-orbit coupling between pure singlet and triplet charge transfer states is forbidden.[13,43,152,153] However, in the case of intermolecular exciplexes, where negligible energy gap between ^{1}CT and ^{3}CT is achieved, hyperfine interactions might become predominant and originate RISC with negligible loss, as no low energy triplet exists below the CT states.

To further understand the properties of the investigated exciplex blend various D-A ratios have been studied (**Figure 7.11b**, **Figure 7.3**, **Figure 7.4**). Remarkably, the ratio between donor–acceptor does not affect exciplex emission at all. All blends show the same CT emission spectrum and lifetime. This is different from the previously observed dependence of the CT energy upon changing the donor-acceptor ratio.[52,135] However, if extremely large excess of PVK is used this leads to inefficient local emission of the donor, which reduces the contribution of efficient exciplex emission. A similar situation may occur in devices, leading to recombination on the PVK, thus reducing EQE. This property shows that using various, but not extreme, PVK : PO-T2T ratios to optimize recombination in the device is a prominent strategy.

It was also found that when using PVKH as the electron blocking layer (EBL), the optimal donor-acceptor ratio is close to 60:40 mass ratio. However, if due to technological limitations an additional EBL cannot be used, then this ratio may be changed without any effect on photophysics, i.e. by increasing amount of PVK to reduce current leakage.

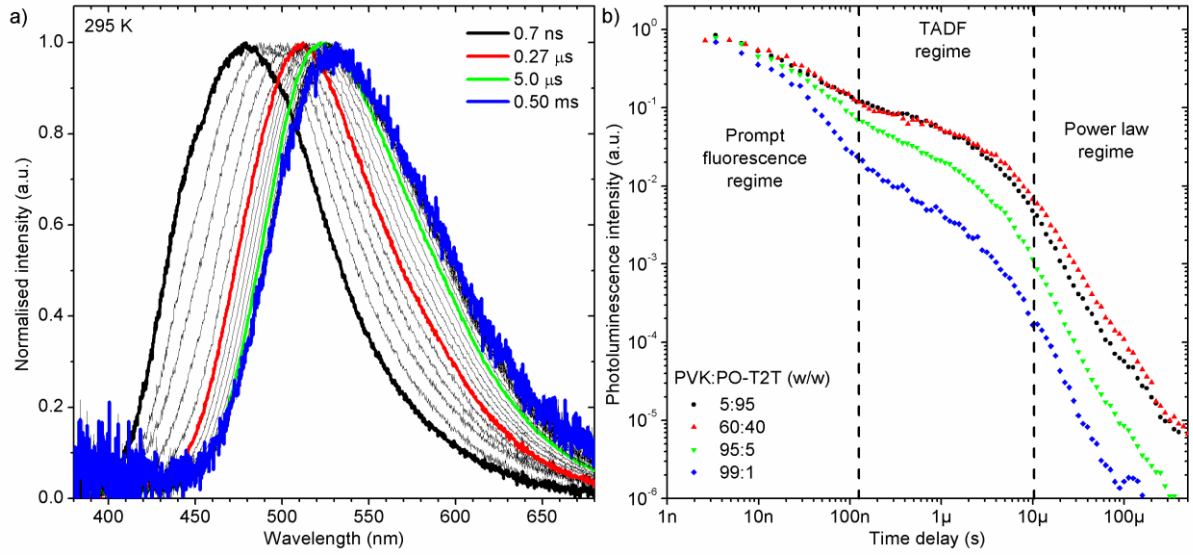

Figure 7.11 a) Time-resolved photoluminescence spectra of PVK:PO-T2T (60:40) exciplex blend at 295 K; b) Photoluminescence decay of PVK:PO-T2T blends at 295 K with various donor-acceptor ratio (λ_{ex} = 355 nm).

7.3 Conclusions

A novel highly luminescent TADF exciplex has been demonstrated, analysed and applied in solution-processed devices. The work presents a novel concept of using polymer-based exciplex blends to obtain efficient TADF emission with good solution-processing properties, and potential use in practical low-cost applications. This opens a new pathway in the use of intermolecular exciplexes in commercial applications, but also paves the way for new fundamental research, regarding the RISC mechanism in these systems. We believe PVK:PO-T2T blend is only a first and not fully optimized example of such polymer-based exciplexes, and further development of new polymers

as donors or acceptors will occur as natural consequence of the concept described in this work. We also show that a variation in the donor-acceptor ratio does not affect the CT state properties at all. However, extreme ratios such as 99:1 may lead to decrease in exciplex formation efficiency and thus cause strong local fluorescence. We also addressed the role of the local triplet states in the RISC mechanism in exciplexes, where the CT state lies below the ^{3}LE. Our results show that the local triplet state does not play a dominant role in the reverse intersystem crossing mechanism in these blends and probably the RISC may involve significant hyperfine interactions.

8 Triplet harvesting in multicolour TADF exciplexes

The material contained within this chapter has been published as:

M. Chapran, **P. Pander**, M. Vasylieva, G. Wiosna-Salyga, J. Ulanski, F. B. Dias and P. Data, *ACS Appl. Mater. Interfaces*, 2019, **11**, 13460–13471.

8.1 Introduction

Exciplex states were introduced to the OLED arena many years ago due to the work of various researchers, including the groups of Kalinowski and Adachi.[11,16,19,154] In general, "single" TADF molecules show higher performance in OLEDs, when compared with bimolecular exciplexes. This is mainly due to the low photoluminescence quantum yield (Φ_{PL}) of exciplexes, but also due to the favourable molecular orientation of the TADF molecules, which is difficult to control in the case of bimolecular systems, but for TADF molecules can be engineered to maximize the intrinsic low light outcoupling efficiency associated with emitting organic layers. [7,155,156]

The relatively weak luminescence of exciplex blends follows a well-known opposite trend between the charge transfer (CT) character of the excited state and the PLQY due to the weak electronic coupling of the excited state with the ground state in molecules with strong charge transfer. This fact has limited the use of exciplexes to fabricate efficient devices, especially in the red region where enhanced internal conversion contributes to quench the triplet population due to the energy-gap law.[157,158] To the best knowledge of the author no efficient red exciplex has been reported to date, which represents a serious problem for the possible application of exciplex blends in white OLEDs. However, exciplexes offer a very interesting alternative approach to realize

multi-colour OLEDs, employing one acceptor and several different donors to simultaneously achieve multi-colour luminescence and efficient triplet harvesting.

Exciplexes also offer a promising alternative to intramolecular TADF molecules, giving the possibility to fabricate OLEDs without using a host material, i.e. the emitting layer in OLEDs using exciplex working cumulatively as the emitter and the host. Therefore, discovering ways to maximize the luminescence efficiency in exciplexes, while keeping strong triplet harvesting, is key for their implementation in the OLED field and important for both intramolecular and intermolecular systems.

A significant breakthrough in exciplex emitters was achieved when the thermally activated delayed fluorescence (TADF) properties of several exciplexes, including the m-MTDATA:PBD system,[154] was discovered by Adachi and co-workers. This idea was later explored by other research groups[12,135,142,150,151,159–161] who showed that very efficient triplet harvesting can be achieved in exciplex systems.

The development of novel exciplex emitters should, therefore, focus on achieving high luminescence efficiencies, while efficient triplet harvesting (TADF) is maintained, so bimolecular systems can compete with their "single" molecule counterparts. This task is complex and requires deep understanding of the photophysics of exciplex blends to unravel the more elusive aspects of the mechanism that affect the luminescence efficiency and lifetime in different regions of the spectrum.

Despite TADF exciplexes have already been used as efficient OLED emitters, they remain in some ways an unsolved puzzle for photophysicists. Some aspects of the theory that is used to explain the formation and decay of these intermolecular excited states are relatively simple, however, their use in practical systems, such as OLEDs, reveal that intermolecular TADF exciplexes are clearly more complex than their intramolecular analogues. For example, the luminescence decay of exciplexes shows prompt and delayed fluorescence components, which are also present on the luminescence decay of TADF molecules, however, more often in the exciplexes than in

the “single” TADF emitters, the luminescence decay includes a luminescence component decaying in a power law fashion, usually observed in the μs to ms region.[118] The origin of these power-law decay is still not clear, but certainly involves long-lived recombination processes. Therefore, the design of more efficient exciplexes, with shorter luminescence lifetimes, requires the understanding of the physical reasons behind power law regimes, so the luminescence quenching due to charge carriers can be minimized in devices. Importantly, recent works showed that some theories that apply to molecules that form intramolecular CT states can be also applied to intermolecular exciplexes, giving grounds to treat mono- and bimolecular CT emitters alike.[134]

Here it is discussed the photophysics of a carefully selected set of intermolecular exciplex blends with emission in the blue to orange regions of the visible spectrum. The motivation is to obtain a clear picture of the photophysical processes that affect the luminescence efficiency of these blends in different regions of the visible spectrum. The photophysics is also correlated with prototype OLED device data. Remarkably, devices with external quantum efficiencies (EQE) up to 20% were achieved in some of these blends, demonstrating the usefulness of exciplexes as OLED emitters, and underlining their major advantages over intramolecular TADF emitters. This includes the easy color tuning of their emission, and the fact that efficient TADF exciplex systems may be produced using already existing molecules, which are often reported in the literature or are even commercially available.

This study brings also clear physical meaning to the transient components observed in the luminescence decays of exciplexes, explaining the observation of luminescence regimes decaying as a power law in many exciplex emitters. These findings will facilitate the design of more efficient exciplex systems in the future.

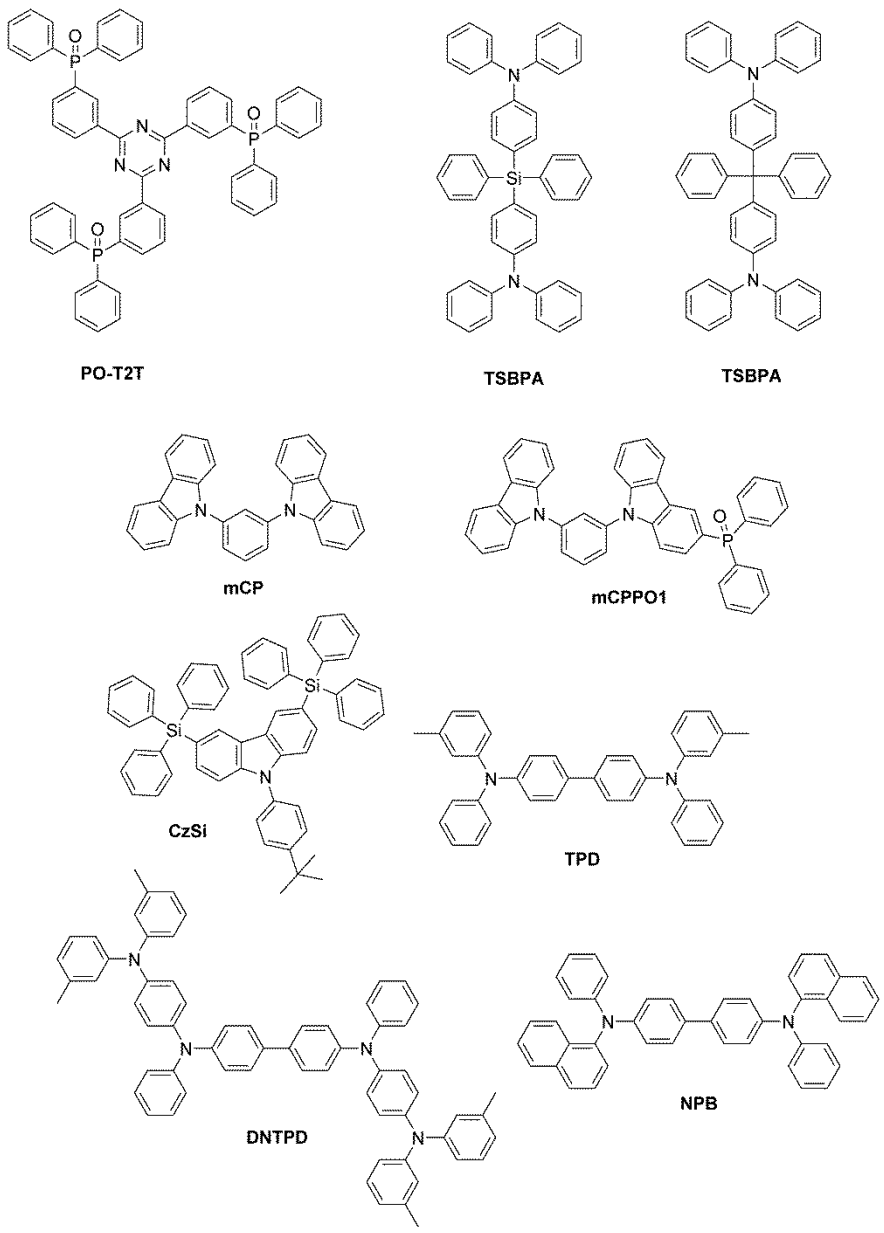

Figure 8.1. Chemical structures of exciplex forming materials used in this work. PO-T2T is used as an electron acceptor to form exciplex-forming blends with other presented molecules (all of them with electron-donating character).

8.2 Results and discussion

Exciplexes can be formed between electron donating (D) and electron-accepting (A) molecules, where the highest occupied molecular orbital (HOMO) is distributed on the D molecule and the lowest unoccupied molecular orbital (LUMO) is located on the A molecule.[154,18,81] The excited state complex is created with extremely small energy difference between singlet and triplet states (ΔE_{ST}) due to the negligible overlap

between HOMO and LUMO. This contributes to very efficient triplet harvesting in OLEDs. **Figure 8.1** shows the chemical structures of the compounds studied in this work. Most of these molecules are currently used as hole (TSBPA, TCBPA, NPD, TPD, DNTPD) or electron (PO-T2T) transport layers, or used as blocking layers (TSBPA, TCBPA), or even as hosts (CzSi, mCP, mCPPO1) in OLEDs. To the best knowledge of the author, exciplex blends formed with these molecules have never been reported before (except for mCP:PO-T2T[162,159] and NPB:PO-T2T[163]).

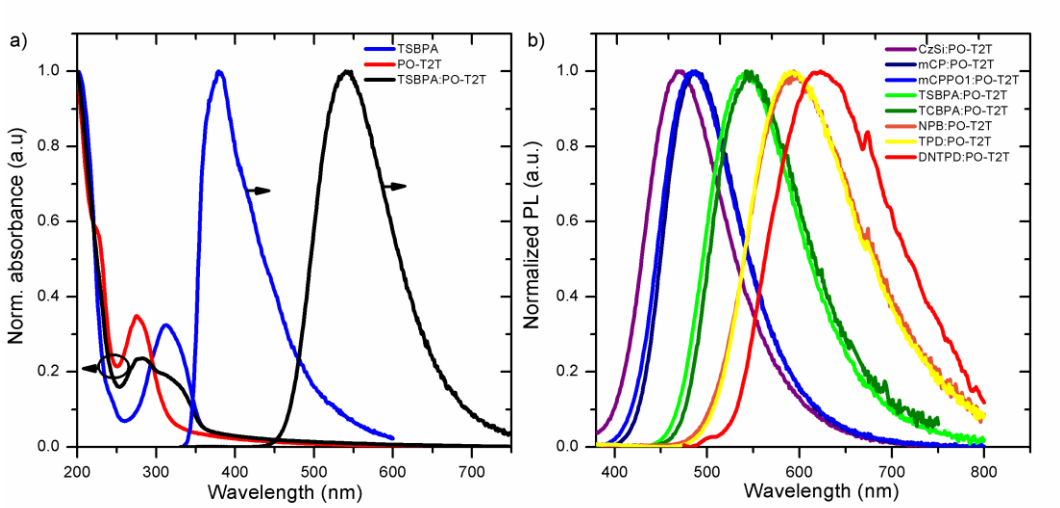

Figure 8.2. a) Normalised absorption and photoluminescence spectra of TSBPA, PO-T2T and their blend in pristine films, note PO-T2T film was found non-emissive at room temperature; b) photoluminescence spectra of all exciplexes obtained in solid films in air. PO-T2T was found to be non-emissive at room temperature. Note: steady-state absorption and fluorescence spectra recorded by M. Chapran. λ_{exc} = 330 nm.

8.2.1 Steady-state spectroscopy

Figure 8.2a shows the absorption and steady-state fluorescence spectra of the individual TSBPA donor and PO-T2T acceptor molecules, as well as their exciplex-forming blend as an exemplar of the exciplex properties of these blends. The absorption spectrum of the blend is simply a superposition of the absorption of the donor and acceptor absorptions, and there is no evidence of formation of CT complexes in the ground state. Similar observations were made for other blends (in supporting information of the published work). **Figure 8.2b** shows the photoluminescence (PL)

spectra of all exciplex blends studied in this work. It is particularly noteworthy that all presented blends show exciplex-only emission, with broad, Gaussian shape, typical of CT state emission,[74] clearly red shifted in respect to the emission of their individual D and A constituents. Moreover, as shown in **Figure 8.3** the ^{1}CT energy is a function of IP_D-EA_A energy difference, similarly to other reported exciplexes[18,50,164] (**Table 8.1**).

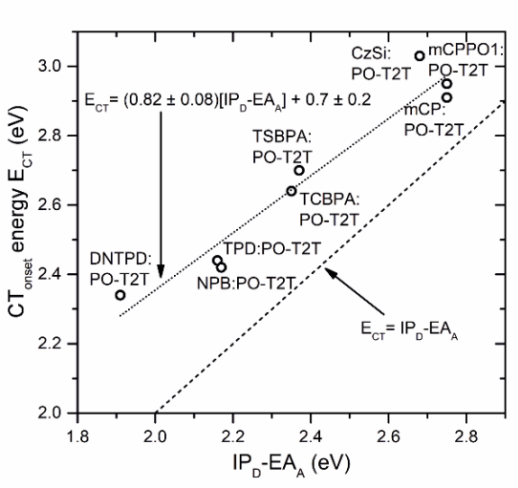

Figure 8.3. Onset CT energy plotted against electrochemically derived IP_D-EA_A energy difference. Note: the electrochemical IP/EA values were determined from cyclic voltammetry measurements performed by M. Vasylieva.

8.2.2 TADF in exciplexes and the role of local triplet states (^{3}LE).

The overlap between the HOMO and LUMO orbitals of the D and A units in exciplexes is minimal, therefore, the energy of the exciplex singlet state (^{1}CT), determined from the onset of the exciplex fluorescence, and the energy of the triplet state (^{3}CT) can be assumed as nearly identical. However, very often the triplet state with lower energy in the system is of local character, i.e. it is localized on the donor (D) or acceptor (A) molecules, and end up controlling the S-T energy gap in the exciplex system. While the CT state energy is a function of donor and acceptor HOMO-LUMO levels, and thus can be tuned, the energy of the local triplet state is determined by the triplet energy of either the donor or the acceptor molecules.[134,40] This implies that each donor-acceptor pair may have different relative energy alignment of the CT state in relation to the local triplet state(s) (^{3}LE), which is in part controlled by the large stabilization of the CT

states, as it is evident from the large Stokes-shift of the exciplex luminescence. This situation leads to one of three cases that have been used to describe the TADF mechanism in exciplexes:[43,41] (**I**) The ^{3}LE lies visibly below the ^{1}CT state, such as in the exciplexes described in previous works;[134] (**II**) The energy of the ^{3}LE state is aligned with the ^{1}CT state, such as in mCP:PO-T2T or mCPPO1:PO-T2T exciplexes; (**III**) The ^{3}LE is clearly above the ^{1}CT state, such as in TSBPA:PO-T2T or TCBPA:PO-T2T.

Case (**II**) is the ideal situation for efficient reverse intersystem crossing (RISC) to occur. Here, the ^{3}LE state has an intermediating role between the ^{1}CT and ^{3}CT states and enables fast RISC due to spin-orbit coupling interaction involving the ^{1}CT/^{3}CT and the ^{3}LE states.[40] In contrast, the lower-lying ^{3}LE state in case (**I**) creates an energy barrier between ^{1}CT and ^{3}LE, which may even be too large for TADF to occur at room temperature. In case (**III**), because ISC and RISC between ^{1}CT and ^{3}CT due to spin-orbit coupling is formally forbidden by symmetry, RISC is expected to be less favorable.[40,42,152,153] This, assuming that the hyperfine coupling between ^{1}CT and ^{3}CT states cannot provide fast exchange.[28,40–43,153] Therefore, the only way to convert triplet states from ^{3}CT to ^{1}CT involves the electronic coupling with the ^{3}LE state, which again generates an energy barrier for TADF.

Surprisingly, our results show that for TSBPA:PO-T2T and TCBPA:PO-T2T exciplexes efficient RISC occurs even when the ^{3}LE states are well above the ^{1}CT state, by 0.20 and 0.32 eV, respectively. Moreover, efficient TADF and high OLED EQE is achieved for both TSBPA:PO-T2T and TCBPA:PO-T2T blends. The exciplex TADF mechanism will be addressed to explain these results later in this work.

Table 8.1. Electronic and photophysical properties of investigated exciplexes.

Exciplex	**IP_D-EA_A, eV[a]**	**CT_{relax}, eV[b]**	**^3LE_D, eV[c]**	**^3LE_A, eV[d]**	**ΔE_{ST}, eV[e]**	**τ_{PF}, ns[f]**	**τ_{DF}, µs[g]**	**DF/PF ratio[h]**
CzSi:PO-T2T	2.68	3.03	3.05	2.93	0.10	36 ± 3	6.3 ± 0.3	5.7
mCP:PO-T2T	2.75	2.91	2.90		≈ 0.01	16 ± 1	1.96 ± 0.07	4.2
mCPPO1:PO-T2T	2.75	2.95	2.96		≈ 0.02	17 ± 3	2.63 ± 0.15	7.3
TSBPA:PO-T2T	2.37	2.70	2.90		≈ 0*	30 ± 6	2.2 ± 0.2	15.1
TCBPA:PO-T2T	2.35	2.64	2.96		≈ 0*	27 ± 6	2.2 ± 0.2	14.9
NPB:PO-T2T	2.17	2.42	2.44		≈ 0*	21 ± 2	0.53 ± 0.04	1.0
TPD:PO-T2T	2.16	2.44	2.45		≈ 0*	19 ± 1	0.37 ± 0.02	2.3
DNTPD:PO-T2T	1.91	2.34	2.43		≈ 0*	12 ± 1	-	-

[a] ionization potential of the donor (IP_D) – electron affinity of the acceptor (EA_A) difference; [b] energy of the relaxed CT emission recorded from delayed fluorescence spectra; note the energy recorded for DNTPD:PO-T2T exciplex, due to lack of TADF, is for prompt fluorescence emission; [c] triplet energy of the donor; [d] triplet energy of the acceptor; [e] singlet-triplet energy splitting; [f] prompt fluorescence lifetime; [g] delayed fluorescence lifetime; [h] delayed fluorescence to prompt fluorescence ratio derived as a ratio of integrated delayed fluorescence (DF) and prompt fluorescence (PF) intensity from the fitted decay curves. * $^1CT - ^3CT$ approaches 0 eV.

As already mentioned, exciplexes usually show low photoluminescence yield (Φ_{PL}). This is direct consequence of a truly distinct HOMO and LUMO orbitals showing vanishingly small overlap. Small, nearly zero integral overlap causes the transition oscillator strength to be very low,[165] with direct impact on the radiative rate of the excited state. This is in fact also a problem in many D-A TADF emitters, and it is believed that in order to obtain good oscillator strength in an exciplex the D and A species must be very close to each other.[166]

The PLQY of TADF molecules in general are obviously affected by the radiative rate constant as in any other molecules. However, particular for the TADF case is the fact that triplets can also contribute to the PLQY. Therefore, the competition between the

RISC rate and the non-radiative rate that affect the triplet decay have to be taken into consideration. For example, considering a system where the RISC rate dominates over the non-radiative decay in the triplet state. In this scenario, any triplet will be up-converted to the singlet manifold, from where it can emit or return back to the triplet state, due to ISC, however as the RISC dominates, once it arrives in the triplet state it will return back to the singlet state, from where it has one more chance to emit. This is known as the recycling process in TADFs. As the PLQY takes into account both prompt and delayed fluorescence components, it can be high even if the radiative rate is relatively slow. The crucial occurrence is that the internal conversion needs to be suppressed. Obviously a larger radiative rate will also help. Given the high Φ_{PL} of the TSBPA and TCBPA blends with PO-T2T, we therefore, speculate that the PO-T2T star-shaped molecule with relatively planar structure should make it easier to minimize the non-radiative internal conversion in these systems. Probably, the D and A molecules in these blends are closer to each other, allowing for relatively large orbital overlap and thus increasing the radiative rate in TSBPA and TCBPA blends with PO-T2T. [137]

8.2.3 Explaining the photoluminescence decay components observed from exciplex blends using time-resolved spectroscopy.

In all photoluminescence decays of the presented exciplex blends there are three clear decay regions, however, this is more evident in some of the cases (**Figure 8.4**). Interestingly, these regions can all be fitted using simple decay laws. Two of these regions can be described using single exponential expressions, these are the short-lived prompt fluorescence and the long-lived TADF region, whereas a third region can only be fitted using a power law decay.[118] It is well known that exponential expressions are able to adequately describe the decay of singlet and triplet populations of "well-behaved" exciplexes, i.e. those that have a very narrow distribution of decay lifetimes. In brief an exponential decay occurs when there is a single species emitting at constant rate. This is often the case in solution. However, in films, power-law decay laws are often needed to describe the luminescence decays. In principle this can be interpreted as

due to the presence in the blend of a broad distribution of decay lifetimes originated by the geometry and distance heterogeneity among the exciplex constituents in the blend. However, it immediately becomes evident that the appearance of power law decays may be in fact caused by a completely different phenomenon.

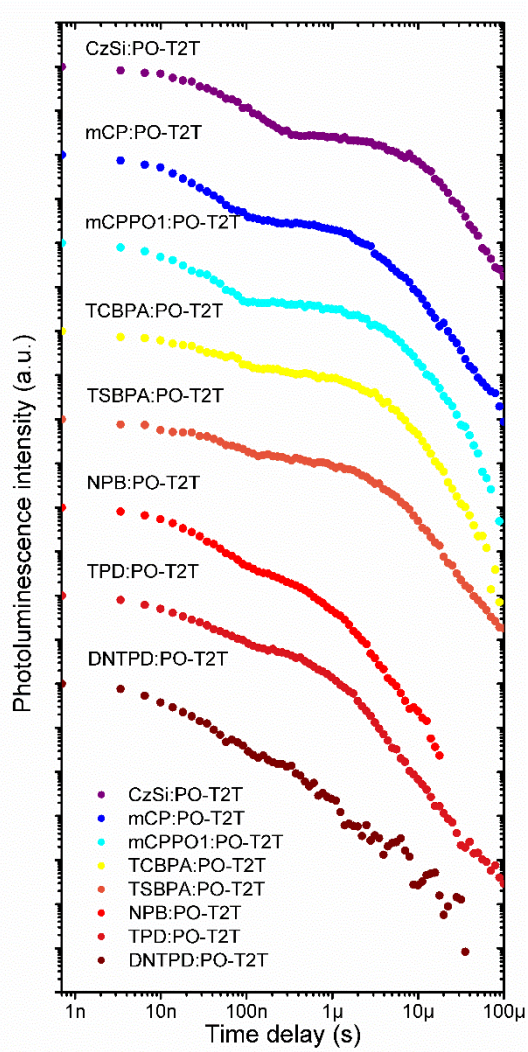

Figure 8.4. Room temperature photoluminescence decay of investigated exciplex blends (λ_{exc} = 355 nm). Note all exciplexes are formed with respective donor and PO-T2T as an acceptor. Note: donor-acceptor ratio is 1:1. Decays recorded in a vacuum at 295 K.

In the light of a recent paper by Kabe and Adachi,[147] it may be that in some situations the exciplex state may dissociate into a separate hole and an electron. This pathway cannot be neglected when describing the recombination of charge carriers in solid films. The explanation given by the authors on the behaviour of their exciplex system appears consistent with the power law decay reported in this work.[147] Both singlet and triplet

exciplex states may dissociate into freely separated hole an electron, which are able to migrate, via hopping, through donor- or acceptor-dominated domains, respectively. These charges when recombining at later time give origin to singlet and triplet exciplex states, which produce delayed exciplex fluorescence (**Figure 8.5**). As their migration pathways vary in a broad range, their recombination lifetime shows a broad distribution, which can only be fitted by a power law decay (**Figure 8.4, Figure 8.6a**). This observation is further supported by a recently published study[166] presenting experimental evidence for formation of polaron pairs in exciplex blends upon light illumination. In this more recent report, the authors suggest the polaron pairs remain a non-radiative evolution pathway of the exciplex state. This is contrary to the explanations suggested by Kabe and Adachi[147] and those presented in this work and would not give origin to decays following a power law. For this reason the incontestable proof for the mechanism suggested in the **Figure 8.5** is yet to be found. However, the experimental evidence is clearly gathering that support this to be a viable mechanism to explain the power-law region appearing in the delayed fluorescence decay of exciplexes.

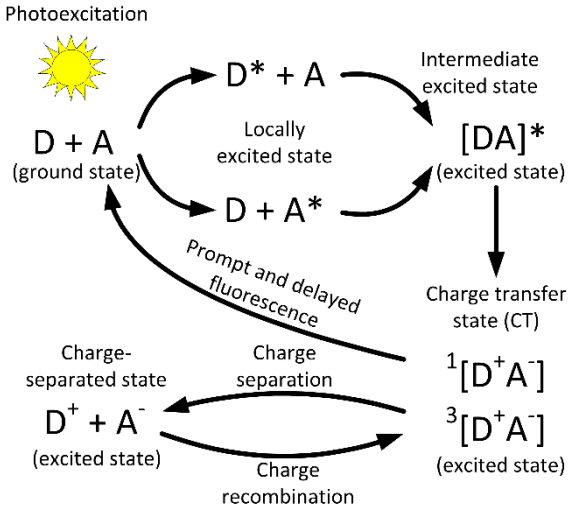

Figure 8.5. Model of photoexcited exciplex blend. Upon absorption of light, the donor (D) or/and acceptor (A) species form an excited state. The excited state molecule interacts with the ground state counterpart to form an excited state complex. A further step is electron transfer that results in the formation of CT states. The CT state can then undergo radiative or non-radiative decay. Another evolution pathway of the CT state is

dissociation into free charge carriers. Holes and electrons migrate all over the D-A blend and eventually recombine giving again CT exciplex states.

8.2.4 Addressing the exciplex TADF behaviour.

As the different exciplex decay regions have now been clarified on the basis of the available results, the differences observed in the exciplexes studied here can be more easily explained:

(1) The blue-emitting exciplexes mCP:PO-T2T; CzSi:PO-T2T; and mCPPO1:PO-T2T are type (II) TADF character. All show visible and strong TADF contribution and a power law decay component is only observed at later times. This is in full agreement with the mechanism explained above, as the ^{1}CT/^{3}CT states are in near resonance with the ^{3}LE state and, therefore, the RISC rate is sufficiently fast to rapidly promote long-lived triplet states into emissive singlets.

(2) The green emitting exciplexes, TSBPA:PO-T2T and TCBPA:PO-T2T show even higher TADF contribution than the blue emitting exciplexes, and both show power law decays at later times.

(3) The orange-yellow exciplexes, TPD:PO-T2T and NPB:PO-T2T, show a decreased amount of TADF contribution in relation to the prompt emission, and the power law decay becomes more pronounced.

Finally, (4) the least energetic orange-red exciplex, DNTPD:PO-T2T, shows no visible contribution of TADF emission and the prompt fluorescence is directly followed by the power law decay. This clearly shows that the DNTPD:PO-T2T blend does not show any classical delayed fluorescence phenomena, but only a delayed fluorescence originated from non-geminate charge-recombination.

The luminescence that is generated from bimolecular charge-recombination is in principle identical with electroluminescence and as such also does not contribute to the triplet harvesting in the OLED device by itself (assuming triplet harvesting is not

effective). In this way, the exciplexes showing only prompt fluorescence and power-law decay will behave like any pure fluorescent emitter in OLEDs, showing very limited triplet harvesting.

The observation of power law and exponential delayed fluorescence decays, therefore, must be distinguished from each other and special care must be taken not to assign the observation of a power law decay to the presence of "multiexponential decaying delayed fluorescence" as this is misleading and may hide a more general phenomenon that contributes to decreasing device efficiency (**Figure 8.6**).

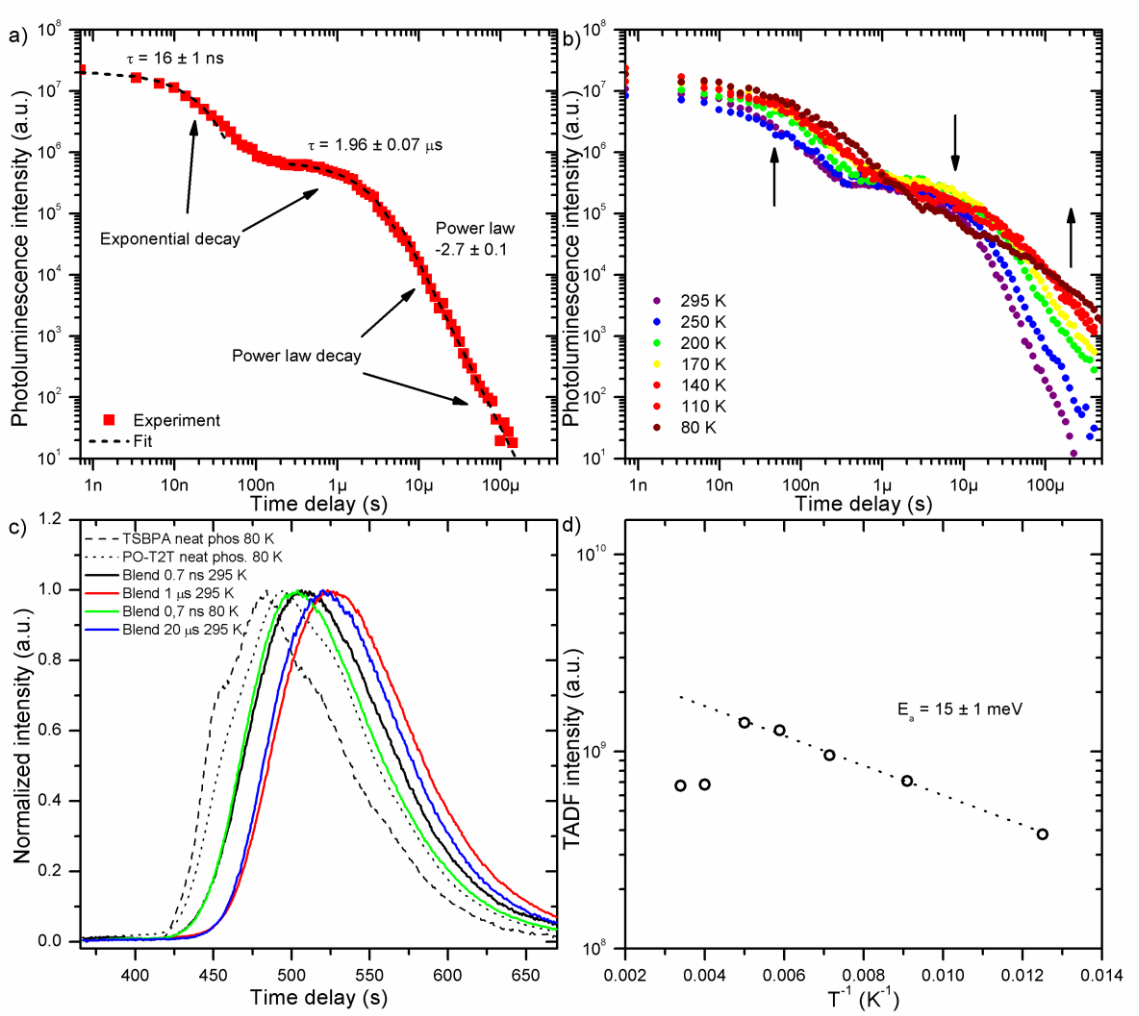

Figure 8.6. a) Photoluminescence decay of mCP:PO-T2T exciplex with fitted decay components. Note the decay components: exponential prompt and delayed fluorescence decay and power-law decay are indicated with arrows; b) photoluminescence decays of CzSi:PO-T2T exciplex at various temperatures. Notable changes to the decay upon temperature decrease are highlighted with arrows; c) prompt and delayed fluorescence spectra of TSBPA:PO-T2T exciplex with phosphorescence spectra of donor and acceptor species for comparison; d) temperature dependence of TADF intensity for mCP:PO-T2T exciplex. Recorded in a vacuum (at 295 K) or in nitrogen at any other temperature. Power law expression used for fitting: $y = ax^b$, where a and b are fitting parameters, while x is time and y is photoluminescence intensity. "Power law:" denotes the exponent b of the fit. λ_{exc} = 355 nm.

Our results are remarkable in the way that some of the exciplexes studied here show very short delayed fluorescence lifetimes. For example, the TADF lifetimes of mCP:PO-T2T, TSBPA:PO-T2T and TCBPA:PO-T2T exciplexes are roughly 2 μs, and are among the shortest values reported for TADF emitters.[5,68,167] A short TADF lifetime is important to facilitate obtaining high EQE in OLEDs with decreasing efficiency roll-

off, as it decreases the probability of triplet-triplet annihilation and triplet-polaron quenching, which are causes of device efficiency roll-off often observed at high brightness.

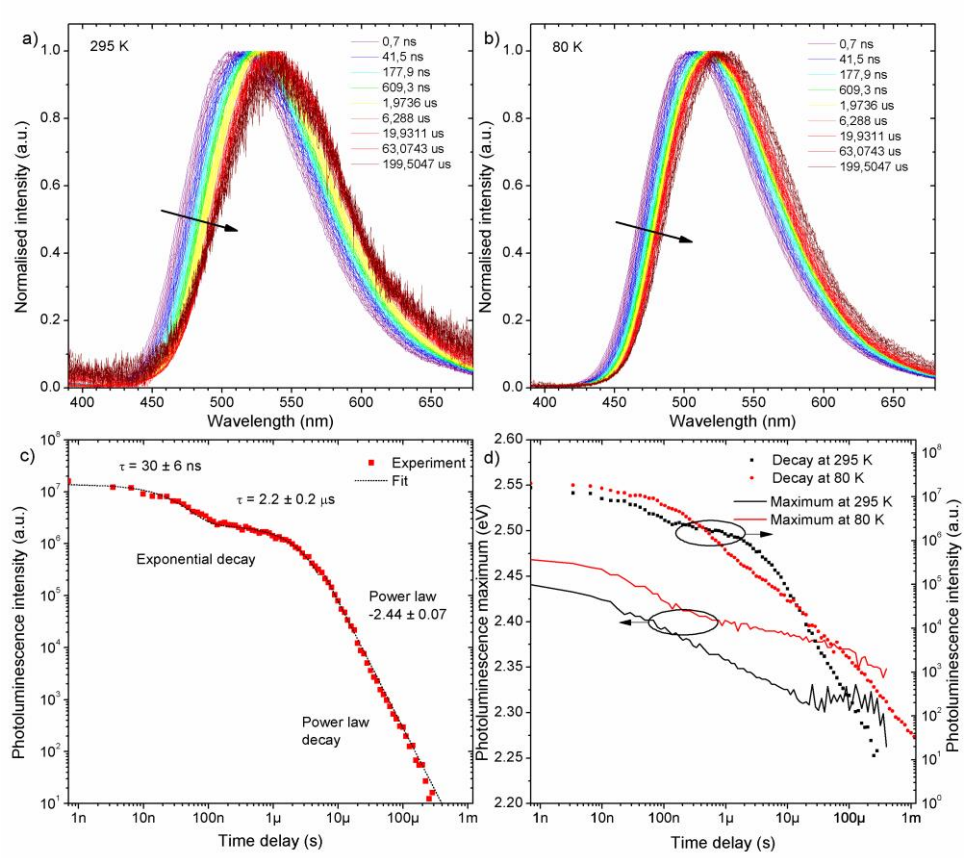

Figure 8.7. TSBPA:PO-T2T exciplex: a) time-resolved photoluminescence spectra at 295 K; b) time-resolved photoluminescence spectra at 80 K; c) photoluminescence decay at 295 K with fitting curves; d) photoluminescence decay and photoluminescence peak position at 295 K and 80 K. Recorded in a vacuum (at 295 K) or in nitrogen at any other temperature. Power law expression used for fitting: $y = ax^b$, where a and b are fitting parameters, while x is time and y is photoluminescence intensity. "Power law:" denotes the exponent b of the fit. λ_{exc} = 355 nm.

It is also worth to note that the longest delayed fluorescence lifetime of 6.3 ± 0.3 μ and the smallest k_{RISC} constant of 1.1×10^6 s^{-1} are observed in CzSi:PO-T2T which is the consequence of the largest singlet-triplet gap in this blend. The S-T gap of CzSi:PO-T2T is calculated as the difference between the relaxed CT energy and the ^3LE_A energy, and equals 0.10 eV in this blend. For mCP:PO-T2T and mCPPO1:PO-T2T S-T singlet-triplet energy gaps below 0.01-0.02 eV are observed, which is within the margin of

error in our determination. These exciplexes show much shorter lifetimes of *ca*. 2-3 μs and moderate k_{RISC} values of 2.7-3.2×10^6 s^{-1}. Consequently, the TCBPA:PO-T2T and TSBPA:PO-T2T exciplexes are expected to have virtually zero S-T gap due to the nearly zero ^{1}CT-^{3}CT energy barrier[118,160,161,168] (see text below for more details). These exciplexes show also very short TADF lifetime, ca. 2 μs, and have the highest TADF contribution, and the largest k_{RISC} constants of 7.2-7.3×10^6 s^{-1}. TPD:PO-T2T and NPB:PO-T2T show the shortest TADF lifetime among all the exciplexes studied here, with TADF decaying with a time constant of just 600 ns. Unfortunately, this is mainly due to increased non-radiative decay affecting the triplet state, as also the DF/PF ratio dramatically decreases[169,12] (**Table 8.1**).

It is notable that no evidence exists to support the observation of phosphorescence at 80K in any of the exciplex blends (except CzSi:PO-T2T, see text below). This is an indication that the singlet-triplet energy gap in these exciplexes is in general very narrow and therefore RISC dominates, even at low temperature. However, an additional weak emission is observed at long delay times, in the CzSi:PO-T2T blend at 80K, which is probably due to the phosphorescence of PO-T2T. This is most likely the consequence of the largest singlet-triplet gap, 0.1 eV, in this blend which slows the RISC rate.

In all the exciplexes herein (except for the obvious case of DNTPD:PO-T2T) the prompt emission is significantly blue shifted in relation to the delayed fluorescence. Interestingly, while the shape of the spectrum is preserved, the position of the emission intensity peak shows a gradual red-shift over time (i.e. see **Figure 8.7**). The time-dependence of this red-shift in the prompt-fluorescence region resembles an exponential decay. This is clear evidence of the CT state relaxation. However, such relaxation may be related to changes in the D-A distance or in their relative orientation, occurring within the first 100 ns. It is, therefore, concluded that the prompt fluorescence mostly occurs from a non-relaxed CT state, whereas the TADF component is mainly produced

from nearly relaxed exciplex states. For this reason, the CT emission that is observed around 1-10μs is the one used for the purpose of explaining the TADF phenomena in the exciplexes studied here, instead of the prompt or steady-state emissions. It is worth to note that the spectrum continuously but slowly red-shifts along the TADF and power law regions.

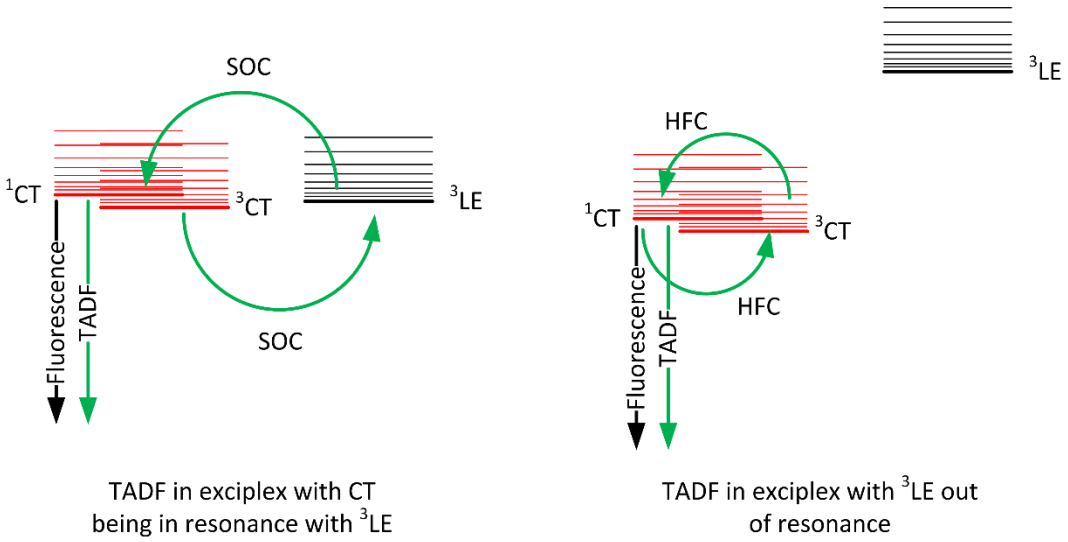

Figure 8.8. Schematic diagram showing how TADF emission is generated in exciplexes with CT – ^{3}LE exchange (left) and without this exchange (right). SOC (spin-orbit coupling) and HFC (hyperfine coupling) indicate the major interactions in each case.

8.2.5 Explaining strong TADF in exciplexes without the involvement of ^{3}LE states.

At this point, it is important to explain how the ^{1}CT - ^{3}CT exchange can be efficient without the involvement of a local ^{3}LE state acting as an intermediate. This is highly relevant for the understanding of the TADF mechanism, since the ^{1}CT - ^{3}CT transition is in general forbidden by symmetry and no TADF should be observed without involvement of local triplet states.

In systems where the ^{1}CT and ^{3}CT states are almost degenerate, hyperfine coupling interaction (HFC) may provide fast enough spin exchange to promote ISC and RISC (**Figure 8.8**).[170,27] In fact, HFC does not require any activation energy as ^{1}CT and ^{3}CT are nearly isoenergetic, but is only effective for very small S-T energy splitting. In our

exciplex systems, the TADF emission shows a temperature-activated regime with an energy barrier of 11-35 meV. This is clearly too large for the ^{1}CT - ^{3}CT energy difference, but it is within the range of energy associated with molecular rotational and vibrational transitions. Therefore, we speculate that the ^{1}CT - ^{3}CT transition associated with HFC may involve crossing from upper vibrational levels of the ^{3}CT state. More importantly, and to conclude this section, our results indicate that regardless of the location of the ^{3}LE state, above or in line with the CT state, the conditions are favourable for TADF because the ^{3}CT state lives long enough in order for efficient RISC to occur. This is the case in TSBPA:PO-T2T and TCBPA:PO-T2T exciplexes. On the other hand, having the ^{3}LE state below the CT state may be not beneficial for TADF. In fact, the ^{3}LE state may even act as a trap and favouring TADF quenching when is too far below the CT state. Note that the activation energy of TADF in TCBPA:PO-T2T and TSBPA:PO-T2T exciplexes is in the range of 10-20 meV, which is significantly lower than the energy difference between the relaxed CT and the lowest local triplet that is 200-300 meV. This undoubtedly demonstrates that the role of the local triplet state is not as crucial in these exciplexes as it has been reported previously in intramolecular systems.[40]

8.2.6 Devices

Organic light emitting diodes using the exciplexes characterised above have been fabricated by M. Chapran (**Table 8.2**). The device structure was based on a typical template, using NPB or TAPC as hole injection layers and PO-T2T as electron transport layer. Top electrode was aluminium with an ultrathin 1 nm layer of LiF for improved electron injection to the organic material.

Table 8.2. OLED device structures using the characterized exciplexes. Note: M. Chapran designed, faricated, and characterised the devices shown in the table below.

Exciplex	**Device**	**Structure**
CzSi:PO-T2T	**B1**	ITO | NPB(10nm) | TCTA(10nm) | CzSi(5nm) | CzSi:PO-T2T(20nm) | PO-T2T(50nm) | LiF(1nm) | Al(100nm)
mCP: PO-T2T	**B2**	ITO | NPB(10nm) | TCTA(10nm) | mCP(5nm) | mCP:PO-T2T(20nm) | PO-T2T(50nm) | LiF(1nm) | Al(100nm)
mCPPO1: PO-T2T	**B3**	ITO | NPB(30nm) | TCTA(10nm) | mCPPO1(5nm) | mCPPO1:PO-T2T(20nm) | PO-T2T(50nm) | LiF(1nm) | Al(100nm)
TSBPA:PO-T2T	**G1**	ITO | NPB(30nm) | TSBPA(10nm) | TSBPA:PO-T2T(20nm) | PO-T2T(50nm) | LiF(1nm) | Al(100nm)
TCBPA: PO-T2T	**G2**	ITO | NPB(40nm) | TCBPA(10nm) | TCBPA:PO-T2T(20nm) | PO-T2T(60nm) | LiF(1nm) | Al(100nm)
TPD: PO-T2T	**O1**	ITO | TAPC (20nm) | NPB (10nm) | NPB:PO-T2T (20nm) | PO-T2T(50nm) | LiF(1nm) | Al(100nm)
NPB: PO-T2T	**O2**	ITO | TAPC (40nm) | TPD (10nm) | TPD:PO-T2T (20nm) | PO-T2T(50nm) | LiF(1nm) | Al(100nm)
DNTPD: PO-T2T	**R1**	ITO | NPB (30nm) | DNTPD (10nm) | DNTPD:PO-T2T (20nm) | PO-T2T(50nm) | LiF(1nm) | Al(100nm)

The devices have shown similar electroluminescence spectra to the respective photoluminescence spectra of exciplex blends (**Figure 8.9**). The turn-on voltage 2.5-4 V suggests a good energy level alignment and no significant barriers for charge injection (**Table 8.3**). The performance of devices, in general, follows Φ_{PL} and TADF performance described above: the brightest and most efficient is device G1 employing the TSBPA:PO-T2T emissive exciplex with maximum luminance of 31000 cd m^{-2} and maximum EQE of 20 %. Interestingly, very similar TCBPA:PO-T2T exciplex, showing nearly identical photophysical characteristics, gives a significantly less efficient device G2. This is ascribed to the formation of electromer by the TCBPA that is not formed by TSBPA. The existence of this electromer has been proven by D. Pereira and the related manuscript is under preparation. The results prove efficient triplet harvesting in those TADF exciplexes which is consistent with their photophysical behaviour.

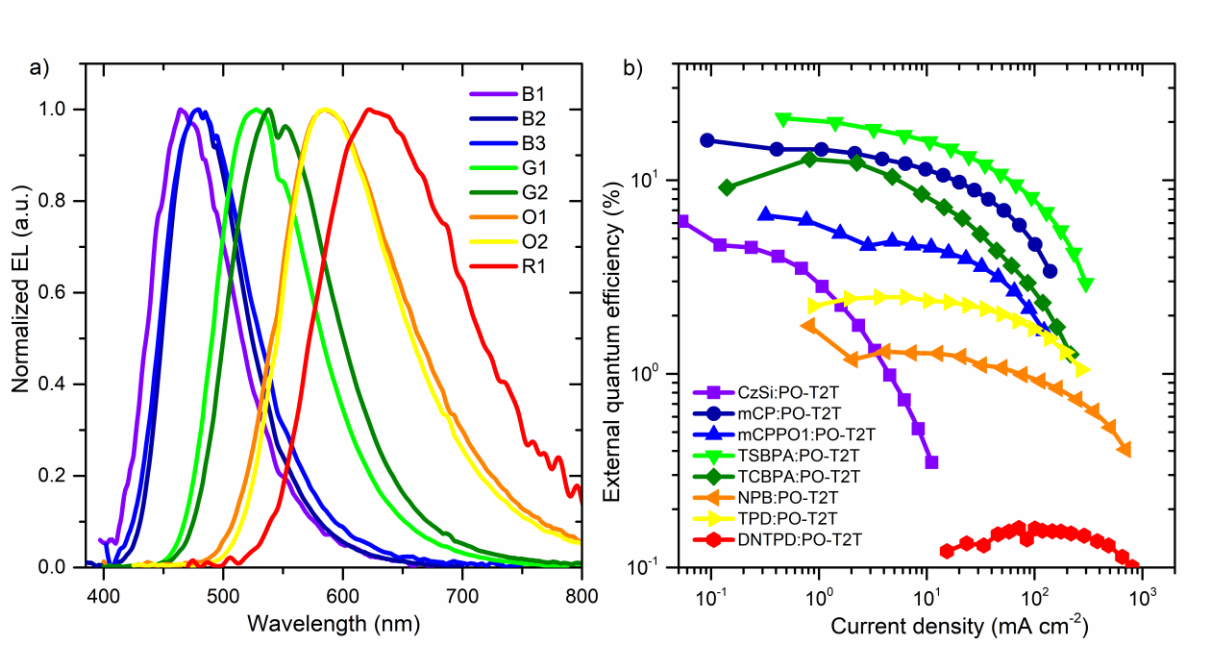

Figure 8.9. a) Electroluminescence spectra of fabricated devices; b) external quantum efficiency of fabricated devices. Note: donor-acceptor ratio is 1:1 in all emissive layers. Note: the OLED devices were fabricated and characterized by M. Chapran.

8.3 Conclusions

A new set of photoluminescent exciplexes has been characterised and new interesting phenomena were found. Local triplet states are believed to be crucial in intramolecular CT compounds as it promotes mixing between the singlet/triplet CT states and enhance SOC accelerating RISC.

Here, it was shown that local triplet states of the donor/acceptor species do not play a vital role in the RISC process in these exciplexes. The efficient triplet up-conversion is achieved without local triplet states being involved.

It is proposed that alternatively to SOC the HFC mechanism is directly involved in the communication between singlet and triplet CT levels and is responsible for the spin exchange in this situation. Furthermore, a phenomenon previously observed in PVK:PBD and PVK:PO-T2T blends: photoluminescence decaying in a power law fashion, has been recognised in small molecule blends. This gives a strong support to claim the phenomenon to be universal to many exciplexes. It was suggested that the

phenomenon occurs due to the presence of free charge carriers that are formed from the normal intermolecular charge-transfer states under strong laser excitation.

Photophysical characterisation of the presented exciplexes revealed remarkably strong photoluminescence and TADF emissions in some of them that were confirmed in prototype OLEDs. The organic light emitting devices fabricated achieved a maximum of 20 % external quantum efficiency, fully proving the concept that nearly 100 % triplet harvesting can be achieved in exciplex systems.

Table 8.3. Photoluminescence quantum yield of exciplexes (Φ_{PL}) and summary of OLEDs performance: turn-on voltage (V_{on}), maximum brightness (L_{max}) and current efficiency ($\eta_{L,max}$), and external quantum efficiency ($\eta_{ext,\,max}$), maxima of EL (λ_{max}) spectra and CIE 1931 color coordinates. Note: the OLED devices were fabricated and characterized by M. Chapran.

	Φ_{PL}		$\mathbf{V_{on}}$ (V)	$\mathbf{L_{max}}$ (cd m^{-2})	$\boldsymbol{\eta}_{\mathbf{L,max}}$ (cd A^{-1})	$\eta_{ext,\,max}$ (%)	λ_{max} EL (nm)	CIE 1931 (x; y)
CzSi:PO-T2T	0.24 ± 0.04	**B1**	3	900	8.9	6.1	465	(0.16;0.21)
mCP: PO-T2T	0.55 ± 0.08	**B2**	3	8960	27	16	480	(0.16;0.28)
mCPPO1: PO-T2T	0.20 ± 0.03	**B3**	3	3920	9.4	6.5	480	(0.18;0.29)
TSBPA:PO-T2T	1.0 ± 0.1	**G1**	2.5	31000	60.9	20	528	(0.33;0.57)
TCBPA: PO-T2T	0.93 ± 0.09	**G2**	2.5	9070	43.7	12.8	542	(0.38;0.56)
TPD: PO-T2T	0.08 ± 0.02	**O1**	3.5	6165	5	2.4	585	(0.53;0.47)
NPB: PO-T2T	0.04 ± 0.01	**O2**	3	6080	2.4	1.7	585	(0.52;0.46)
DNTPD: PO-T2T	< 0.01	**R1**	4	925	0.1	0.15	628	(0.60;0.39)

9 General conclusions of the thesis

Solid state photophysics is at the core of the investigations aimed to fully understand photoluminescence mechanisms in emitters designed to be used in OLEDs. This work focuses on photophysical studies aimed to characterise triplet-harvesting mechanisms occurring in excitonic, excimer and exciplex systems. Exciton, excimer and exciplex are three types of excited states primarily used to harvest triplets in OLED. This work provided not only a summary or basic characteristics of these complex emitters, but also presented an in-depth look into their photophysics, providing essential novelties into the topic. The author supported their photophysical results with prototype OLED devices: either fabricated by vacuum-deposition or solution-processed.

Triplet-harvesting exciton emitters are primarily either TADF or phosphorescent molecules. Both types have been characterised in this work. A novel TADF sky-blue emitter with narrow emission spectrum and record high ΔE_{ST} = 0.45 eV has been introduced. The study showed that by varying the nature of the lowest triplet state, either ππ* or nπ*, thus affecting their radiative lifetime, may promote either TADF or RTP properties in large $\Delta E_{ST} \approx$ 0.4-0.5 eV molecules.

Energy transfer processes from blend hosts (such as mixtures of electron and hole transport materials) to triplet-harvesting dopants is a complicated phenomenon. There are short-lived singlet states that undergo normal FRET to the dopant, and longer-lived triplet states that mostly undergo a quick Dexter energy transfer. However, there are also states that live considerably longer than the triplet excitons of the dopant, even up to milliseconds at 80 K. These states are trapped within the host and tend to migrate. Once they hit a triplet-harvesting dopant molecule, they induce emission of light, but at much longer delay after excitation, than would normally be expected. These states are responsible for long-lived and temperature-dependent power law luminescence decays observed in photoexcited PVK:PBD blends with low dopant concentration. Apparently,

that complicated photophysics does not relate to device performance as in OLEDs the dopant molecules are excited by direct charge injection.

Exciplex TADF emitters have been investigated in-depth within the recent years. Yet, they still remain an unsolved puzzle. The work presented here has given an insight into singlet-triplet relations in the exciplex, including the questionable involvement of the local triplet state. This work demonstrates that in some cases the local triplet state is not involved in an efficient RISC process. Furthermore, it has been shown, step by step, how to properly record and interpret photophysical properties of a TADF exciplex. Finally, a phenomenon previously observed in a doped PVK:PBD blend, which is related to the power law emission decays is reproduced in a TADF exciplex blend. This suggests the phenomenon might be caused by free migrating charge carriers. Finally, one of the characterised exciplexes gave 20 % external quantum efficiency in a prototype OLED.

Excimer-forming Pt(II) complexes have been primarily used in thermally evaporated OLEDs due to their low solubility. In this work highly soluble, excimer-forming molecules that achieve high efficiency in either solution-processed or thermally-evaporated devices were investigated. These molecules show variable contribution of excimer and exciton emissions upon changing their weight concentration in the OLED host. A significant red shift of the excimer-related emission band at higher complex concentrations and in neat film is observed. Time-resolved studies and excitation spectra suggested the red shift to be attributed to the coexistence of excimer and aggregate emissions (of which the latter becomes more significant at higher concentrations).

Exciton, excimer, and exciplex emitters – all can be utilised in OLED devices, however, due to electroluminescent and photoluminescent characteristics their potential use is limited to specific applications. In example: exciplex and excimer emitters, and most of the CT excitonc TADF emitters generally show broad photo- and electroluminescence

spectra. For this reason these emissive systems can only find their application in white light OLED technology for lighting. By mixing emission of two or more exciton emitters or exciplexes it is possible to achieve white light. Excimer emitters due to their dual emissive nature are potentially suitable to produce white light by using a single emissive compound by properly balancing blue-greenish exciton emission with yellow-orange excimer emission. White light can also be achieved by combination of the abovementioned methods. Exciton CT and non-CT TADF emitters and metalorganic phosphorescent emitters can be designed in a way to produce narrow photo- and electroluminescence spectra, thus their target application are electroluminescent displays, where colour purity of the emissive pixels is an important factor. Beyond the visible electromagnetic spectrum, among near infrared emitters the excimer-forming metal complexes may be of superior performance. This is because the interaction of two metal centres significantly increases radiative rate constant of the triplet state which is crucial in near infrared emitters due to the energy gap law.

In summary, this work presents examples of exciton, excimer, and exciplex triplet-harvesting emitters that have been characterised in-depth and well understood. Their performance has been evaluated in efficient OLEDs. The results contained in this work will have an impact on the understanding of these excited states giving a useful reference for further research in the area.

10 References

1 B. Geffroy, P. le Roy and C. Prat, *Polym. Int.*, 2006, **55**, 572–582.

2 J. N. Bardsley, *IEEE J. Sel. Top. Quantum Electron.*, 2004, **10**, 3–9.

3 H. Yersin, *Top. Curr. Chem.*, 2004, 1–26.

4 C. W. Tang and S. A. VanSlyke, *Appl. Phys. Lett.*, 1987, **51**, 913–915.

5 Y. Tao, K. Yuan, T. Chen, P. Xu, H. Li, R. Chen, C. Zheng, L. Zhang and W. Huang, *Adv. Mater.*, 2014, **26**, 7931–7958.

6 D.-H. Kim, A. D'Aléo, X.-K. Chen, A. D. S. Sandanayaka, D. Yao, L. Zhao, T. Komino, E. Zaborova, G. Canard, Y. Tsuchiya, E. Choi, J. W. Wu, F. Fages, J.-L. Brédas, J.-C. Ribierre and C. Adachi, *Nat. Photonics*, 2018, **12**, 98–104.

7 H. Uoyama, K. Goushi, K. Shizu, H. Nomura and C. Adachi, *Nature*, 2012, **492**, 234–238.

8 C. Adachi, M. A. Baldo, M. E. Thompson and S. R. Forrest, *J. Appl. Phys.*, 2001, **90**, 5048–5051.

9 G. A. Crosby and J. N. Demas, *J. Phys. Chem.*, 1971, **75**, 991–1024.

10 F. B. Dias, *Philos. Trans. R. Soc. A Math. Phys. Eng. Sci.*, 2015, **373**, 20140447–20140447.

11 J. Kalinowski, M. Cocchi, D. Virgili, V. Fattori and J. A. G. Williams, *Adv. Mater.*, 2007, **19**, 4000–4005.

12 K.-H. Kim, S.-J. Yoo and J.-J. Kim, *Chem. Mater.*, 2016, **28**, 1936–1941.

13 F. B. Dias, J. Santos, D. Graves, P. Data, R. S. Nobuyasu, M. A. Fox, A. S. Batsanov, T. Palmeira, M. N. Berberan-Santos, M. R. Bryce and A. P. Monkman, *Adv. Sci.*, 2016, **201600080**, 1–10.

14 M. Cocchi, J. Kalinowski, D. Virgili and J. A. G. Williams, *Appl. Phys. Lett.*, 2008, **92**, 113302.

15 P. Data, P. Pander, M. Okazaki, Y. Takeda, S. Minakata and A. P. Monkman, *Angew. Chemie Int. Ed.*, 2016, **55**, 5739–5744.

16 M. Sarma and K.-T. Wong, *ACS Appl. Mater. Interfaces*, 2018, **10**, 19279–19304.

17 T. Hatakeyama, K. Shiren, K. Nakajima, S. Nomura, S. Nakatsuka, K. Kinoshita, J. Ni, Y. Ono and T. Ikuta, *Adv. Mater.*, 2016, **28**, 2777–2781.

18 P. Pander, A. Kudelko, A. Brzeczek, M. Wroblowska, K. Walczak and P. Data, *Disp. Imaging*, 2017, **2**, 265–277.

19 M. Cocchi, D. Virgili, C. Sabatini and J. Kalinowski, *Chem. Phys. Lett.*, 2006, **421**, 351–355.

20 J. Kalinowski, M. Cocchi, L. Murphy, J. A. G. Williams and V. Fattori, *Chem. Phys.*, 2010, **378**, 47–57.

21 J. McMurry, *Organic Chemistry*, Brooks/Cole Cengage Learning, 2011.

22 A. Jablonski, *Nature*, 1933, **131**, 839–840.

23 J. R. Lakowicz, *Principles of Fluorescence Spectroscopy*, Springer US, 2007.

24 H. Yersin, *Top Curr Chem*, 2012, **241**, 1–26.

25 N. J. Bunce, *J. Chem. Educ.*, 1987, **64**, 907.

26 D. J. Griffiths, *Am. J. Phys.*, 1982, **50**, 698–703.

27 T. Ogiwara, Y. Wakikawa and T. Ikoma, *J. Phys. Chem. A*, 2015, **119**, 3415–3418.

28 J. Gibson, A. P. Monkman and T. J. Penfold, *ChemPhysChem*, 2016, **17**, 2956–2961.

29 G. Spavieri and M. Mansuripur, *Phys. Scr.*, 2015, **90**, 85501.

30 H. Yersin, *Highly Efficient OLEDs with Phosphorescent Materials*, Wiley, 2008.

31 S. R. Forrest, *Nature*, 2004, **428**, 911–918.

32 D. Yokoyama, *J. Mater. Chem.*, 2011, **21**, 19187.

33 H. Nakanotani, T. Higuchi, T. Furukawa, K. Masui, K. Morimoto, M. Numata, H. Tanaka, Y. Sagara, T. Yasuda and C. Adachi, *Nat. Commun.*, 2014, **5**, 4016.

34 M. J. Leitl, V. A. Krylova, P. I. Djurovich, M. E. Thompson and H. Yersin, *J. Am. Chem. Soc.*, 2014, **136**, 16032–16038.

35 R. Czerwieniec, J. Yu and H. Yersin, *Inorg. Chem.*, 2011, **50**, 8293–8301.

36 P. Pander, R. Bulmer, R. Martinscroft, S. Thompson, F. W. Lewis, T. J. Penfold, F. B. Dias and V. N. Kozhevnikov, *Inorg. Chem.*, 2018, **57**, 3825–3832.

37 V. N. Kozhevnikov, Y. Zheng, M. Clough, H. A. Al-Attar, G. C. Griffiths, K. Abdullah, S. Raisys, V. Jankus, M. R. Bryce and A. P. Monkman, *Chem. Mater.*, 2013, **25**, 2352–2358.

38 G. Li, R. S. Nobuyasu, B. Zhang, Y. Geng, B. Yao, Z. Xie, D. Zhu, G. Shan, W. Che, L. Yan, Z. Su, F. B. Dias and M. R. Bryce, *Chem. - A Eur. J.*, 2017, **23**, 11761–11766.

39 R. Czerwieniec and H. Yersin, *Inorg. Chem.*, 2015, **54**, 4322–4327.

40 F. B. Dias, J. Santos, D. R. Graves, P. Data, R. S. Nobuyasu, M. A. Fox, A. S. Batsanov, T. Palmeira, M. N. Berberan-Santos, M. R. Bryce and A. P. Monkman, *Adv. Sci.*, 2016, **3**, 1600080.

41 M. K. Etherington, F. Franchello, J. Gibson, T. Northey, J. Santos, J. S. Ward, H. F. Higginbotham, P. Data, A. Kurowska, P. L. Dos Santos, D. R. Graves, A. S. Batsanov, F. B. Dias, M. R. Bryce, T. J. Penfold and A. P. Monkman, *Nat. Commun.*, 2017, **8**, 14987.

42 R. S. Nobuyasu, Z. Ren, G. C. Griffiths, A. S. Batsanov, P. Data, S. Yan, A. P. Monkman, M. R. Bryce and F. B. Dias, *Adv. Opt. Mater.*, 2016, **4**, 597–607.

43 M. K. Etherington, J. Gibson, H. F. Higginbotham, T. J. Penfold and A. P. Monkman, *Nat. Commun.*, 2016, **7**, 13680.

44 S. A. Jenekhe and J. A. Osaheni, *Science (80-.).*, 1994, **265**, 765–768.

45 V. Jankus, P. Data, D. Graves, C. McGuinness, J. Santos, M. R. Bryce, F. B. Dias and A. P. Monkman, *Adv. Funct. Mater.*, 2014, **24**, 6178–6186.

46 P. Kurunczi, K. . Martus and K. Becker, *Int. J. Mass Spectrom.*, 2003, **223**–**224**, 37–43.

47 S. Develay and J. A. G. Williams, *Dalt. Trans.*, 2008, 4562.

48 K. Tuong Ly, R.-W. Chen-Cheng, H. Lin, Y. Shiau, S. Liu, P. Chou, C. Tsao, Y. Huang and Y. Chi, *Nat. Photonics*, 2017, **11**, 63–68.

49 R. J. Gillespie, *J. Chem. Educ.*, 2004, **81**, 298.

50 M. Gordon and W. R. Ware, Eds., *The Exciplex*, Academic Press, 1975.

51 P. Data, A. Kurowska, S. Pluczyk, P. Zassowski, P. Pander, R. Jedrysiak, M. Czwartosz, L. Otulakowski, J. Suwinski, M. Lapkowski and A. P. Monkman, *J. Phys. Chem. C*, 2016, **120**, 2070–2078.

52 J. Li, H. Nomura, H. Miyazaki and C. Adachi, *Chem. Commun.*, 2014, **50**, 6174–6176.

53 W.-Y. Hung, G.-C. Fang, S.-W. Lin, S.-H. Cheng, K.-T. Wong, T.-Y. Kuo and P.-T. Chou, *Sci. Rep.*, 2015, **4**, 5161.

54 J. C. de Mello, H. F. Wittmann and R. H. Friend, *Adv. Mater.*, 1997, **9**, 230–232.

55 A. M. Brouwer, *Pure Appl. Chem.*, 2011, **83**, 2213–2228.

56 S. Pluczyk, M. Vasylieva and P. Data, *J. Vis. Exp.*, 2018, e56656.

57 P. Pander, R. Motyka, P. Zassowski, M. Lapkowski, A. Swist and P. Data, *J. Phys. Chem. C*, 2017, **121**, 11027–11036.

58 V. Nadaraj, S. Thamarai Selvi and S. Mohan, *Eur. J. Med. Chem.*, 2009, **44**, 976–980.

59 J. P. Dheyongera, W. J. Geldenhuys, T. G. Dekker and C. J. Van der Schyf, *Bioorg. Med. Chem.*, 2005, **13**, 689–698.

60 R. Hegde, P. Thimmaiah, M. C. Yerigeri, G. Krishnegowda, K. N. Thimmaiah and P. J. Houghton, *Eur. J. Med. Chem.*, 2004, **39**, 161–177.

61 N. Bahr, E. Tierney and J.-L. Reymond, *Tetrahedron Lett.*, 1997, **38**, 1489–1492.

62 A. Świst, J. Cabaj, J. Sołoducho, P. Data and M. Łapkowski, *Synth. Met.*, 2013, **180**, 1–8.

63 D. a K. Vezzu, J. C. Deaton, M. Shayeghi, Y. Li and S. Huo, *Org. Lett.*, 2009, **11**, 4310–4313.

64 B. K. Sharma, A. M. Shaikh, N. Agarwal and R. M. Kamble, *RSC Adv.*, 2016, **6**, 17129–17137.

65 9(10H)-Acridanone, www.sigmaaldrich.com/catalog/product/aldrich/150215, (accessed 10 January 2018).

66 P. Data, A. Swist, M. Lapkowski, J. Soloducho, K. Darowicki and A. P. Monkman, *Electrochim. Acta*, 2015, **184**, 86–93.

67 S. Miyamoto, N. Miyake, L. F. Jarskog, W. W. Fleischhacker and J. A. Lieberman, *Mol. Psychiatry*, 2012, **17**, 1206–1227.

68 F. B. Dias, T. J. Penfold and A. P. Monkman, *Methods Appl. Fluoresc.*, 2017, **5**, 12001.

69 M. Okazaki, Y. Takeda, P. Data, P. Pander, H. Higginbotham, A. P. Monkman and S. Minakata, *Chem. Sci.*, 2017, **8**, 2677–2686.

70 H. Tanaka, K. Shizu, H. Nakanotani and C. Adachi, *J. Phys. Chem. C*, 2014, **118**, 15985–15994.

71 Z. Yang, Z. Mao, Z. Xie, Y. Zhang, S. Liu, J. Zhao, J. Xu, Z. Chi and M. P. Aldred, *Chem. Soc. Rev.*, 2017, **46**, 915–1016.

72 A. Endo, M. Ogasawara, A. Takahashi, D. Yokoyama, Y. Kato and C. Adachi, *Adv. Mater.*, 2009, **21**, 4802–4806.

73 H. Kaji, H. Suzuki, T. Fukushima, K. Shizu, K. Suzuki, S. Kubo, T. Komino, H. Oiwa, F. Suzuki, A. Wakamiya, Y. Murata and C. Adachi, *Nat. Commun.*, 2015, **6**, 1–8.

74 F. B. Dias, K. N. Bourdakos, V. Jankus, K. C. Moss, K. T. Kamtekar, V. Bhalla, J. Santos, M. R. Bryce and A. P. Monkman, *Adv. Mater.*, 2013, **25**, 3707–3714.

75 R. Komatsu, H. Sasabe, Y. Seino, K. Nakao and J. Kido, *J. Mater. Chem. C*, 2016, **4**, 2274–2278.

76 P. L. dos Santos, J. S. Ward, M. R. Bryce and A. P. Monkman, *J. Phys. Chem. Lett.*, 2016, **7**, 3341–3346.

77 P. Data, P. Pander, M. Okazaki, Y. Takeda, S. Minakata and A. P. Monkman, *Angew. Chemie Int. Ed.*, 2016, **55**, 5739–5744.

78 M. N. Berberan-Santos and J. M. M. Garcia, *J. Am. Chem. Soc.*, 1996, **118**, 9391–9394.

79 C. Baleizão and M. N. Berberan-Santos, *J. Chem. Phys.*, 2007, **126**, 204510.

80 H. Higginbotham, K. Karon, P. Ledwon and P. Data, *Disp. Imaging*, 2017, **2**, 207–216.

81 P. Data, R. Motyka, M. Lapkowski, J. Suwinski, S. Jursenas, G. Kreiza, A. Miasojedovas and A. P. Monkman, *Electrochim. Acta*, 2015, **182**, 524–528.

82 X.-L. Chen, C.-S. Lin, X.-Y. Wu, R. Yu, T. Teng, Q.-K. Zhang, Q. Zhang, W.-B. Yang and C.-Z. Lu, *J. Mater. Chem. C*, 2015, **3**, 1187–1195.

83 T. Hofbeck, U. Monkowius and H. Yersin, *J. Am. Chem. Soc.*, 2015, **137**, 399–404.

84 P. Pander, A. Swist, J. Soloducho and F. B. Dias, *Dye. Pigment.*, 2017, **142**, 315–

322.

85 S. Mukherjee and P. Thilagar, *Chem. Commun.*, 2015, **51**, 10988–11003.

86 G. He, W. Torres Delgado, D. J. Schatz, C. Merten, A. Mohammadpour, L. Mayr, M. J. Ferguson, R. McDonald, A. Brown, K. Shankar and E. Rivard, *Angew. Chemie - Int. Ed.*, 2014, **53**, 4587–4591.

87 S. Hirata, K. Totani, J. Zhang, T. Yamashita, H. Kaji, S. R. Marder, T. Watanabe and C. Adachi, *Adv. Funct. Mater.*, 2013, **23**, 3386–3397.

88 Y. Gong, G. Chen, Q. Peng, W. Z. Yuan, Y. Xie, S. Li, Y. Zhang and B. Z. Tang, *Adv. Mater.*, 2015, **27**, 6195–6201.

89 B. K. Sharma, A. M. Shaikh, N. Agarwal and R. M. Kamble, *RSC Adv.*, 2016, **6**, 17129–17137.

90 P. Pander, A. Swist, P. Zassowski, J. Soloducho, M. Lapkowski and P. Data, *Electrochim. Acta*, 2017, **257**, 192–202.

91 M. Y. Wong, M.-G. La-Placa, A. Pertegas, H. J. Bolink and E. Zysman-Colman, *J. Mater. Chem. C*, 2017, **5**, 1699–1705.

92 T. Serevičius, T. Nakagawa, M. Kuo, S. Cheng, K.-T. Wong, C.-H. Chang, R. C. Kwong, S. Xia and C. Adachi, *Phys. Chem. Chem. Phys.*, 2013, **15**, 15850.

93 M. Kim, S. K. Jeon, S. Hwang and J. Y. Lee, *Adv. Mater.*, 2015, **27**, 2515–2520.

94 J. Lee, K. Shizu, H. Tanaka, H. Nomura, T. Yasuda and C. Adachi, *J. Mater. Chem. C*, 2013, **1**, 4599.

95 D. R. Lee, M. Kim, S. K. Jeon, S. Hwang, C. W. Lee and J. Y. Lee, *Adv. Mater.*, 2015, **27**, 5861–5867.

96 P. L. dos Santos, J. S. Ward, A. S. Batsanov, M. R. Bryce and A. P. Monkman, *J. Phys. Chem. C*, 2017, **121**, 16462–16469.

97 H. Tanaka, K. Shizu, H. Nakanotani and C. Adachi, *J. Phys. Chem. C*, 2014, **118**, 15985–15994.

98 S. T. Hoffmann, P. Schrögel, M. Rothmann, R. Q. Albuquerque, P. Strohriegl and A. Köhler, *J. Phys. Chem. B*, 2011, **115**, 414–421.

99 M. C. Castex, C. Olivero, G. Pichler, D. Adès and A. Siove, *Synth. Met.*, 2006, **156**, 699–704.

100 J. Li, Q. Zhang, H. Nomura, H. Miyazaki and C. Adachi, *Appl. Phys. Lett.*, 2014, **105**, 13301.

101 R. Huang, J. Avó, T. Northey, E. Chaning-Pearce, P. L. dos Santos, J. S. Ward, P. Data, M. K. Etherington, M. A. Fox, T. J. Penfold, M. N. Berberan-Santos, J. C. Lima, M. R. Bryce and F. B. Dias, *J. Mater. Chem. C*, 2017, **5**, 6269–6280.

102 C. Baleizão and M. N. Berberan-Santos, *ChemPhysChem*, 2011, **12**, 1247–1250.

103 J. S. Ward, R. S. Nobuyasu, A. S. Batsanov, P. Data, A. P. Monkman, F. B. Dias and M. R. Bryce, *Chem. Commun.*, 2016, **52**, 3–6.

104 R. Pashazadeh, P. Pander, A. Lazauskas, F. B. Dias and J. V Grazulevicius, *J.*

Phys. Chem. Lett., 2018, **9**, 1172–1177.

105 V. N. Kozhevnikov, B. Donnio and D. W. Bruce, *Angew. Chemie - Int. Ed.*, 2008, **47**, 6286–6289.

106 J. A. G. Williams, S. Develay, D. Rochester and L. Murphy, *Coord. Chem. Rev.*, 2008, **252**, 2596–2611.

107 K. R. Graham, Y. Yang, J. R. Sommer, A. H. Shelton, K. S. Schanze, J. Xue and J. R. Reynolds, *Chem. Mater.*, 2011, **23**, 5305–5312.

108 M. Osawa, I. Kawata, R. Ishii, S. Igawa, M. Hashimoto and M. Hoshino, *J. Mater. Chem. C*, 2013, **1**, 4375–4387.

109 M. Z. Shafikov, A. F. Suleymanova, R. Czerwieniec and H. Yersin, *Chem. Mater.*, 2017, **29**, 1708–1715.

110 M. Aydemir, V. Jankus, F. B. Dias and A. Monkman, *Phys. Chem. Chem. Phys.*, 2014, **16**, 21543–21549.

111 J.-H. Jou, C.-Y. Hsieh, P.-W. Chen, S. Kumar and J. H. Hong, *J. Photonics Energy*, 2014, **4**, 43598.

112 J.-H. Jou, Y.-T. Su, S.-H. Liu, Z.-K. He, S. Sahoo, H.-H. Yu, S.-Z. Chen, C.-W. Wang and J.-R. Lee, *J. Mater. Chem. C*, 2016, **4**, 6070–6077.

113 X. Yang, B. Jiao, J.-S. Dang, Y. Sun, Y. Wu, G. Zhou and W.-Y. Wong, *ACS Appl. Mater. Interfaces*, 2018, **10**, 10227–10235.

114 P. Pander, R. Bulmer, R. Martinscroft, S. Thompson, F. W. Lewis, T. J. Penfold, F. B. Dias and V. N. Kozhevnikov, *Inorg. Chem.*, 2018, **57**, 3825–3832.

115 J. R. Sommer, R. T. Farley, K. R. Graham, Y. Yang, J. R. Reynolds, J. Xue and K. S. Schanze, *ACS Appl. Mater. Interfaces*, 2009, **1**, 274–278.

116 G. Turnbull, J. A. G. Williams and V. N. Kozhevnikov, *Chem. Commun.*, 2017, **2**, 1–4.

117 S. D. Cummings and R. Eisenberg, *Inorg. Chem.*, 1995, **34**, 2007–2014.

118 D. Graves, V. Jankus, F. B. Dias and A. Monkman, *Adv. Funct. Mater.*, 2014, **24**, 2343–2351.

119 C. M. Cardona, W. Li, A. E. Kaifer, D. Stockdale and G. C. Bazan, *Adv. Mater.*, 2011, **23**, 2367–2371.

120 P. Data, P. Pander, M. Lapkowski, A. Swist, J. Soloducho, R. R. Reghu and J. V. Grazulevicius, *Electrochim. Acta*, 2014, **128**, 430–438.

121 P. Data, R. Motyka, M. Lapkowski, J. Suwinski and A. P. Monkman, *J. Phys. Chem. C*, 2015, **119**, 20188–20200.

122 J. H. Burroughes, D. D. C. Bradley, A. R. Brown, R. N. Marks, K. Mackay, R. H. Friend, P. L. Burns and A. B. Holmes, *Nature*, 1990, **347**, 539–541.

123 D. D. . Bradley, A. . Brown, P. . Burn, J. . Burroughes, R. . Friend, A. . Holmes, K. . Mackay and R. . Marks, *Synth. Met.*, 1991, **43**, 3135–3141.

124 X. Yang, G. Zhou and W. Y. Wong, *J. Mater. Chem. C*, 2014, **2**, 1760–1778.

125 J. H. Cook, J. Santos, H. A. Al-Attar, M. R. Bryce and A. P. Monkman, *J. Mater. Chem. C*, 2015, **3**, 9664–9669.

126 C. Li, R. S. Nobuyasu, Y. Wang, F. B. Dias, Z. Ren, M. R. Bryce and S. Yan, *Adv. Opt. Mater.*, 2017, **5**, 1–9.

127 P. Murto, A. Minotto, A. Zampetti, X. Xu, M. R. Andersson, F. Cacialli and E. Wang, *Adv. Opt. Mater.*, 2016, **4**, 2068–2076.

128 M. Auer-Berger, R. Trattnig, T. Qin, R. Schlesinger, M. V. Nardi, G. Ligorio, C. Christodoulou, N. Koch, M. Baumgarten, K. Müllen and E. J. W. List-Kratochvil, *Org. Electron.*, 2016, **35**, 164–170.

129 Q. Zhang, D. Tsang, H. Kuwabara, Y. Hatae, B. Li, T. Takahashi, S. Y. Lee, T. Yasuda and C. Adachi, *Adv. Mater.*, 2015, **27**, 2096–2100.

130 P. L. dos Santos, J. S. Ward, D. G. Congrave, A. S. Batsanov, J. Eng, J. E. Stacey, T. J. Penfold, A. P. Monkman and M. R. Bryce, *Adv. Sci.*, 2018, 1700989.

131 Y.-K. Wang, S.-H. Li, S.-F. Wu, C.-C. Huang, S. Kumar, Z.-Q. Jiang, M.-K. Fung and L.-S. Liao, *Adv. Funct. Mater.*, 2018, **28**, 1706228.

132 L.-S. Cui, Y.-M. Xie, Y.-K. Wang, C. Zhong, Y.-L. Deng, X.-Y. Liu, Z.-Q. Jiang and L.-S. Liao, *Adv. Mater.*, 2015, **27**, 4213–4217.

133 W.-Y. Hung, G.-C. Fang, S.-W. Lin, S.-H. Cheng, K.-T. Wong, T.-Y. Kuo and P.-T. Chou, *Sci. Rep.*, 2015, **4**, 5161.

134 P. L. Dos Santos, F. B. Dias and A. P. Monkman, *J. Phys. Chem. C*, 2016, **120**, 18259–18267.

135 V. Jankus, P. Data, D. Graves, C. McGuinness, J. Santos, M. R. Bryce, F. B. Dias and A. P. Monkman, *Adv. Funct. Mater.*, 2014, **24**, 6178–6186.

136 V. Cherpak, A. Gassmann, P. Stakhira, D. Volyniuk, J. V Grazulevicius, A. Michaleviciute, A. Tomkeviciene and G. Barylo, *Org. Electron.*, 2014, **15**, 1396–1400.

137 V. Cherpak, P. Stakhira, B. Minaev, G. Baryshnikov, E. Stromylo, I. Helzhynskyy, M. Chapran, D. Volyniuk, Z. Hotra, A. Dabuliene, A. Tomkeviciene, L. Voznyak and J. V. Grazulevicius, *ACS Appl. Mater. Interfaces*, 2015, **7**, 1219–1225.

138 D. Volyniuk, V. Cherpak, P. Stakhira, B. Minaev, G. Baryshnikov, M. Chapran, A. Tomkeviciene, J. Keruckas and J. V. Grazulevicius, *J. Phys. Chem. C*, 2013, **117**, 22538–22544.

139 V. Jankus, K. Abdullah, G. C. Griffiths, H. Al-Attar, Y. Zheng, M. R. Bryce and A. P. Monkman, *Org. Electron.*, 2015, **20**, 97–102.

140 L. Song, Y. Hu, Z. Liu, Y. Lv, X. Guo and X. Liu, *ACS Appl. Mater. Interfaces*, 2017, **9**, 2711–2719.

141 P. Data, M. Lapkowski, R. Motyka and J. Suwinski, *Electrochim. Acta*, 2013, **87**, 438–449.

142 X.-K. Liu, Z. Chen, J. Qing, W.-J. Zhang, B. Wu, H. L. Tam, F. Zhu, X.-H. Zhang and C.-S. Lee, *Adv. Mater.*, 2015, **27**, 7079–7085.

143 J. H. Cook, H. A. Al-Attar and A. P. Monkman, *Org. Electron.*, 2014, **15**, 245–250.

144 H. A. Al Attar and A. P. Monkman, *Adv. Mater.*, 2016, **28**, 8014–8020.

145 C. Murawski, K. Leo and M. C. Gather, *Adv. Mater.*, 2013, **25**, 6801–6827.

146 V. Jankus and A. P. Monkman, *Adv. Funct. Mater.*, 2011, **21**, 3350–3356.

147 R. Kabe and C. Adachi, *Nature*, 2017, **550**, 384–387.

148 P. L. Santos, J. S. Ward, P. Data, A. S. Batsanov, M. R. Bryce, F. B. Dias and A. P. Monkman, *J. Mater. Chem. C*, 2016, **4**, 3815–3824.

149 V. Jankus, C. J. Chiang, F. Dias and A. P. Monkman, *Adv. Mater.*, 2013, **25**, 1455–1459.

150 W. Hung, T. Wang, P. Chiang, B. Peng and K. Wong, *ACS Appl. Mater. Interfaces*, 2017, **9**, 7355–7361.

151 W. Liu, J.-X. Chen, C. Zheng, K. Wang, D. Chen, F. Li, Y.-P. Dong, C.-S. Lee, X.-M. Ou and X.-H. Zhang, *Adv. Funct. Mater.*, 2016, **26**, 2002–2008.

152 B. T. Lim, S. Okajima, A. K. Chandra and E. C. Lim, *J. Chem. Phys.*, 1982, **77**, 3902–3909.

153 C. M. Marian, *J. Phys. Chem. C*, 2016, **120**, 3715–3721.

154 K. Goushi, K. Yoshida, K. Sato and C. Adachi, *Nat. Photonics*, 2012, **6**, 253–258.

155 T.-L. Wu, M.-J. Huang, C.-C. Lin, P.-Y. Huang, T.-Y. Chou, R.-W. Chen-Cheng, H.-W. Lin, R.-S. Liu and C.-H. Cheng, *Nat. Photonics*, 2018, **12**, 235–240.

156 H. Kaji, H. Suzuki, T. Fukushima, K. Shizu, K. Suzuki, S. Kubo, T. Komino, H. Oiwa, F. Suzuki, A. Wakamiya, Y. Murata and C. Adachi, *Nat. Commun.*, 2015, **6**, 8476.

157 W. Zeng, H.-Y. Lai, W.-K. Lee, M. Jiao, Y.-J. Shiu, C. Zhong, S. Gong, T. Zhou, G. Xie, M. Sarma, K.-T. Wong, C.-C. Wu and C. Yang, *Adv. Mater.*, 2018, **30**, 1704961.

158 S. Wang, X. Yan, Z. Cheng, H. Zhang, Y. Liu and Y. Wang, *Angew. Chemie Int. Ed.*, 2015, **54**, 13068–13072.

159 J.-H. Lee, S.-H. Cheng, S.-J. Yoo, H. Shin, J.-H. Chang, C.-I. Wu, K.-T. Wong and J.-J. Kim, *Adv. Funct. Mater.*, 2015, **25**, 361–366.

160 W. Hung, G. Fang, Y. Chang, T. Kuo, P. Chou, S. Lin and K. Wong, *ACS Appl. Mater. Interfaces*, 2013, **5**, 6826–6831.

161 T. Zhang, B. Chu, W. Li, Z. Su, Q. M. Peng, B. Zhao, Y. Luo, F. Jin, X. Yan, Y. Gao, H. Wu, F. Zhang, D. Fan and J. Wang, *ACS Appl. Mater. Interfaces*, 2014, **6**, 11907–11914.

162 Z. Wu, L. Yu, F. Zhao, X. Qiao, J. Chen, F. Ni, C. Yang, T. Ahamad, S. M.

Alshehri and D. Ma, *Adv. Opt. Mater.*, 2017, **5**, 1700415.

163 J.-H. Lee, H. Shin, J.-M. Kim, K.-H. Kim and J.-J. Kim, *ACS Appl. Mater. Interfaces*, 2017, **9**, 3277–3281.

164 P. Data, A. Kurowska, S. Pluczyk, P. Zassowski, P. Pander, R. Jedrysiak, M. Czwartosz, L. Otulakowski, J. Suwinski, M. Lapkowski and A. P. Monkman, *J. Phys. Chem. C*, 2016, **120**, 2070–2078.

165 S. Hirata, Y. Sakai, K. Masui, H. Tanaka, S. Y. Lee, H. Nomura, N. Nakamura, M. Yasumatsu, H. Nakanotani, Q. Zhang, K. Shizu, H. Miyazaki and C. Adachi, *Nat. Mater.*, 2015, **14**, 330–336.

166 T.-C. Lin, M. Sarma, Y.-T. Chen, S.-H. Liu, K.-T. Lin, P.-Y. Chiang, W.-T. Chuang, Y.-C. Liu, H.-F. Hsu, W.-Y. Hung, W.-C. Tang, K.-T. Wong and P.-T. Chou, *Nat. Commun.*, 2018, **9**, 3111.

167 W.-C. Chen, C.-S. Lee and Q.-X. Tong, *J. Mater. Chem. C*, 2015, **3**, 10957–10963.

168 B. Frederichs and H. Staerk, 2008, **460**, 116–118.

169 X. Wei, Y. Chen, R. Duan, J. Liu, R. Wang, Y. Liu, Z. Li, Y. Yi, Y. Yamada-Takamura, P. Wang and Y. Wang, *J. Mater. Chem. C*, 2017, **5**, 12077–12084.

170 A. M. Scott and M. R. Wasielewski, *J. Am. Chem. Soc.*, 2011, **133**, 3005–3013.